

DISSERTATION

Modelling Analysis of Fluidised Bed Reactor Systems for Chemical-Looping Combustion

ausgeführt zum Zwecke der Erlangung des akademischen Grades eines
Doktors der technischen Wissenschaften unter der Leitung von

Univ.-Prof. Dr. Hermann Hofbauer
E 166
Institut für Verfahrenstechnik, Umwelttechnik und Technische
Biowissenschaften

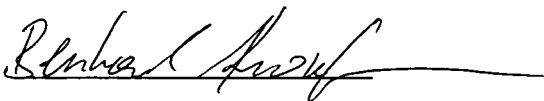
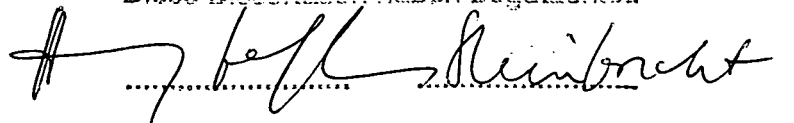
eingereicht an der Technischen Universität Wien
Fakultät für Maschinenwesen und Betriebswissenschaften

von

Dipl.-Ing. Bernhard Kronberger
Matr. Nr.: 9426340
In der Straß 4
4816 Gschwandt

Wien, im März 2005

Diese Dissertation haben begutachtet:

The most exciting phrase to hear in science,
the one that heralds the most discoveries,
is not "Eureka!" (I've found it!) but "That's
funny..."

Isaac Asimov

Acknowledgement

To Prof. Hermann Hofbauer, my supervisor, for giving me the chance to carry out this work along with the many interesting research projects. Thank you for your excellent scientific supervision and for the guidance through these years.

To Doctor Gerhard Löffler. His patience and profound advice during countless discussions over the last few years raised my motivation and gave me strong support throughout my thesis.

To Prof. Dieter Steinbrecht, University of Rostock, for critically and carefully reading my manuscript and giving me his advice.

To my former diploma workers Christoph Tagwerker, Pablo Navarro Marco, Raquel Valenciano, Ana Luengo and Elisabeth Wopienka for their valuable contributions to this work.

To the GRACE and CCCC project partners and co-workers for the pleasure it was to work with them and the time spent in many valuable discussions. On behalf of the many people I would like to mention Prof. Anders Lyngfelt and Eva Johansson, Chalmers University of Technology, Sweden, and Markus Luisser. I also want to acknowledge the financial support by the European Union for the research projects GRACE- Grangemouth Advanced CO₂ Capture Project (GRACE ENK5-CT-2001-005712) and CCCC-CO₂ Capture in Coal Combustion (ECSC contract No 7220-PR-125) .

To all my past and present colleagues at the Institute of Chemical Engineering, and to my fellow research associates and friends at the JRC Ispra. All the exchanges of thoughts and ideas made this time an enjoyable experience. A special thanks goes to Doctor Fesil Mushtaq, who did most of the language proofreading of my papers.

Finally, I would like to give a huge thank-you to my family for always being there for me, and for encouraging me in my work during times of happiness or dissatisfaction.

Abstract

This thesis conveys the research work carried out for the further development of a novel combustion technology known as chemical-looping combustion (CLC). The CLC concept is based on the transfer of oxygen from solid oxide materials in a reducing atmosphere of gaseous fuels. In a cyclic fashion those oxide materials are recycled in a separate oxidation stage, wherein they are re-oxidised to their original state for re-use. The key feature of this process is its ability to produce an essentially pure CO₂ stream that is ready for sequestration.

The work on the development of the oxygen carrier material focuses on the thermodynamics aspects. A parameter model of mass and energy balances of a CLC system shows, for different operating conditions, the importance of designing the unit specifically to the type of active metal. From the analysis, it follows that for oxides of the metals Fe, Cu, Ni, and Mn, and for reasonable small temperature differences between the two reactors, an oxygen carrier mass flow of about 0.005kg s⁻¹ kW⁻¹ is sufficient for natural gas and synthesis gas from coal gasification.

Fluid dynamics of CLC reactor concepts at different scales were studied not only experimentally with the use of flow models but also by mathematical modelling. CLC reactor system design issues are discussed and critical fluid dynamic parameters such as the solids circulation rate and gas leakage intensively analysed. The findings of the experimental part show the suitability of the concepts for the planned applications. In connection with the mathematical descriptions the results provide a reliable foundation for a combustion system scale-up.

A global CLC combustor model and its integration into a power plant concept are outlined. Results and models of detailed analysis on fluid dynamics and thermodynamics are integrated directly into the model. The influence of the metal oxide type and the operating temperatures of the reactors, as well as, the conditions of the inlet and outlet streams are evaluated to form the basis for further power plant concept optimisation.

An integrated assessment of the CLC technology is presented. By way of a case study detailed analyses and developments of other research institutions are reviewed. Technology scale-up issues are analysed and the potential of CLC as a possible key process for the continued use of fossil fuel resources as clean and efficient energy sources is evaluated.

Kurzfassung

Die vorliegende Dissertation umfasst Forschungsarbeiten zur Weiterentwicklung einer neuartigen Verbrennungstechnologie, dem Chemical-Looping Combustion (CLC). Das CLC Verfahren basiert auf Sauerstoffbereitstellung für die Verbrennung von gasförmigen Brennstoffen durch feste Oxide. In einem zyklischen Verfahren werden die Oxide in einem separaten Oxidationsprozess wieder bis zur ursprünglichen höheren Oxidationstufe aufoxidiert. Hauptmerkmal des Verfahrens ist die Bereitstellung eines weitgehend reinen CO₂ Abgasstromes, der für nachfolgende Sequestrierung zur Verfügung steht.

Hauptaugenmerk an der Weiterentwicklung von Sauerstoffträgermaterialien ist die Analyse der Thermodynamik. Ein Parametermodell der Massen- und Energiebilanzen von CLC Systemen wird vorgestellt und stellt die Bedeutung der spezifischen Auslegung für die jeweiligen Betriebsbedingungen dar. Es zeigt sich, dass für die Metalloxide von Fe, Cu, Ni und Mn und für akzeptable Temperaturdifferenzen zwischen den beiden Reaktoren ein Sauerstoffträgermassenstrom von etwa $0.005\text{kg}\cdot\text{s}^{-1}\cdot\text{kW}^{-1}$ zur Verbrennung von Erdgas bzw. Synthesegas aus Kohle ausreicht.

Die Fluidynamik von CLC Reaktorkonzepten verschiedener Maßstäbe wurde experimentell mithilfe von Kaltmodellen untersucht und zusätzlich durch mathematische Modelle analysiert. Verschiedene Aspekte der Reaktorauslegung werden diskutiert und entscheidende Parameter wie der Feststoffumlauf und die Gasvermischung untersucht. Die experimentellen Ergebnisse zeigen, dass die ausgelegten Reaktorkonzepte für die jeweilige Anwendung geeignet sind. In Kombination mit der mathematischen Beschreibung ergibt sich eine belastbare Grundlage für die fluiddynamische Maßstabsübertragung des Verbrennungssystems.

Ein umfassendes Modell sowie dessen Integration in ein Kraftwerkskonzept wird für den CLC-Brenner vorgestellt. Die Ergebnisse und Modelle von Detailuntersuchungen von Thermodynamik und Fluidynamik bilden die Basis für das Brennermodell. Mithilfe des Modells werden Einflüssen von Oxidtyp und Betriebstemperatur etc. untersucht sowie die Auswirkungen der Zustände der verschiedenen Stoffströme analysiert. Das Modell bildet die Basis für weitere CLC Prozesssimulation zur Optimierung des Konzeptes.

Anhand einer Fallstudie werden Detailergebnisse und technische Entwicklungen der CLC Technologie beurteilt. Aspekte der Maßstabsvergrößerung des Verfahrens werden analysiert und das Potential hinsichtlich des möglichen Einsatzes als weitestgehend saubere und effiziente Technologie zur Energieumwandlung aus fossilen Brennstoffen bewertet.

Table of contents

ACKNOWLEDGEMENT	III
ABSTRACT	IV
KURZFASSUNG	V
TABLE OF CONTENTS	1
1 INTRODUCTION	4
1.1 Background	4
1.2 CO₂-sequestration for fossil fuel power plants	6
1.2.1 Technological options for fossil fuel power plants	6
1.2.2 Energy conversion processes with inherent CO ₂ separation	7
1.3 Scope and outline of this thesis	8
2 CHEMICAL-LOOPING COMBUSTION	10
2.1 Technical background	10
2.2 Reactor design	12
2.3 Particle development	13
2.4 System analysis – process integration of CLC	16
3 THERMODYNAMIC ASPECTS OF CLC REACTOR SYSTEMS	18
3.1 Mass and energy balances	18
3.2 Parameter variations	20
3.3 Results and discussion	20
3.3.1 Variation of solids conversion and active metal content.....	20
3.3.2 Comparison of oxygen carrier types for base case	26
3.3.3 Conclusions	28
4 FLUID DYNAMICS OF CLC REACTOR SYSTEMS	29
4.1 Technical background on CLC -CFB systems	29
4.2 Methodologies	30
4.2.1 Flow modelling	30
4.2.2 Experimental techniques	32
4.2.3 Mathematical modelling	33
4.2.4 Overview of investigated CLC designs and scales.....	33
4.3 Laboratory scale unit	34
4.3.1 Reactor concept and design of the flow model.....	34
4.3.2 Experimental procedure and design variations	36
4.3.3 Results and discussion	37

4.3.4	Conclusions and design of the laboratory reactor system.....	44
4.4	Bench scale unit	45
4.4.1	General design issues	45
4.4.2	CFB reactor concept of the CLC prototype	47
4.4.3	Design aspects specific to the cold flow model	50
4.4.4	Pressure loop analysis.....	51
4.4.5	Solids circulation rate measurements.....	52
4.4.6	Gas leakage.....	55
4.4.7	Residence time distribution of solids in the CLC prototype fuel reactor	57
4.4.8	Design of bench-scale unit and operation results.....	65
4.5	Pilot and large-scale unit.....	67
4.5.1	CFB system description	67
4.5.2	Experimental programme	69
4.5.3	Experimental results for solids circulation and gas leakage.....	69
5	MATHEMATICAL MODELLING OF FLUID DYNAMICS OF CLC REACTOR SYSTEMS	75
5.1	Global model description	75
5.2	CFB-components models.....	76
5.2.1	The riser model.....	76
5.2.2	Fuel and air reactor.....	82
5.2.3	Loop seals.....	83
5.2.4	Cyclone	86
5.3	Simulation results and discussion	86
5.3.1	Static pressure distribution - pressure loop	86
5.3.2	Solids circulation rate.....	87
5.4	Conclusions	88
6	AN INTEGRATED CHEMICAL-LOOPING COMBUSTOR MODEL	90
6.1	Model structure and background	90
6.2	Simulation results and discussion	91
7	A CASE STUDY OF AN INDUSTRIAL CLC POWER PLANT	93
7.1	Development of a conceptual design	93
7.1.1	Boiler layout and process flow diagram.....	93
7.1.2	Techno-economic evaluation of the large-scale-concept	96
7.1.3	Future development and conclusions for industrial scale CLC boilers.....	100
8	SUMMARY AND CONCLUDING REMARKS	101
9	LIST OF PUBLICATIONS INCLUDED IN THIS WORK.....	105
10	REFERENCES	107

11	NOMENCLATURE	117
11.1	Greek letters	119
11.2	Acronyms.....	119
11.3	Indices.....	120
12	CURRICULUM VITAE.....	122

1 Introduction

1.1 *Background*

Economic development and growth in the developed countries depend on the provision and supply of affordable energy. The current situation in the energy field is marked by three issues that endanger the fragile stability: Firstly, energy demand is projected to grow rapidly by over 60% up to 2030 (IEA, 2002), whereby about 80% of this energy is supplied by fossil fuels (IPCC, 2001). Secondly, the high energy demand requires fossil fuels that are limited and mainly located in regions of unstable political situation, which threatens the access and thus costs for energy. Thirdly, concern over climate change is rapidly increasing, and the combustion of fossil fuels is accused of being a major source of greenhouse gas emissions.

Currently, energy policy looks for solutions to all these trends with different intensity and success. Although a huge potential for effectively tackling the problems in the energy field is attributed to the use of renewable fuels, by 2010 renewable energy is only expected to represent 15% of all primary energy use. As also nuclear power use is seen ambiguously, fossil fuels are widely acknowledged to play a significant role world-wide for future energy supply.

Having accepted that in the foreseeable future the effects of the use of fossil fuels must be addressed, and referring to the greenhouse gas emissions aspect, it is essential that when these fuels are burnt, they are burnt cleanly and efficiently with minimum associated emissions.

World average emissions of CO₂ per capita and the reductions required for atmospheric stabilisation at 550 or 450 ppm are depicted in Figure 1-1.

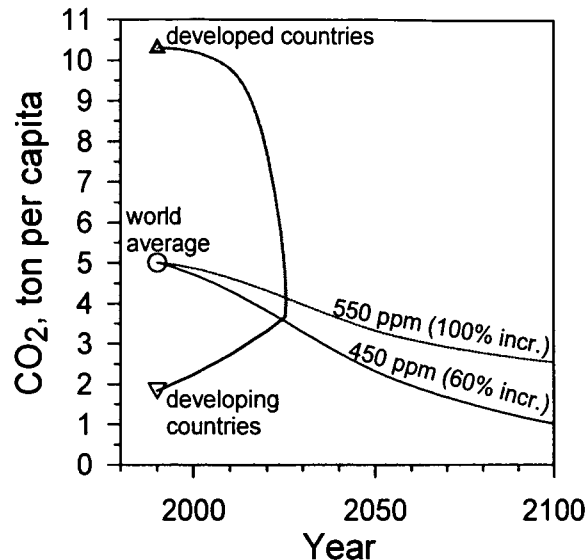


Figure 1-1: World average emissions of CO₂ per capita. %-increase refers to pre-industrial level (280 ppm) (source: Lyngfelt, 2004a).

The annual world average amount of CO₂ emissions is about 5 tonnes per capita, resulting from 5 times higher emissions from developed countries compared to developing countries. Today, the concentration of CO₂ in the atmosphere is about 370 ppm, which is 30% higher than the pre-industrial level of 280 ppm. This concentration is currently growing by about 2 ppm per annum and, because emissions of developing countries are projected to become a significant proportion of the global emissions, stabilisation will be impossible without actions by developing countries to control their emissions. Stabilisation of the CO₂ level at twice the pre-industrial level, 100% increase or 550 ppm, giving an expected temperature rise of 2°C (reference scenario of the EU, UK, Germany) will require a reduction of the average global CO₂ emissions per capita by a factor of two before the year 2100. Actions on a shorter timescale or lower stabilisation level (e.g. 450ppm) will require even more dramatic reductions for developed-world economies.

CO₂ capture and storage (CCS) - carbon management - is an approach that can support these necessary actions. However, it must be said that CCS is a strategy that can "buy time" but in view of the limited fossil fuel resources more sustainable CO₂ free energy solutions must be developed.

The projected quantities of CO₂, which would need to be captured and stored to meet significant global reductions as mentioned above, are huge. The extent to which CCS could be applied is widely unknown. Firstly, because mature technologies do not exist and, secondly, neither do steady quantifications of impacts on world economy and energy markets. In addition, the attractiveness of CCS compared to alternative mitigation options, such as increasing renewable energy or nuclear power use are unclear at the time being.

1.2 CO₂-sequestration for fossil fuel power plants

1.2.1 Technological options for fossil fuel power plants

The CO₂ capture options for fossil fuelled power plants are commonly grouped into three categories (e.g. Simbeck, 2004): These are

- post combustion CO₂ capture
- pre combustion CO₂ capture
- oxyfuel technology - post combustion in-situ CO₂ capture with oxygen firing.

Figure 1-2 shows a general description of Energy-conversion cycles and CO₂-capture methods as presented by Leithner (2004).

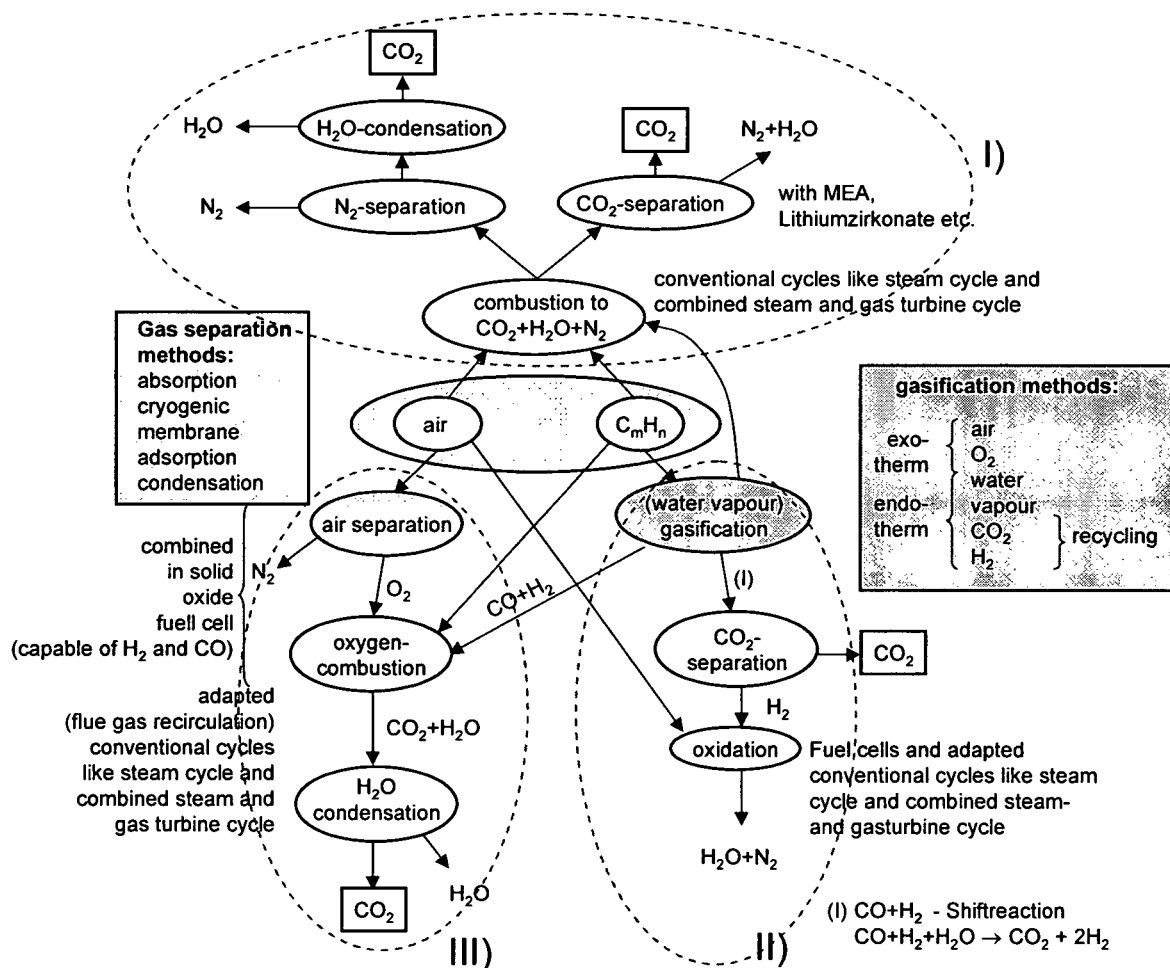


Figure 1-2: Energy-conversion cycles and CO₂-capture methods (modified from Leithner, 2004)

The three pathways marked by the cycles in Figure 1-2 can be described as follows:

- I. Post combustion is an “end of pipe technology”. A conventional combustion is followed by a CO₂ separation step from other flue gas components like N₂, water vapour etc.

- II. Pre combustion capture of CO₂ uses the “hydrogen route”, i.e. hydrogen is separated from CO₂ before combustion in a gasification process.
- III. Oxyfuel technology is referred to as combustion with oxygen from an additional air separation unit (ASU). Usually, the combustion takes place in an oxygen/CO₂ atmosphere, which allows the limitation of the combustion temperatures. This process is referred to as (classical) oxyfuel technology. A second group of processes in this category are fuel oxidation technologies with integrated advanced air separation technologies. These processes have the advantage of avoiding the energy penalty for the ASU and are characterised by in-situ CO₂ separation.

1.2.2 Energy conversion processes with inherent CO₂ separation

Fuel oxidation processes with inherent CO₂ separation have, equally to all other oxyfuel cycles, two separated flue gas flows. One is a depleted air stream and the other a stream of CO₂ and water vapour. The CO₂ separation technology requirements additional to the combustion are reduced to a condensation step of the water vapour for the latter stream. As mentioned above, these processes avoid the energy penalty associated with all other CO₂ separation processes but, in addition, most of them have the theoretical possibility of higher cycle efficiencies compared to conventional combustion.

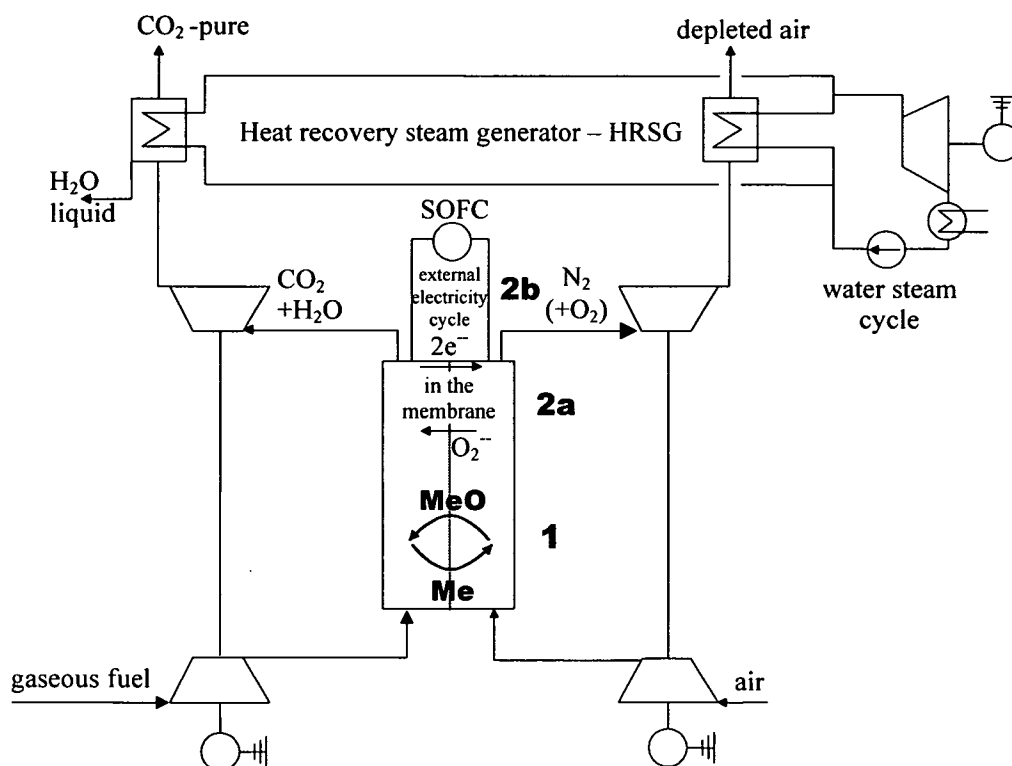


Figure 1-3: Basic principles of energy conversion processes with inherent CO₂-separation (MeO - Metal oxide, Me - Metal) (Leithner, 2004).

The processes in this group are firstly, metal oxide cycles, and secondly, oxygen ions transporting membrane cycles. In Figure 1-3 the basic principles are drawn for the first

process (1) and two options for the second process (2) for the integration into a combined cycle power plant concept. These two options for oxygen transport through membranes are an internal backflow of the ions in the membrane itself (2a) or an external backflow via an electricity cycle as Solid Oxide Fuel Cells (SOFC) (2b).

Membranes with an internal ions exchange are called mixed conducting membranes. The Zirconina oxide (ZrO_2) with Perovskit- or Fluorit-structure makes them selective to oxygen ions and permeation takes place as a consequence of the difference of the partial differential pressure of oxygen in the air and in the fuel or flue gas respectively. A technical research project based on this principle is the AZEP (Advanced Zero Emission Plant) process (Eklund et al., 2003).

SOFCs have a ZrO_2 -membrane, which is permeable to oxygen ions only. The electrons are conducted via an external electricity circuit back to the cathode. SOFCs are operated at temperatures of about 1000°C with a high electrical efficiency of about 50% and they can be fuelled with H_2 but also CO. An example of an integration of an SOFC in a large-scale CO_2 capture project is the ZECA (Zero Emission Coal Alliance) process (Lackner and Ziock, 2001).

Metal oxide cycles use solid metal oxides for oxygen transport from air to the fuel oxidizer. The metals (Fe, Cu, Ni, Mn, Co, Cd) are in a second step transported back to the air, where the metals are again oxidised and the cycle starts again. Detailed basic principles are presented in chapter 2.

Currently, these technologies have passed a “proof of concept” status and they are entering a pre-demonstration stage. Despite this disadvantage in comparison to mature processes such as the amine scrubbing process for post combustion CO_2 capture, their high potential in terms of efficiency for energy conversion including CO_2 capture makes it well worth to follow these research routes.

1.3 Scope and outline of this thesis

This thesis deals with detailed technical analysis of a novel combustion process called chemical-looping combustion (CLC). The process integrates a new technique for CO_2 capture in fossil fuelled power plants with the potential to separate CO_2 from a power generation process with only small penalties in efficiency. The oxygen for the fuel oxidation process is provided by metal oxide particles instead of ambient air. The oxide particles in reduced form are in a second step re-oxidised by air and act such as an oxygen carrier from the air to the fuel.

The aim of this thesis is to evaluate the impact of important process and design parameters on the performance of chemical-looping technology. To this end, the work includes investigations that are relevant to the basic research for this process, namely the study of particle development aspects, fluid dynamics, and thermodynamics. Experimental and mathematical modelling was carried out with the aims of identification of crucial design

aspects. Optimisation of the reactor design and the creation of a basis for further scale-up of the technology form the core of this work.

The work was conducted as part of two European research projects: The "Grangemouth Advanced CO₂ Capture Project" (GRACE) project focused on the development of CLC for firing of refinery gas at atmospheric conditions. The project "Capture of CO₂ in Coal Combustion" (CCCC) targets research for CLC application in coal combustion by firing coal synthesis gas at atmospheric and pressurised conditions. In both projects the activities of Vienna University covered reactor design and reactor fluidization studies, mathematical modelling and reactor scale-up issues.

In chapter 2 the technical background and previous work on CLC are provided. A detailed introduction on oxygen carrier development and a comprehensive overview on the research status in other topics in the field of CLC are given.

Chapter 3 includes the mathematical modelling of thermodynamics of the fuel oxidation process, based on papers Ia/Ib. Selected results and parameter studies are presented for atmospheric pressure for different fuel types and oxygen carrier types.

In chapter 4 the fluid dynamics of CLC reactor systems are analysed. The section contains an introduction on fluidised bed fluid dynamics and scaling issues. Results of experimental modelling work of CLC reactor concepts at laboratory -, bench-, and pilot scale published in papers IIa/IIb, III, IV, V are presented. Details on mathematical modelling (paper V) are given in chapter 5. Parts of the included work originate from a number of diploma theses that were supervised by the author.

Chapter 6 is dedicated to process simulation of mass and energy balances of CLC. Results of fluid dynamic, thermodynamic, and reaction engineering analyses are the basis for model of the CLC – combustor. The work presented in this chapter refers to paper VI and focuses on the energetic efficiency of the combustor but also on integration into a power plant process.

Chapter 7 contains techno-economic analysis of CLC technology and is based on a case study. The work (included in papers VII, VIIIa, VIIIb, VIIIc, IX, and X) gives an integrated assessment of chemical-looping combustion and shows its potential and critical issues.

Finally, chapter 8 presents a summary and a general discussion on the major results in this thesis. Further, recommendations are given for continued research.

2 Chemical-Looping combustion

2.1 Technical background

Chemical-looping combustion (CLC) is a novel combustion technology with inherent separation of the greenhouse gas CO₂. The technique, first mentioned by Knoche and Richter (1986, 1983) involves the combustion of fuel using a metal oxide as an oxidant instead of ambient oxygen. Direct contact between fuel and combustion air is avoided, and the products from combustion are kept separated from the rest of the flue gases, e.g. nitrogen and any remaining oxygen.

The system consists of two reactors, a fuel reactor (FR) and an air reactor (AR), and an oxygen carrier in the form of a metal oxide (MeO) that transports oxygen from the air to the fuel. In the FR the metal oxide is reduced, and in the AR the reduced metal oxide (Me) is re-oxidised by the air. The outlet gas stream of the AR consists of nitrogen and non-reacted oxygen, while the outlet gas from the FR consists of water and CO₂.

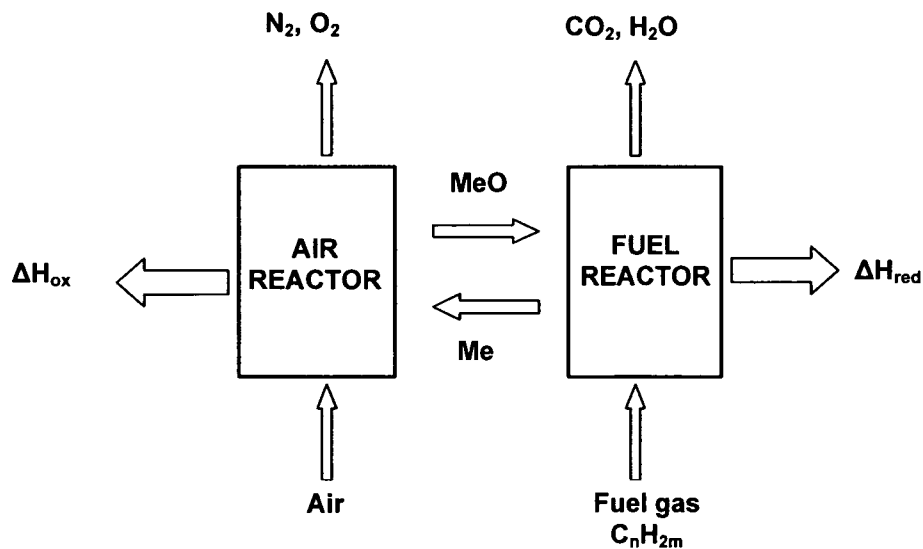
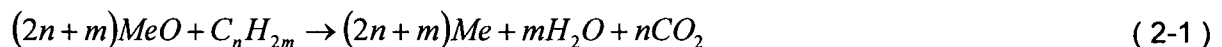


Figure 2-1: Principle of chemical-looping combustion. MeO and Me denote oxidised and reduced oxygen carriers.

According to the scheme shown in Figure 2-1 the gaseous fuel introduced to the fuel reactor reacts with the oxygen carrier according to:



In a second step the reduced metal is then circulated to the air reactor where it is oxidised and thus regenerated (2-2):



The flue gas from the air reactor contains N_2 and any non-reacted O_2 . Reaction (2-1) is often endothermic and reaction (2-2) is always exothermic. The net chemical reaction over the two reactors is the same as for normal combustion with an equal amount of heat released. Also, the total amount of heat evolved is equal to normal combustion of the same fuel (2-3):

$$\Delta H_c = \Delta H_{ox} + \Delta H_{red} \quad (2-3)$$

Major advantages of this system are:

- (i) CO_2 and H_2O are separated inherently from the rest of the flue gases..
- (ii) No additional energy is required for the CO_2 separation
- (iii) Reduction of the combustion irreversibilities (Ishida et al., 1994, Anheden et al. 1996, 1998, 2000, Wolf et al., 2001).
- (iv) Elimination of the formation of nitrogen oxides (Ishida et al., 1996a).
- (v) Existing equipment can be used, no new components are required.
- (vi) Retrofit of CFB power plant is feasible (Kronberger et al., 2004a).

Historically, the main benefit was seen in the reduction of combustion irreversibilities. This depends on the reaction path and thermodynamics of the two-step CLC reaction. The reactions are performed in a more ordered way than the conventional combustion reaction since direct contact between fuel and the combustion air is prevented, similar to fuel cells. The reaction between the fuel and the oxygen carrier MeO is usually (2-1) endothermic and takes place at a medium-low temperature with recovery of heat at a medium temperature level. The re-oxidation of the oxygen carrier is exothermic and according to Hess's law; the sum of heat of reaction for reactions (2-1) and (2-2) is equal to the heat of combustion. This means that the oxidation reaction (2-2) must have a higher heat of reaction than the conventional combustion reaction. As a result, more heat is released at a high temperature in the air reactor through recovery of thermal energy at a low temperature in the fuel reactor. The chemical-looping combustion system is thereby acting as a "chemical heat pump" in upgrading the low-level energy to high-level energy. When this energy is utilised efficiently in the subsequent power generation system, the overall thermal efficiency can be increased.

Later the potential was assigned towards the elimination of nitrogen oxide emissions. As fuel and air pass through different reactors with no flame an opportunity to thoroughly suppress the generation of NO_x is provided (Ishida et al., 1996).

Only, in the 90s the advantage of inherent CO_2 separation was recognised and the integration of this into a CLC power plant concept is presented in Figure 1-3. The combustion products CO_2 and H_2O leave the reduction reactor as a separate stream undiluted by excess air. All that is needed to get an almost pure CO_2 product is to condense the water vapour and remove the liquid water and any other impurities like unburned combustibles.

Recent research activities are all located around the CCS topic (CO₂ Capture and Storage) and motivated by the objective to develop a technology for the combustion of fossil fuels in an efficient power process providing CO₂ for further sequestration. Research and development in this field can be grouped into the following three areas:

- 1) Reactor design
- 2) Oxygen carrier development and
- 3) System analysis – process integration of CLC

2.2 Reactor design

A suitable reactor design for chemical-looping combustion was first proposed by Harvey (1994). Two isothermal fluidised beds with alternating valves allow the operation of each reactor as oxidizer and reducer, respectively. The main advantage of this configuration is that no solids transport is required. The oxidizer is run under atmospheric conditions and the reduction reactor is pressurised. Notable is also that the heat requirements of the two reactors are exactly matched.

Batch experiments and general feasibility analysis of Lyngfelt et al. (2001) showed that a circulating fluidised bed (CFB) reactor concept is suitable for chemical-looping combustion. The riser is thereby planned to work as an air reactor and the fuel reactor is put as a bubbling bed reactor into the return leg between downcomer and solids valve. Loop seals separate both reactors and a cyclone is used for particle separation from the air reactor exit flow.

Johansson and co-workers (2002, 2003) have outlined cold flow modelling results of different layouts of small laboratory scale reactor systems for chemical-looping combustion. A small laboratory scale unit based on a twin reactor system with less stringent gas sealing was developed and tested.

Adanez et al. (2003) have presented a kinetic fuel reactor model that allows optimisation of the reactor geometry based on kinetic models and experimental results. Ryu and colleagues (2002) showed a preliminary design of a 50 kW_{th} unit based on pressurised circulating fluidised bed technology.

Ishida et al. (2002) have shown experimental data from a small laboratory unit using a mixture of hydrogen with 33% Argon. The system consists of two interconnected columns in an oven, and seems to have no particle locks. The principles of the circulation system are not reported and since the two exiting gas streams were mixed before gas analysis it is not possible to judge if there was any gas mixing between the two reactors.

The authors performed tests at 600, 900 and 1200°C with complete conversion at the two higher temperatures. Gas conversion data are presented for a 5-hour test at 1200°C. The particles were made of a mixture of NiO and Al₂O₃, and it is interesting to note the high temperature used. In the frame of the EU co-funded GRACE (Grangemouth Advanced CO₂

Capture Project) project a 10kW_{th} CLC-CFB unit was run successfully for over 100 hours of operation by Lyngfelt et al. (2004b, 2004c).

2.3 Particle development

The most crucial aspect in the development of chemical-looping combustion is the identification of suitable oxygen carrier material. Research in this area has been carried out only by a small number of international institutions. A number of publications related to the development of oxygen-carrier particles have been issued by:

- i. Tokyo Institute of Technology, Research Laboratory of Resources Utilisation; (Ishida et al., 1996, 1997, 1998, 2002 and Jin et al., 1998, 1999, 2001, 2002).
- ii. National Institute for Resources and Environment in Japan (Hatanaka and co-workers, 1997)
- iii. Chalmers University of Technology (Mattisson et al., 2000, 2001a, 2001b, 2001c, 2002, 2004a and Cho et al., 2002, 2004).
- iv. Korea Institute of Energy Research, Advanced Industrial Science and Technology (Ryu et al., 2001, 2002a, 2002b, 2003a, 2003b, 2004a, 2004b, 2004c and Song et al., 2003)
- v. TDA Inc (Copeland and co-workers, 2000, 2001, 2002)
- vi. CSIC-ICB in Zaragoza (Adanez and co-workers, 2004a, 2004b)
- vii. Politecnico di Milano (Villa et al., 2003)
- viii. SINTEF & Norwegian University of Sci. and Technol., NTNU (Blom et al., 2004)

The development of chemical-looping combustion relies on the availability of redox materials able to match the following requirements:

- (i) good redox reactivity with high selectivity towards complete oxidation products and air respectively;
- (ii) high oxygen exchange efficiency, i.e. ratio of the oxygen mass involved in the redox process to the total mass of the solids;
- (iii) regenerability, i.e. stability during repeated redox cycles at relatively high temperatures (above 800°C);
- (iv) mechanical resistance to the friction stresses associated with recirculation of solid powders;
- (v) availability of a large scale particle production process;
- (vi) environmentally sound;
- (vii) low cost.

Metal oxides with metals from families 7B, 8B and 1B of the periodic table, such as Fe, Ni, and Cu, were initially suggested to be suitable as oxygen carriers from a thermodynamic

point of view (Richter and Knoche, 1983, Harvey, 1994). Later Mn and Co and mixtures such as Fe/Cu and Co/NiO₂ were also investigated. In Table 2-1 the capacity of a metal to carry oxygen from the air reactor to the fuel reactor is shown in the second column. R₀ gives the mass fraction of oxygen in the carrier in its fully oxidised state. Values up to 37% can be found, which gives the basic suitability for CLC. However, it must be considered that thermodynamic limitations avoid the practical use of few material/fuel gas combinations.

In Table 2-1 also an overview on possible reactions of methane with active metals at their possible oxidation states is given. The heats of reactions are presented for metal oxidation and reduction and it can be seen that the sum (based on equal metal moles) is equal to that of direct combustion (2-3). Division of the reaction enthalpy of oxidation with that for direct combustion of methane results in the heat release in the air reactor relative to that of direct combustion. This shows that most active metals give a heat release in the air reactor, which corresponds to the endothermic reactions in the fuel reactor.

Table 2-1: Oxidation and reduction reactions for CH₄ and various active metals (modified from Ryu et al, 2004b)

#	R ₀	Oxidation	ΔH _{ox} [kJ.mol ⁻¹]	Reduction	ΔH _{red} [kJ.mol ⁻¹]	ΔH _{ox} / ΔH _c [-]
0	--	O ₂ +1/2CH ₄ → 1/2CO ₂ +H ₂ O	445.16	Direct combustion	--	1.00
1	0.1002	O ₂ +4/3Fe→ 2/3Fe ₂ O ₃	547.55	CH ₄ +4/3Fe ₂ O ₃ → CO ₂ +2H ₂ O+8/3Fe	204.78	1.23
2	0.0334	O ₂ +4FeO→ 2Fe ₂ O ₃	584.92	CH ₄ +4Fe ₂ O ₃ → CO ₂ +2H ₂ O+8FeO	279.53	1.31
3	0.2142	O ₂ +4Fe ₃ O ₄ → 6Fe ₂ O ₃	461.08	CH ₄ +12 Fe ₂ O ₃ → CO ₂ +2H ₂ O+8 Fe ₃ O ₄	31.84	1.04
4	0.2135	O ₂ +2Ni→ 2NiO	481.16	CH ₄ +4NiO→ CO ₂ +2H ₂ O+4Ni	72.01	1.08
5	0.2658	O ₂ +2Co→ 2CoO	477.81	CH ₄ +4CoO→ CO ₂ +2H ₂ O+4Co	65.31	1.07
6	0.0664	O ₂ +3/2Co→ 1/2Co ₃ O ₄	452.50	CH ₄ +Co ₃ O ₄ → CO ₂ +2H ₂ O+3Co	14.69	1.02
7	0.2011	O ₂ +6CoO→ 2Co ₃ O ₄	376.56	CH ₄ +4Co ₃ O ₄ → CO ₂ +2H ₂ O+12CoO	137.19	0.85
8	0.1118	O ₂ +2Cu→ 2CuO	310.45	CH ₄ +4CuO→ CO ₂ +2H ₂ O+4Cu	269.41	0.70
9	0.1006	O ₂ +4Cu→ 2Cu ₂ O	334.72	CH ₄ +4Cu ₂ O→ CO ₂ +2H ₂ O+8Cu	220.87	0.75
10	0.3681	O ₂ +2Cu ₂ O→ 4CuO	286.19	CH ₄ +8CuO→ CO ₂ +2H ₂ O+4Cu ₂ O	317.94	0.64
11	0.2255	O ₂ +Mn→ MnO ₂	520.07	CH ₄ +2MnO ₂ → CO ₂ +2H ₂ O+2Mn	149.83	1.17
12	0.1840	O ₂ +2Mn→ 2MnO	769.86	CH ₄ +4MnO→ CO ₂ +2H ₂ O+4Mn	649.40	1.73
13	0.1013	O ₂ +2MnO→ 2Mn ₂ O ₃	270.29	CH ₄ +4Mn ₂ O ₃ → CO ₂ +2H ₂ O+4MnO	349.74	0.61
14	0.0699	O ₂ +4MnO→ 2Mn ₂ O ₃	374.05	CH ₄ +4 Mn ₂ O ₃ → CO ₂ +2H ₂ O+8MnO	142.21	0.84
15	0.0920	O ₂ +6MnO→ 2Mn ₃ O ₄	463.59	CH ₄ +4 Mn ₃ O ₄ → CO ₂ +2H ₂ O+12MnO	36.86	1.04
16	0.1227	O ₂ +2Mn ₂ O ₃ → 4MnO	166.52	CH ₄ +8MnO→ CO ₂ +2H ₂ O+4Mn ₂ O ₃	557.27	0.37
17	0.0338	O ₂ +Mn ₃ O ₄ → 3MnO	173.64	CH ₄ +6MnO→ CO ₂ +2H ₂ O+2Mn ₃ O ₄	543.04	0.39
18	0.3006	O ₂ +4Mn ₃ O ₄ → 6Mn ₂ O ₃	194.97	CH ₄ +12 Mn ₂ O ₃ → CO ₂ +2H ₂ O+8Mn ₃ O ₄	500.36	0.44

The metal oxides are circulating in the system in the form of fine particles, which explains the aforementioned CFB technology as a suitable reactor system. The oxygen carrier is not only formed by a metal oxide or a metal oxide mixture but inert materials must be added to the particles. This is justified by the need of mechanical and thermal stability; particular important in this context is the issue of agglomeration at the relatively high operation temperatures of chemical-looping combustion. Further, the inert phase causes an increase of the porosity and thus, the diffusion rate of reactants and products to and from the interior of the particle. This, in turn leads to an increased overall reaction rate. The inert

material plays the role of an oxide ion conductor to enhance the ion permeability in the solid. The following inert materials have been used for the development of oxygen carriers: YSZ (Yttria Stabilised Zirconia), TiO_2 or Al_2O_3 , and MgO has been suggested by Ishida and co-workers and Adanez and co-workers.

Chalmers University also tested Kaolin with starch added for pore formation in some cases (Cho et al., 2004). Ryu and co-workers (2002a, 2002b, 2003a, 2003b, 2004a, 2004b, 2004c) at the Korean Institute of Energy Research have also analysed the effect of Bentonite and Hexaaluminate addition on NiO as support material. Issues such as carbon and NO_x formation were studied besides reaction kinetics by application of an unreacted core model.

Nakano and co-workers (1986) at the Tokyo Institute of Technology performed experimental work by investing Fe_2O_3 with Al_2O_3 and Fe_2O_3 with Ni as support using a thermogravimetric analyser (TGA). Since then Ishida, Jin and co-workers (Ishida et al, 1996, 1998, 2002; Jin et al, 1998, 2002) have investigated oxides of Fe, Ni and Co with Al_2O_3 , yttria-stabilised zirconia, TiO_2 and MgO as support using TGA mostly with H_2 as fuel. Also some work with fixed bed reactors and in continuous CLC reactors with gas chromatography (GC) has been presented. Operating temperatures up to 1200°C for Fe and Ni based carriers were tested and particle production methods are given.

Hatanaka and co-workers (1997) investigated NiO with methane as fuel. Copeland and co-workers at TDA Research Inc. investigated iron, copper and nickel based oxygen carriers with H_2 and synthesis gas as fuel. The particularity of their SETS (Sorbent Energy Transfer System) system is that the oxide mixture is chosen to set the heat of reaction in the fuel reactor to zero, results in the heat of reaction in the air reactor equal to conventional combustion.

Mattisson and co-workers (Mattisson et al, 2000, 2001c, 2004a; Cho et al, 2002, 2004) at Chalmers University of Technology investigated iron ore, $\text{Fe}_2\text{O}_3/\text{Al}_2\text{O}_3$ and $\text{Fe}_2\text{O}_3/\text{MgO}$ in fixed bed and fluidised bed conditions as well as oxides of nickel, copper, cobalt and manganese supported by alumina with TGA using methane as fuel. Oxygen carriers were produced by freeze granulation or impregnation and sintering at various temperature levels. The sintering temperature was found to be an important factor influencing the reactivity (decreasing with increasing temperature) and the mechanical stability (increasing with increasing temperature). Tests showed high enough reactivity for CLC but Cu particles agglomerated and may not be suitable for CLC although tested at a lower temperature (850°C) compared to Fe, Ni and Mn (950°C). Samples of iron oxide with aluminium oxide support showed signs of agglomeration. Ni oxide shows the highest reduction rate but limited strength. For Mn and Co oxides the extent of reaction was found to be limited by a high degree of spinel formation at all temperatures.

Villa et al. (2003) investigated redox properties of Ni-Al-O and Ni-Mg-Al-O mixed oxides with H_2 and CH_4 reducing agents. Pulse tests as well as repeated oxidation/reduction cycles were carried out. Mg was found to improve regenerability upon repeated redox cycles. Coke formation was found and co-feeding of H_2O along with CH_4 was confirmed as suitable

measure for avoidance. Limitations of the redox materials for practical use are given by the poor selectivity towards deep oxidation products.

Alstom (2003) have performed a detailed study on the feasibility of using CaS as oxygen carrier. Unfortunately, no further details are given but conclusions from a study by Löffler et al. (2003b) show that due to thermodynamic equilibrium in the air reactor small SO₂ concentrations up to 100ppm must be expected.

In the investigations above the reaction rates during oxidation and reduction varied in a wide range depending upon the metal oxide used, as well as reaction parameters. In general, nickel based carriers seem to have the highest reduction reactivity compared to iron. Manganese and copper-based carriers have not been studied to the same extent and frequently cause agglomeration. However, Ni based carriers have the drawback of a thermodynamic limitation and thus, incomplete fuel conversion.

Another issue that is discussed in several studies is the formation of carbon during the fuel oxidation procedure. Ishida and Jin (1997) report that this causes degradation of the physical strength of particles. Water addition to the fuel is recommended to avoid the formation of carbon. Carbon deposition conditions for Ni based carriers were mapped by Ryu (2002) and no formation above 900°C was observed for low concentrations of CH₄ (>95% N₂ balanced).

2.4 System analysis – process integration of CLC

The successful layout of a chemical-looping combustion concept depends upon the optimised integration of technological units such as fuel pre-treatment, combustor, power cycle, CO₂ treatment and sequestration. Research in this field was carried by Wolf et al., (2001, 2005), Anheden et al., (1996, 1998, 2000), Brandvoll et al., (2002a), Bolland et al., (2001), Naquvi et al., (2004) Consonni et al., (2004), Copeland et al., (2000, 2002), Jin and Ishida (1997).

Most studies focus on process integration based on natural gas and an integration of CLC into a combined cycle (NGCC) system. Thereby, the optimum turbine inlet temperature of the gases is either reached by assuming the same temperature level as for the air reactor or by NG fuelled topping burners. Wolf (2001) reports electrical efficiencies of up to 53% for the overall process with a turbine inlet temperature (TIT) of 1200°C. The use of topping burners for a temperature increase from the CLC operating temperature to the TIT causes a reduction of the CO₂ capture efficiency by roughly 50%. The assumption of a TIT of 1000°C and without the use of topping burners reduces the efficiency to about 46 – 48%. Anheden (1996) has carried a study for coal combustion in CLC with an oxygen gasification unit. Results show that a CLC power plant can also be operated at high efficiencies.

Another approach for integration of coal gasification and chemical-looping was made shown by Marion et al., (2004) and similarly by Rizeq et al., (2003). Chemical-looping gasification, as envisioned by those groups, uses two primary chemical loops in the process

to produce both a relatively pure CO₂ stream and a medium calorific gas. The oxygen used in the gasification process is provided by a solid oxygen carrier and a regenerative carbonate cycle is used for CO₂ capture.

A novel path for application of chemical-looping combustion was proposed by Stobbe (1999), Mattisson et al., (2004b), and Wolf et al., (2004), and the concept is referred as chemical-looping reforming. In this process a chemical-looping system as described previously is used for partial oxidation and production of hydrogen rich synthesis gas. However, experimental work with this concept needs to show proof the viability first. Both technologies have a promising potential but are under early stages of development.

3 Thermodynamic aspects of CLC reactor systems

A mathematical model for parameter studies on CLC thermodynamics

As was shown in the previous chapter the choice of the oxygen carrier type depends on a number of aspects. A crucial parameter is the thermodynamic behaviour of the oxygen carrier in reaction with a fuel gas. For a systematic analysis of this issue a mathematical model of a CLC system with an integrated solution of the mass and energy balances was developed (paper Ia/Ib). Evaluation of the effect of numerous design and operating parameters, such as fuel gas composition and reactor cooling arrangement, were carried out for different oxygen carrier types.

3.1 Mass and energy balances

The capacity of a metal to carry oxygen from the air reactor to the fuel reactor is a basic quantity in the design of CLC. In this study it is referred to as the oxygen ratio, R_0 , and denotes the mass fraction of oxygen in the carrier in its fully oxidised state and is given by (3-1):

$$R_0 = \frac{M_{f,ox} - M_{f,red}}{M_{f,ox}} \quad (3-1)$$

where $M_{f,ox}$ and $M_{f,red}$ are the molar masses of the carrier in its fully oxidised and reduced states, respectively. Similarly, the conversion of the oxygen carrier is given by (3-2):

$$X_{OC} = \frac{M_{f,ox} - M_{actual}}{M_{f,ox} - M_{f,red}} \quad (3-2)$$

where M_{actual} is the molar mass of the carrier in its partially oxidised state. The mass flow of the oxygen carrier m_{circ} from the fuel reactor to the air reactor for fuel gas oxidation is given by (3-3):

$$m_{circ} = \frac{m_{O_2}}{\Delta X_{OC} \cdot w_{MeO}} \quad (3-3)$$

m_{O_2} is the mass flow of oxygen required for fuel gas conversion, ΔX the difference of oxygen carrier metal conversion between AR and FR and w_{MeO} is the content of active metal in the oxygen carrier in its fully oxidised state. The requirement for an inactive fraction of the oxygen carrier derives from the need of high mechanical stability and reactivity. The purity of CO_2 can be defined as the molar fraction of CO_2 in the water-free FR exit gas flow (3-4):

$$\eta_{CO_2} = x_{CO_2,FR,exit,dry} \quad (3-4)$$

The conversions of the oxygen carrier and the fuel gas are determined by thermodynamic equilibrium between the metal oxide and the fuel gas components. The simulation can handle CO, H₂, and numerous hydrocarbons up to pentane as well as trace substances like sulphur dioxide (SO₂). For each oxidation reaction *k* of a fuel molecule, e.g. CO to CO₂, the thermodynamic equilibrium constant is defined as shown in equation (3-5).

$$K_{x,k} = \frac{x_{CO_2}}{x_{CO}} = \exp\left(\frac{-\Delta G_{f,k}}{R \cdot T_{FR}}\right) \quad (3-5)$$

The material properties for the calculation of $G_{f,k}$ are taken from Barin (1995) and Burcat (2001).

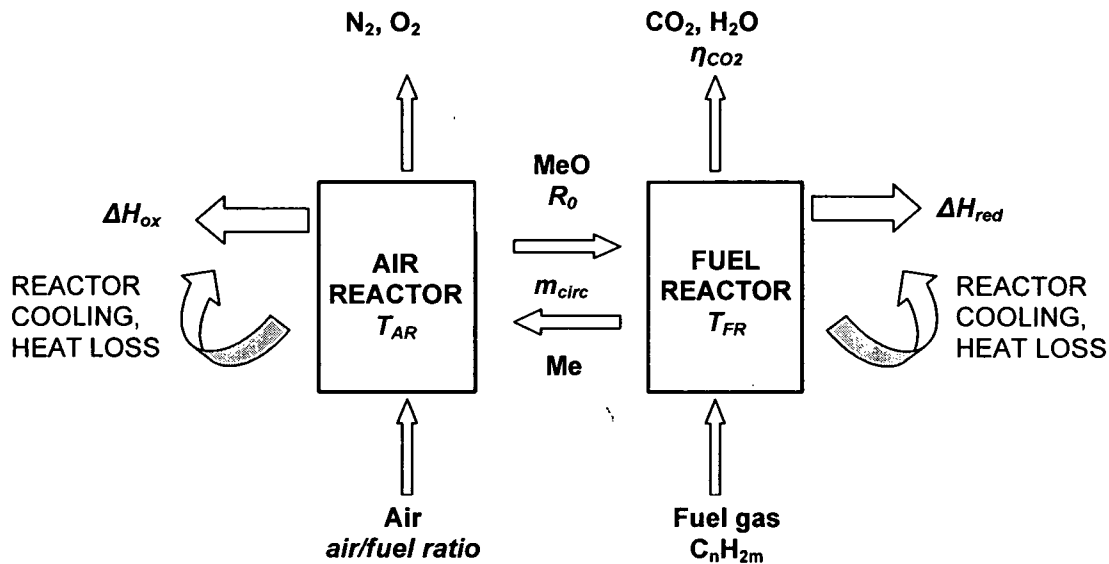


Figure 3-1: Principle of chemical-looping combustion. MeO and Me denote oxidised and reduced oxygen carriers.

From mass and energy balances of the fuel reactor, and the entire CLC system according to, it emerges that the mass flow of the oxygen carrier is decisive for the temperature levels of both reactors. The oxygen carrier coming from the air reactor is at the temperature of the air reactor and transports sensible heat to the fuel reactor. Thus, the mass flow of oxygen carrier in a chemical-looping combustion system is not only determined by the amount of oxygen that needs to be transported (3-3), but also by the heat balance of the entire combustion system. This includes also heat losses of the reactors and reactor cooling corresponding to the heat duty of heat exchangers.

To ensure sufficient rates for the relevant reactions, and to prevent melting of the oxygen carrier the temperature should be about 900°C in both reactors and the temperature difference between the air reactor and the fuel reactor should be less than 50°C approximately.

3.2 Parameter variations

To evaluate the effects of the different design and operating parameters (thermal power, fuel, oxygen carrier type, mass fraction of inert material, solids conversion, air-to-fuel ratio, reactor cooling, reactor heat loss) on the performance of a CLC system, parameter variations were carried out in a wide range. These include thermal power, fuel type, air-to-fuel ratio, and cooling and heat loss of both reactors, and the oxygen carrier type and composition. For the four metals in question the following oxide pairs form the basis for the model: CuO-Cu, Fe₂O₃-Fe₃O₄-FeO-Fe, Mn₂O₃-Mn₃O₄-MnO, NiO-Ni. The gas inlet flows enter the process at 25°C and in Table 3-1 an overview of the conditions investigated is given.

Table 3-1: Overview of parameters investigated. The frames indicate the parameters that specify the standard conditions for CH₄ and CO/H₂

Parameter					1	1
Thermal Power	[kW]				CH ₄	CO/H ₂
Fuel	[-]				Ni	Mn
Oxygen Carrier	[-]	Fe	Cu			
Solids conversion	[%]				0-100	0-100
Cooling	[%]				50	60
Mass fraction of act. material	[w-%]	100	80	60	40	20
Inert material	[-]				SiO ₂	
Air-to-fuel ratio	[-]				1.2	
Heat loss	[%]				0	

3.3 Results and discussion

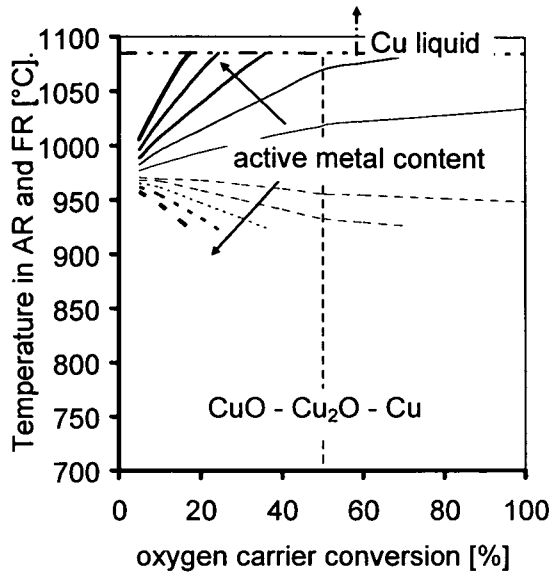
Additional cooling and heat losses at each reactor can be chosen as these determine the temperature level of the system as they affect the amount of energy extracted from the system. The cooling is assumed to be performed for all test runs in the air reactor, where the more exothermic reaction usually takes place. As there is no difference in the effect of cooling and heat losses, respectively, the heat losses are assumed to be zero. For the air fuel ratio a value of 1.2 is assumed, which constitutes a conventional value for combustion processes.

3.3.1 Variation of solids conversion and active metal content

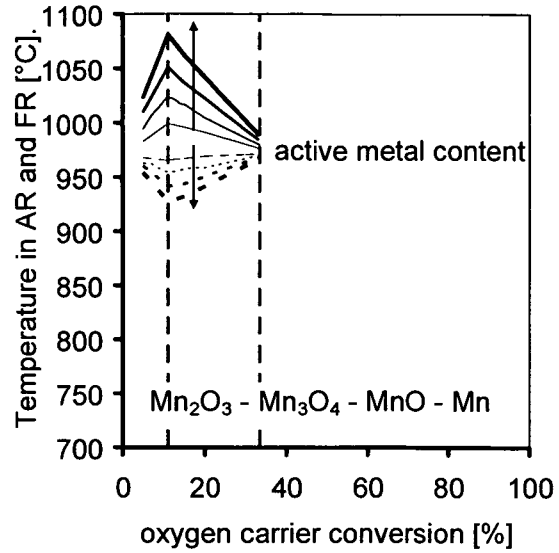
Natural gas as fuel for CLC

Figure 3-2 presents the temperatures in both reactors versus the solids conversion for different active material mass fraction for natural gas (100% CH₄ as model fuel) assumed.

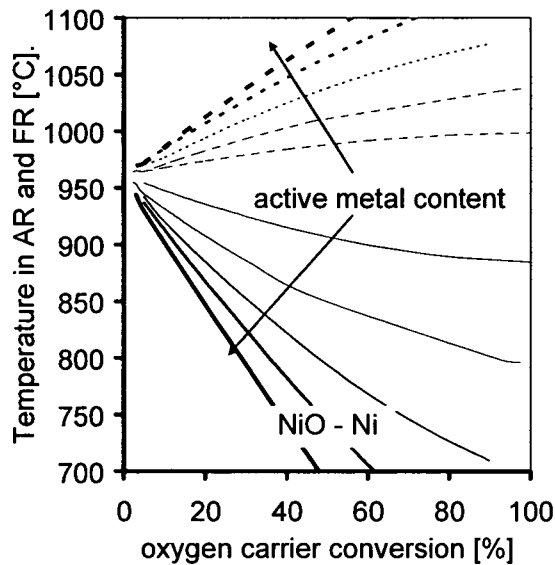
(a) Cu



(b) Mn



(c) Ni



(d) Fe

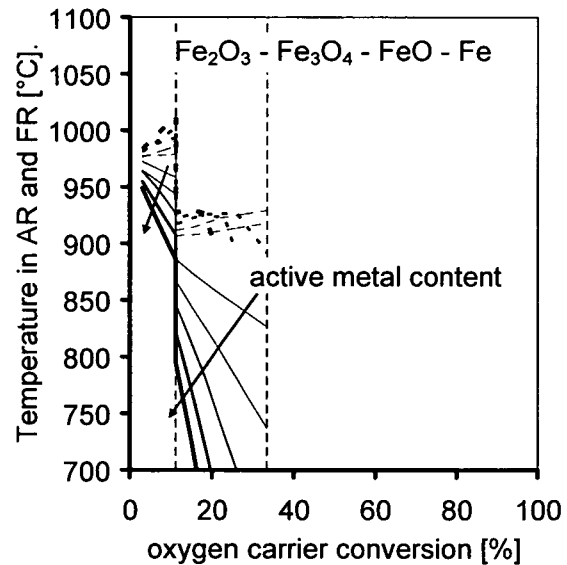


Figure 3-2: Temperatures [°C] of the AR (dotted line) and FR (solid line) vs. oxygen carrier conversion for different active material mass fractions.

Fuel: CH₄, act. material: (a) Cu, (b) Mn, (c) Ni, (d) Fe, act. material content 20, 40, 60, 80, 100%, inactive material: SiO₂, AR cooling: 50 % of thermal power, air-to-fuel ratio 1.2.

It can be seen that for all four active metals the temperature difference between the two reactors is very small in the cases of low solids conversions, which is equivalent to high solids circulation rates. Also, in the cases of Cu and Mn, the fuel reactor is always at a higher temperature than the air reactor. This is due to the differences in the heat tone of the active metals reacting with CH₄: The reduction of Cu to CuO and Mn₃O₄ to Mn₂O₃ with methane are exothermic reactions in the FR, whereas all Ni and Fe reductions are endothermic. Although

reduction from Mn_3O_4 to MnO is endothermic the fuel reactor temperature still remains above the air reactor for oxygen conversions for Mn higher than 11.1% because the heat of reaction of the next higher oxide pair is prevailing.

It must be kept in mind that these results are produced assuming a certain cooling in the air reactor. Although the tendency cannot be changed, a strong influence of cooling of the two reactors on the temperature distribution between the reactors is obvious.

For higher oxygen carrier mass flows the situation is very different for the four metals. Copper shows an increase of the temperature in the air reactor with increasing solids conversion and active metal content. Both aspects can be explained by the lower mass flows between the reactors, which increases the difference in the temperature levels. The limitation for high mass fraction of active metal in the oxygen carrier is given by reaching the melting point of Cu.

Mn shows a distinct change in the effects at a conversion of about 11%, which is caused by the change in the oxidation state from Mn_3O_4 to MnO , and causes the temperatures in the reactors to approach. Conversions higher than 33.3% (the change of MnO to Mn) cannot arise as under present conditions MnO cannot be reduced. On the other hand, a further reduction of the oxygen mass flow can be forced on the system, leading to incomplete combustion of the fuel gas. This, in turn leads to a drastic reduction of the reactor temperatures, due to the assumption of a constant cooling based on the thermal power of the fuel at the inlet.

Nickel shows, from a comparison of the temperatures in the reactors, a rather similar behaviour to Cu. However, the main difference is that melting and decomposition temperatures are much higher, which results in different options of implementing a Ni CLC-unit into a power plant concept.

Fe, like Mn, can form three different oxidation states and the limits also are at 11.1% and 33.3% solids conversion. For high active metal contents the reactions are stopped due to low temperatures in the FR, which do not allow a sufficient fuel conversion. A strong decrease of the temperature in particular in the AR occurs at conversions higher than 11.1vol-%, whereas at lower conversions smaller deviations can be observed. At solids conversions above 11.1% FeO in the fuel reactor reduced CO_2 -purity results (as shown in Figure 3-6). No oxygen carrier conversion higher than 33.3% can be realised, as also FeO cannot be reduced at the gas concentrations necessary to maintain the temperature in the fuel reactor.

The simulation model allows, as part of the investigation of the temperatures, the study of gas outlet concentrations. In Figure 3-3, the concentrations of CO and H_2 are plotted, for the same abovementioned conditions, i.e. equal temperatures versus the solids material conversion for Fe and Ni.

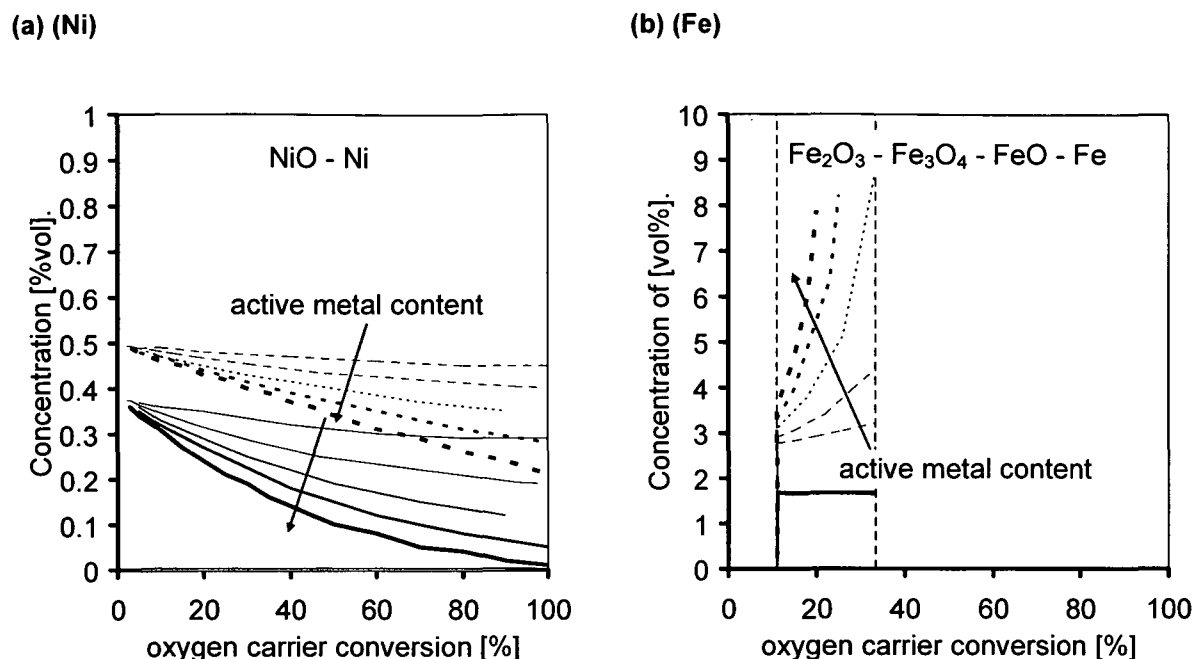


Figure 3-3: Concentrations [vol-%] of H₂ (dotted line) and CO (solid line) vs. oxygen carrier conversion for different mass fraction of active material.

Fuel: CH₄, act. material: (a) Ni, (b) Fe, act. material content 20, 40, 60, 80, 100%, inactive material: SiO₂, cooling: 60 % of thermal power, air/fuel ratio 1.2.

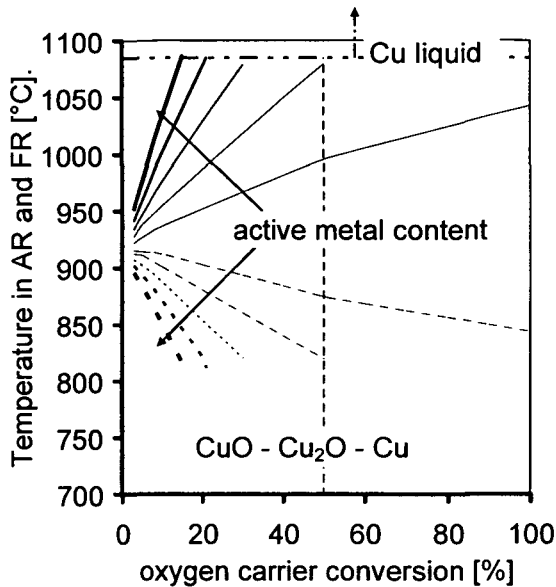
Complete CO₂-purity in the FR exit gas flow (dry basis) exists for both Mn and Cu. As can be seen in Figure 3-3 (a) for Ni as active material incomplete conversion occurs in the entire range of the solids conversion, although no CH₄ remains. Due to the endothermic heat tone of H₂ and CO, their conversion increases with decreasing temperature in the fuel reactor causing an increase of the oxygen carrier conversion (as shown in Figure 3-5). The concentrations of unconverted species are decreasing from about 0.5vol-% at low oxygen carrier conversions to very low values at high oxygen carrier conversions. In literature experimental work on carbon deposition in the case of Ni-based oxygen carrier particles (Ryu et al., 2002) shows the formation of carbon at temperatures below about 900°C. However, as in this system high gas conversion is desired, carbon formation can only occur close to the inlet of the fuel, where the CO partial pressure is high. This carbon would be gasified by CO₂ or H₂O again in regions of higher gas conversion. It is concluded that carbon formation is not relevant for this work.

Methane is converted entirely in the case of Fe as the active metal up to 11.1%. Above the state change from Fe₃O₄ to FeO incomplete conversion occurs. While the concentration of CO is equal for all active metal contents 1.7vol-%, the hydrogen concentration shows a strong increase at higher active metal contents as well as conversions. This gives a clear explanation for the significant temperature drop of both reactors in this region as incomplete fuel conversion also reduces the heat released in the process, whereby the volume flows remain almost constant. Thus, a higher proportion of the heat is withdrawn by the exit gas flows and the cooling in the air reactor.

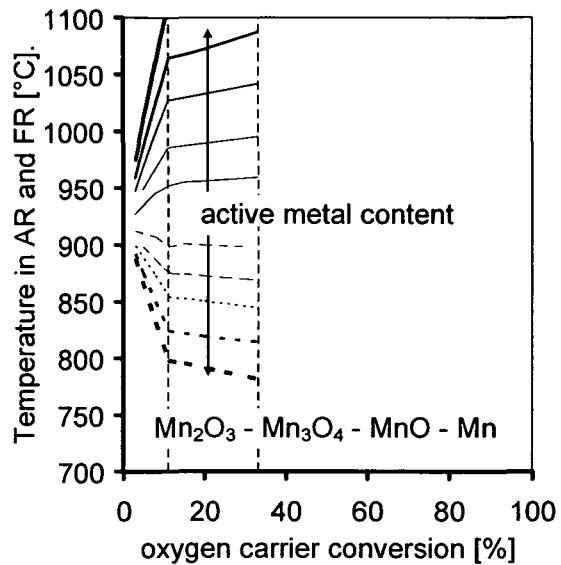
Coal synthesis gas as fuel for CLC

An analysis was also carried out for a coal gasification synthesis gas as second likely fuel gas for CLC, presented in Figure 3-4 and Figure 3-5. For simplicity reasons a mixture of 50vol-%CO and 50vol-%H₂ was used.

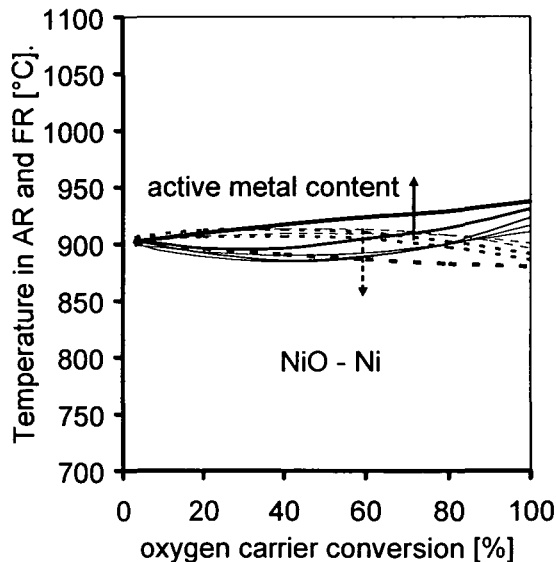
(a) Cu



(d) Mn



(c) Ni



(d) Fe

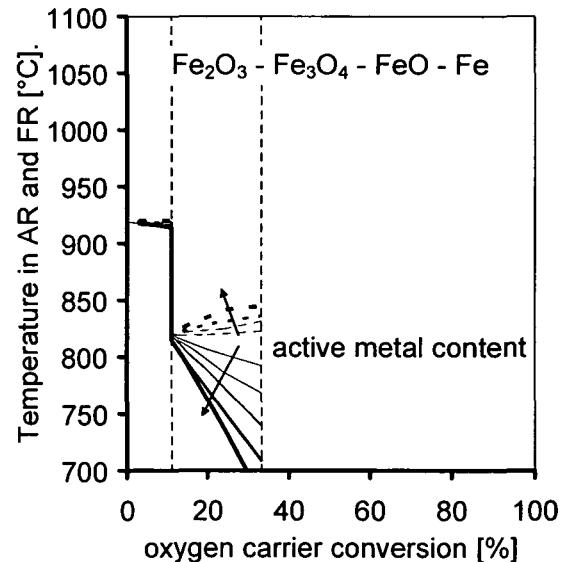


Figure 3-4: Temperatures [°C] of the air reactor (dotted line) and fuel reactor (solid line) vs. oxygen carrier conversion for different mass fraction of active material.

Fuel: CO/H₂, act. material: (a) Fe, (b) Cu, (c) Ni, and (d) Mn, act. material content 20, 40, 60, 80, 100%, inactive material: SiO₂, cooling: 60 % of thermal power, air-to-fuel ratio 1.2.

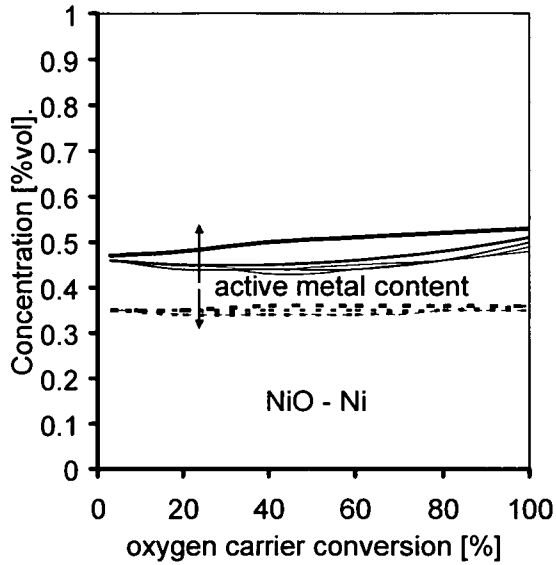
The results of these test runs are based on a cooling rate of 60% in the AR. To maintain a similar temperature level in the reactors a higher cooling rate than for CH₄ is required as consequence of the lower flue gas flows.

Whereas for copper no significant difference appears, a change at conversion higher than 11.1% is observed for Mn. Further increasing the temperature in the fuel reactor, in turn, causes a lower air reactor temperature. Again, the temperature differences are higher for increased active metal material contents of the oxygen carrier as this results in lower solids circulation rates and also lower heat transfer between the two reactors for the given oxygen carrier conversion (3-4).

Nickel also shows a completely different behaviour, and at conversions lower than about 40 to 50% the temperature in the air reactor decreases with increasing conversion. This tendency changes at high values for the solids conversion and a comparison with Figure 3-5 (a) shows that this is not influenced by the amount of unconverted fuel gas. For the current conditions this was found to be almost constant over the entire range of the conversion.

In the case of Fe as the active material for the combustion of CO and H₂, both temperatures are almost equal up to the boundary of Fe₃O₄ and FeO. At this point (11.1% conversion) a drop of the reactor temperatures of about 100°C occurs, which goes along with a stepwise increase of CO and H₂ concentrations to values of about 2.5vol-%. At lower circulation rates, i.e. higher conversions, the AR temperature increases as well as the hydrogen concentration and the FR temperature drops.

a) (Ni)



b) (Fe)

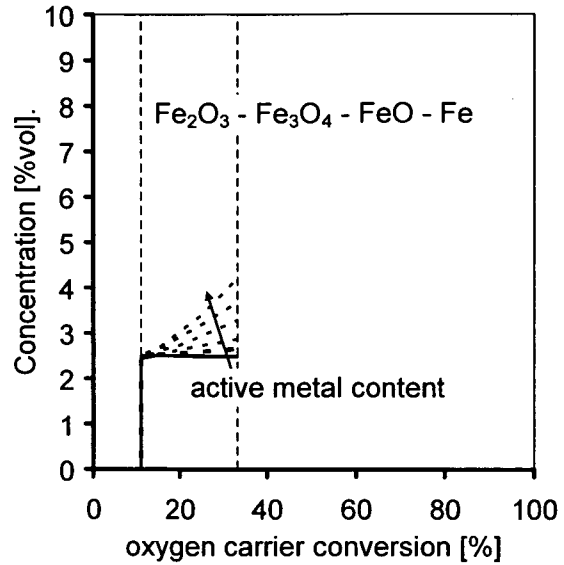


Figure 3-5: Concentrations [vol-%] of H₂ (dotted line) and CO (solid line) vs. solids conversion for different mass fraction of active material.

Fuel: CO/H₂, act. material: (a) Ni, (b) Fe, act. material content 20-100%, inactive material: SiO₂, cooling: 60 % of thermal power, air-to-fuel ratio 1.2.

3.3.2 Comparison of oxygen carrier types for base case

As discussed above, the conversion and the fraction of active material determines the necessary solids circulation rate. In Figure 3-6, the temperature difference between the two reactors is shown versus the specific solids circulation rate for both model fuels. Additionally, the purity of CO₂ in the FR exit gas flow (dry basis) is plotted in separate charts.

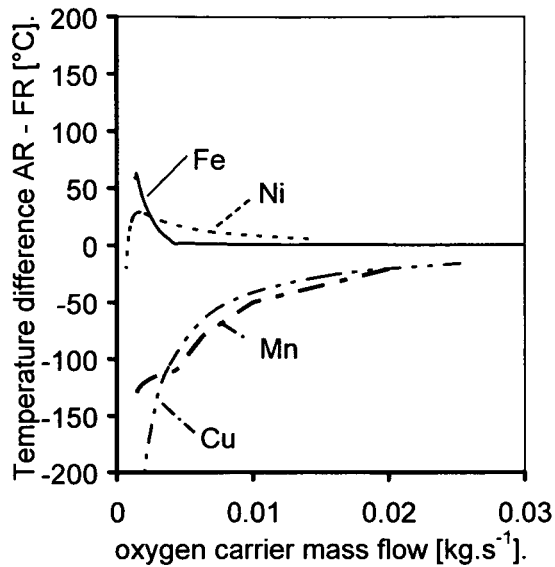
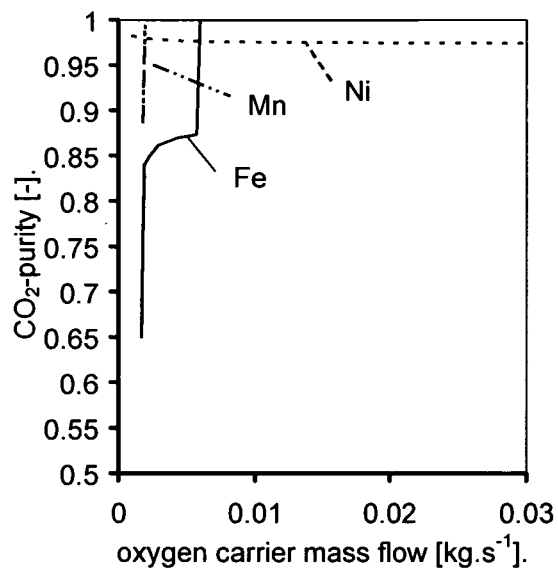
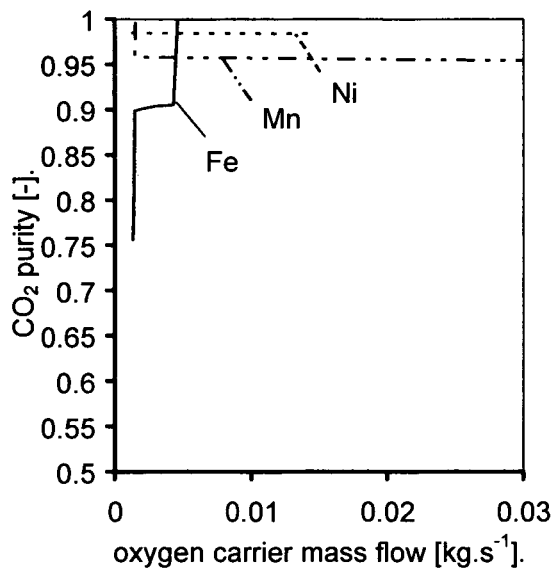
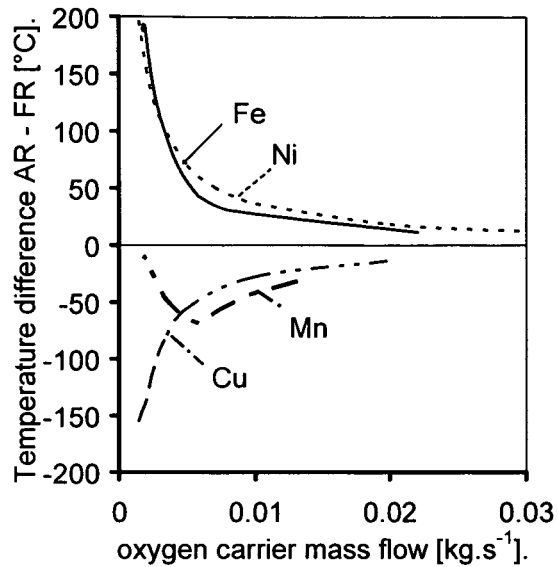
(a) CO/H₂(b) CH₄

Figure 3-6: Comparison of temperature difference between AR and FR and fuel gas conversion for base cases for CO/H₂ (a) and CH₄ (b).

In the case of CO/H₂ as fuel gas at the given conditions (cooling of 60% in the AR) Cu and Ni cause a larger temperature difference than Fe and Mn. For the latter two a specific solids flow of about 0.002kg s⁻¹ kW⁻¹ is sufficient to maintain a temperature difference lower than 50°C, whereas for Cu and Ni about 0.008kg s⁻¹ kW⁻¹ is required for the same limitation. The CO₂-purity as the second characteristic determining the choice of an appropriate solids mass flow, shows that for Cu full gas conversion is always achieved and for Mn for mass flows above 0.002kg s⁻¹ kW⁻¹. Ni has a constant CO₂-purity of about 98%. For Fe, however, circulation rates lower than 0.005kg s⁻¹ kW⁻¹ cause a dilution of the CO₂ - H₂O mixture to about 90% purity.

If CH_4 is used as the fuel gas a situation arises where all four metals require a mass flow of about $0.005\text{kg}\cdot\text{s}^{-1}\cdot\text{kW}^{-1}$ for a temperature difference of less than 50°C . Only Mn has very similar temperatures in the AR and FR at low oxygen carrier mass flows. Again, Ni causes some unconverted CO and H_2 to be in the flue gas and Fe has incomplete conversion for mass flows lower than about $0.005\text{kg}\cdot\text{s}^{-1}\cdot\text{kW}^{-1}$.

3.3.3 Conclusions

The presented mathematical model of the mass and energy balances of a chemical-looping combustion system constitutes a suitable tool to support the selection of oxygen carrier types for the process. From the analysis, it follows that for all four metal oxides and for reasonable small temperature differences a specific oxygen carrier mass flow of about $0.005\text{kg}\cdot\text{s}^{-1}\cdot\text{kW}^{-1}$ is sufficient. At this value full fuel gas conversion, equivalent to 100% CO_2 purity after H_2O is removed from the FR exit gas flow, can be expected for all active metal types except Ni, which always produces unconverted CO and H_2 in the range of about 0.5vol-% in the flue gas.

For many parameter variations, limitations in operating conditions for the use of certain types of active metal have been identified, caused either by the attainment of the melting or decomposition point or by the thermodynamic equilibrium.

The model allows the identification of possible operating ranges in terms of temperature levels of the reactors in conjunction with purity of the CO_2 , which is used as measure for the energy need for further CO_2 sequestration. Both of these aspects are crucial to the implementation of chemical-looping combustion into a large-scale power plant concept and it shows that considerable differences appear for the demand of a CLC system.

In order to optimise chemical-looping combustion for efficient power production the system integration and the metal oxide type must be matched. If this is considered, CLC can constitute a viable solution for CO_2 sequestration during the combustion of fossil fuels.

4 Fluid dynamics of CLC reactor systems

4.1 Technical background on CLC -CFB systems

Due to the heterogeneous nature of the reaction and the required solids transport between the fuel reactor and the air reactor in CLC units, a circulating fluidised bed (CFB) concept is the preferred reactor type. Dual fluidised beds are used in a multitude of processes where good contact between solids and gas and/or heat transfer between reaction zones are required, such as biomass pyrolysis (Haslinger et al. 1999) and gasification (Hofbauer, 1995). Additionally, such a system can guarantee the consideration of the following criteria that are also crucial for reliable operation of a CLC unit:

- high solids material circulation between the two reactors for fulfilling process requirements
- sufficient particle inventory in each reactor for high conversion of solids or gas
- minimum gas mixing between reaction zones

The proposed dual fluidised-bed concept is built up by a riser acting as the air reactor and a stationary fluidised bed reactor as the fuel reactor. Gas mixing between the reactors is minimised by installation of loop seals and most designs use a cyclone for solid separation of the air reactor exit flow. The design of such a CFB concept is shown in Figure 4-1.

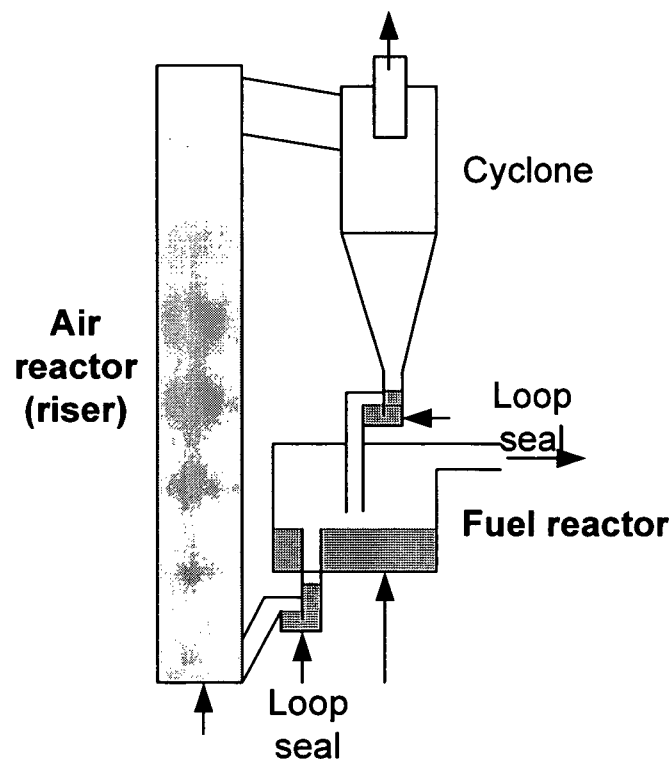


Figure 4-1: CFB reactor concept for CLC.

In this work a total number of four flow models was analysed experimentally, whereby differences are mainly in scale and the type of fuel gas. Further, differences exist in the objectives of the modelling. Some models were built mainly to form a design basis for "hot" laboratory CLC units and others predominately for securing scale-up to the next development step of CLC; design variations form a third category. It is therefore evident that the design requirements are somewhat different for all units.

Generally, for the design of a CLC reactor it is necessary to gain understanding of the fluid dynamics. Influences of operating factors and limitations of the unit are to be examined and are key for successful designing. Results also form the basis for material and energy balances as presented in chapter 3. Special aspects of interest of this study are effects of design particularities and operating parameters in view of reaction engineering aspects that are critical for chemical-looping combustion performance. This comprises the reactor geometry and solids mass-flux on solids (mean) residence time, solids residence time distribution in reactors on the gas-solid contacting, and gas leakage on the separation principle of the two exit gas flows.

4.2 Methodologies

4.2.1 Flow modelling

For the fluid dynamic analysis of fluidised beds that operate at a high temperature and/or a high pressure the use of flow models working at ambient conditions has been found advantageous. Easy handling, minimal requirements on experimental equipment and control techniques and the possibility for visual observation of macroscopic flow structures make flow models be a cheap, comfortable and reliable source of necessary and important fluid dynamic data for scale-up purposes. These are the pressure profiles of riser sections, the solids circulation rate, gas leakage, and residence time distribution of the reactors. An important issue on the use of flow models is the comparability of results and conclusions for the original unit. Numerous authors have worked on developing scaling criteria and a discussion on this is presented in this section.

Fluid dynamic scaling relationships for fluidised beds

Scale-up of reactors is amongst the most important procedures for the development of industrial processes. Apart of heat and mass transfer, and chemical reaction the fluid dynamics are of particular importance for fluidized bed scaling. Objective of research in this area is the derivation of scaling laws that allow an easy correlation of data at small and large-scale units. Also, reliable scaling laws allow the analysis of fluid dynamics in flow models and drawing conclusions for reactors operating at high temperature and/or pressure.

Several attempts exist in literature on developing scaling relationships (Horio et al, 1986, Zhang and Yang, 1987, Foscolo et al, 1990, Chan and Louge, 1992). Glicksman and his co-workers, however, developed scaling laws that are widely used and proofed reliability. For the design of the flow models reported in this thesis also Glicksman's scaling criteria were applied.

Based on governing equation for the gas and solids motion in a fluidized bed, the governing dimensionless parameters are derived by non-dimensionalising the equations. The complete set of dimensionless parameters can be written as (Glicksman, 1984):

$$\frac{u^2}{g \cdot L}, \frac{\rho_p}{\rho_f}, \frac{\rho_p \cdot u \cdot d_p}{\eta^2}, \frac{\rho_f \cdot u \cdot L}{\eta}, \frac{G_s}{\rho_p \cdot u}, \text{bed_geometry}, \Phi, PSD \quad (4-1)$$

Equation (4-1) can be rewritten in an alternate form when Froude number, Reynolds number, and the Archimedes number are combined as follows:

$$\frac{\rho_f \cdot \rho_p \cdot d_p^3 \cdot g}{\eta^2}, \frac{\rho_p}{\rho_f}, \frac{u^2}{g \cdot L}, \frac{L}{d_p}, \frac{D}{d_p}, \Phi, PSD, \text{bed_geometry} \quad (4-2)$$

$$\text{with the particle Reynolds number } Re_p = \frac{\rho_f \cdot u \cdot d_p}{\eta} \quad (4-3)$$

Equation(4-2) is the most general case and it drastically limits the degrees of freedom for designing scale models as all fluid and solids parameters must be matched simultaneously. For this reason for certain Reynolds number this set can be reduced. For Re_p below 4 (viscous limit) the following dimensionless numbers should be kept constant:

$$\frac{g \cdot d_p}{u^2}, \frac{\eta}{\rho_p \cdot u \cdot d_p}, \frac{L}{d_p}, \frac{D}{d_p}, \Phi, PSD, \text{bed_geometry} \quad (4-4)$$

In this case the density ratio needs not to be considered and the choice for the fluidisation gas in the flow model is only limited by the viscosity.

In case the Re_p is higher 400 (inertial limit) the fluid viscosity is unimportant to the bed dynamics. The governing parameters are:

$$\frac{g \cdot d_p}{u}, \frac{\rho_f}{\rho_p}, \frac{L}{d_p}, \frac{D}{d_p}, \Phi, PSD, \text{bed_geometry} \quad (4-5)$$

Glicksman et al (1993) proposed a simplified form of the scaling relationships. It was shown that these relationships should be exact at the limit of high and low particle Reynolds numbers. These relationships allow more flexibility in the bed width so that a laboratory model can simulate a larger prototype. The simplified set of scaling parameters is as follows:

$$\frac{u^2}{g \cdot L}, \frac{\rho_p}{\rho_f}, \frac{u}{u_{mf}}, \frac{G_s}{\rho_s \cdot u}, \text{bed_geometry}, \Phi, PSD \quad (4-6)$$

4.2.2 Experimental techniques

All in- and outgoing gas flows of the cold flow models were measured using mass flow controllers (Type MKS flows 5-200l_N/min (basis nitrogen) and commercial diaphragm gas meters (Type Elster BK). For very low gas flows and for calibration purposes a gas bubble meter was also utilised. A total number of up to 20 pressure transducers, type Honeywell, Micro Switch were used.

The solids circulation rate was determined by a short interruption of the fluidisation of the lower particle lock. Repeated measurements of the time necessary to fill a dedicated volume in the downcomer were used to determine the solids flux. Total measurement error was found to be below ± 6 per cent with deviations attributed to variations of the bulk behaviour due to electrostatic charges caused by changing air humidity. The test methodology itself, instead, proved to have a very high accuracy.

For the unit described in chapter 4.2.4 a very simple tracer technique was developed for determining the solids circulation rate. As the bed material is of white colour, a very fine black powder (ground coal dust) was used to mark the top surface of a moving particle column in the downcomer section. The time for the tracer "point" to move a certain distance was measured, giving the velocity of the particle column. Because the bulk density is known, the solids circulation rate can be determined.

Second measurement method used for determination of the solids flow behaviour for small CFBs was as follows: A small ball was introduced in the downcomer, which was taken along by the moving solids column. The movement of a thin thread connected to the ball indicated the velocity of the moving solids column and therefore also the mass flow. This method was used to validate the previous methodology as the type for flow behaviour in the column (mass or core flow) would lead to different results for both methods. Similar results were found and average values of both methods of a minimum of five measurements were used.

The residence time distribution tests in fluidised bed reactors were carried out by adaptation of the tracer measurement technique of Rhodes et al. (1991). A pulse function of sodium chloride was injected into the solids flow and bed material samples were taken at the downcomer of the fuel reactor particle overflow at given time intervals. The concentration of the solids sample is determined by a conductivity method and the RTD distribution function is derived by standard methods.

For gas leakage measurements a tracer gas method was applied. The tracer gas (propane, and in some cases oxygen, if the fluidisation gas used was not ambient air) was added to the inlet fluidisation gas flows and the concentration of propane was measured with a flame ionisation detector in the in- and outgoing gas flows. By solving the mass balances of this over-determined set of equations the gas leakage flows could be determined.

Gas leakage values are defined as follows: absolute gas leakage flow into the reactor divided by the (inlet) fluidisation gas flow of the concerned reactor. In the context of CLC,

however, a gas stream of special interest is the fuel reactor outlet flow, i.e. the CO₂/H₂O mixture, because a too large dilution of the CO₂ produced could give technical problems. If not stated explicitly, this definition is used as basis for the data representation.

For the operation of the prototype it is important to keep the loss of solids very low. The performance of the particle separators was determined by fractional separation efficiency.

4.2.3 Mathematical modelling

Different approaches can be found for mathematical modeling of detailed analysis of CFB reactors and CFB pressure loops and Pugsley et al., 1996 and Löffler et al. 2004 have classified the CFB reactor models into three types: prediction of i) axial solids suspension density only, often based on experimental data, ii) axial and radial variations by assuming two or more regions (e.g. core-annulus flow structure) and, iii) dynamics of the two-phase gas-solid flow by employment of the fundamental equations of fluids.

In this study (chapter 5) for the CFB riser a type ii) model is applied because, as mentioned by Pugsley et al. (1996), these are best suited as design tools and they can easily be coupled with reaction kinetics to study the performance of the reactor. For other CFB loop components (fluidised bed orifices, loop seals, gas-solids separator, stationary fluidised beds etc) type i) models were chosen.

The mathematical models of this study can be used for detailed analysis and thus comprehension of the fluidised bed systems but also represent an excellent tool for data and know-how repository. Models support design and scale-up of specific designs and design variations but results on solids distribution and residence time behaviour also form the basis for kinetic reactor modelling.

4.2.4 Overview of investigated CLC designs and scales

Throughout the work of this thesis four different CFB concepts were designed, manufactured, and analysed by mathematical and flow modelling. An overview is given in Table 4-2 and it can be seen that the main difference is in the scale of the unit, which follows the corresponding research stage. For each unit a specific assignment existed prior to the design start and manufacture. A detailed description of the design procedure for all CLC units is given in Kronberger et al., (2005b) and GRACE and CCC technical project reports.

Table 4-1: Overview of flow models (scale and purpose)

Flow model #	Scale of reactor system	Assignment	Particular design criteria
1	Laboratory scale (100-300W)	Small unit for particle testing	Placed in an oven. No heat balance needs to be considered
2	Bench scale (5-10kW)	Prototype operation	Safety margin for allowing a variation of particles and gas and for securing continuous operation
3	Bench scale	Conceptual study of an alternative solids return concept	
4	Pilot (demonstration) scale (2MWth)	Demonstration of CFB concept as used in large scale CLC	"Close to real life" approach including special features like solid splitters and secondary air injection

4.3 Laboratory scale unit

From previous research a need arose to study different oxygen carrier particles in a continuous mode. The purpose of this work is therefore to develop a small CLC laboratory reactor to be used for i) the study of the process, and ii) testing of different oxygen carriers. The unit is characterised by a simple possible design of circulating fluidised beds, having a small bed inventory, which reduces the drawback of high production expenditure for the oxygen carrier materials.

4.3.1 Reactor concept and design of the flow model

The design chosen for this CLC system is a two-compartment fluidised bed having a thermal power range of 100 – 300W_{th} for the original reactor. This design type was first proposed by Chong et al., (1986) and He et al., (1993) to be used as an oil shale retort. A further application was presented later by Fang et al., (2003) for producing a middle heating values synthesis gas by coal gasification. A sketch of the two-compartment fluidised bed is shown in Figure 4-2.

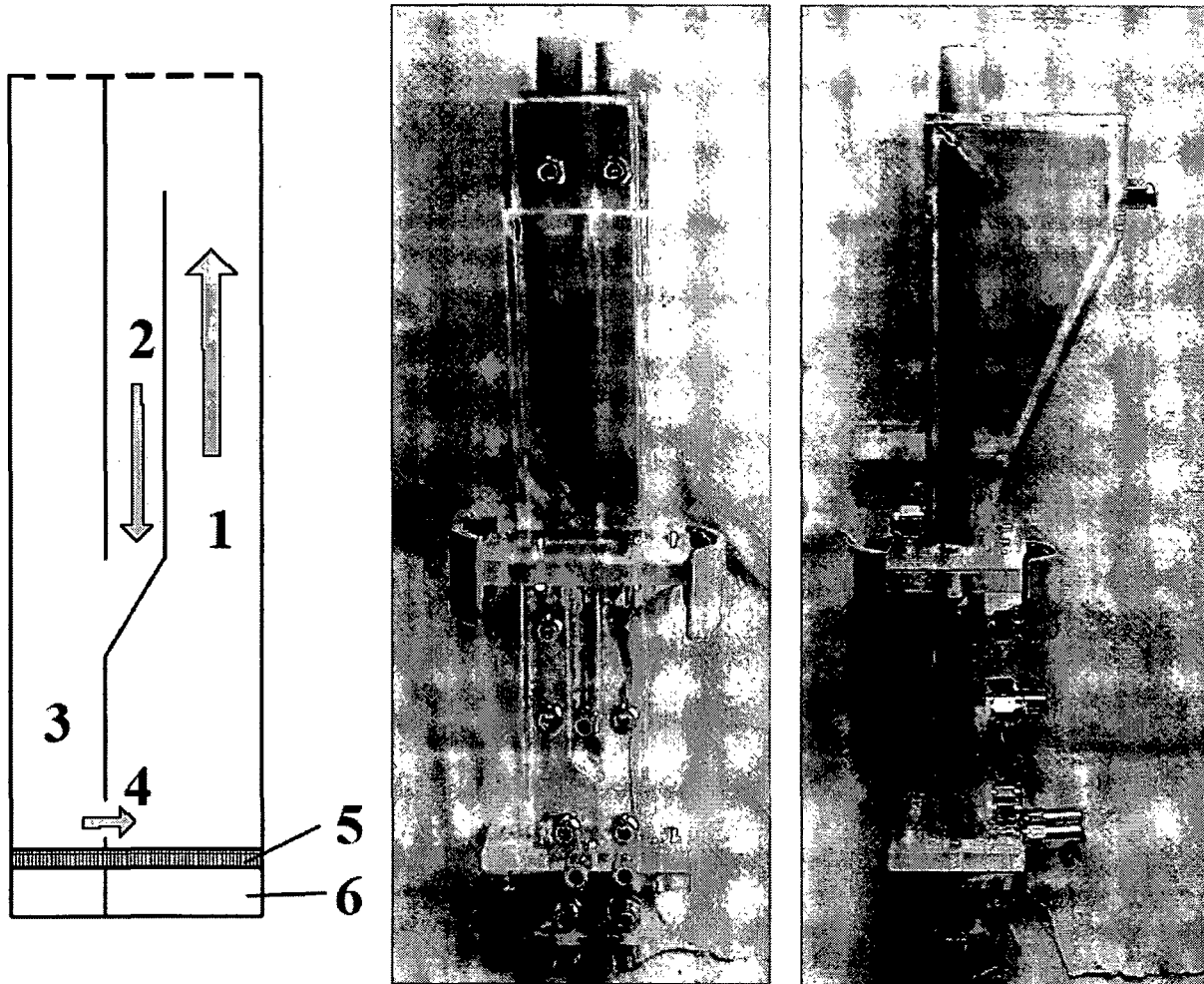


Figure 4-2: Two-compartment fluidised bed. 1) air reactor, 2) downcomer, 3) fuel reactor, 4) slot, 5) gas distributor, 6) wind boxes (not shown in the scheme).

The reactor consists of two adjacent fluidised beds divided by a vertical wall with two orifices. At one side the air reactor, (1), has a higher velocity causing particles to be thrown upwards, and some of them fall into a downcomer, (2), that has a bottom opening leading to the fuel reactor, (3). There is a slot, (4), in the bottom of the wall between the two reactors, and the particles move through this slot from the fuel reactor to the air reactor. The driving force for the solids circulation is the gas velocity in the air reactor throwing particles upwards. A part of these particles falls down in the downcomer and creates a particle column. This produces a pressure drop, which in turn results in a higher pressure in the fuel reactor and presses particles back into the air reactor via the slot. Not shown in the schematic figure are the solid/gas separators at the top of each reactor, which are designed as gravity settling chamber type by enlargement of the cross section of the fluidised bed reactor freeboard.

As fuel gas for the reactor a model fuel of 50/50vol% H_2 and CO is assumed, representing synthesis gas of coal gasification. The standard bed material particles are defined by a particle density of $2300 \text{ kg} \cdot \text{m}^{-3}$ and mean particle diameter of $95 \mu\text{m}$. Application of the scaling laws of Glicksman (1984) shows that a scaling factor of 0.75 is to be used for length, and for the fluidisation gas a gas mixture of, for example, helium/nitrogen is required. To simulate this, a suitable particle for the flow model is powder used for fluid catalytic

cracking (FCC), with a particle density of $1500 \text{ kg}\cdot\text{m}^{-3}$ and a mean particle diameter of $70 \text{ }\mu\text{m}$. In order to investigate the hydrodynamics of the system for alternative particle properties glass beads (GB) with a mean diameter of $68 \text{ }\mu\text{m}$ and a particle density of $2500 \text{ kg}\cdot\text{m}^{-3}$ were also used.

The dimensions of the system are very small and for this reason surface effects may not be negligible. The scaling rules are based on similarity in hydrodynamics and effects between particles and walls are neglected. This should be kept in mind when the results are transferred between the flow model and the hot unit, but might not be crucial. The difference in size between the flow model and the hot laboratory unit is quite small, although the hot unit is somewhat bigger than the flow model. Therefore the wall effects may be less significant in the hot unit in favour of the particle recirculation rate.

4.3.2 Experimental procedure and design variations

The flow model had some fixed dimensions and some that could be varied slightly. The cross-sections of the fuel reactor and the air reactor (in the bottom) are constant. The AR top section next to the downcomer was smaller with the width of either 15 or 17 mm, depending on the variable downcomer width. Further, the height from the bottom plate to the slot was 4 mm, the height from the bottom plate to the downcomer exit 38 mm, and the total height of the downcomer, including the sloped part, was 85 mm. The height of the slot between the reactors was varied between 1.2 and 8 mm. The profile of the wall beneath the slot was altered from the shape of an "I" to a "T" by adding a horizontal plate beneath the slot. The width of the downcomer was also altered between 9 and 11 mm. The different designs and the main dimensions are presented in Table 4-2.

Table 4-2: Design variations and main dimensions

design	FR dimension	AR dimension (bottom)	downcomer width	slot height	slot profile
	[mm]	[mm]	[mm]	[mm]	
A	19 x 19	19 x 27	9	8	I
B	19 x 19	19 x 27	9	4.5	I
C	19 x 19	19 x 27	11	1.5	I
D	19 x 19	19 x 27	11	1.2	T

The flow model was with total solids inventories of 40 to 70 g. The gas volume flow in the air reactor varied from 5 to $7 \text{ l}\cdot\text{min}^{-1}$. This gives a velocity in the narrow part of the riser of 0.26 to $0.36 \text{ m}\cdot\text{s}^{-1}$ for designs A and B, and a velocity of 0.29 to $0.41 \text{ m}\cdot\text{s}^{-1}$ for designs C and D. The reason for the different gas velocities is due to the change in downcomer width, causing a change in the riser cross-sectional area. The gas flow in the fuel reactor was varied between 1.1 and $3 \text{ l}\cdot\text{min}^{-1}$ giving the velocities of 0.05 to $0.14 \text{ m}\cdot\text{s}^{-1}$, corresponding to a power of 100 to 300 W in the hot unit. In addition to variations of the slot design and gas velocities the additional fluidisation of the downcomer was tested.

4.3.3 Results and discussion

Pressure loop

In Figure 4-3 a typical pressure profile of the unit are presented, whereby measured values are complemented with theoretical correlations as presented later in this section. The pressure values are pressure differences to atmosphere and data were recorded for design C and for FCC bed material.

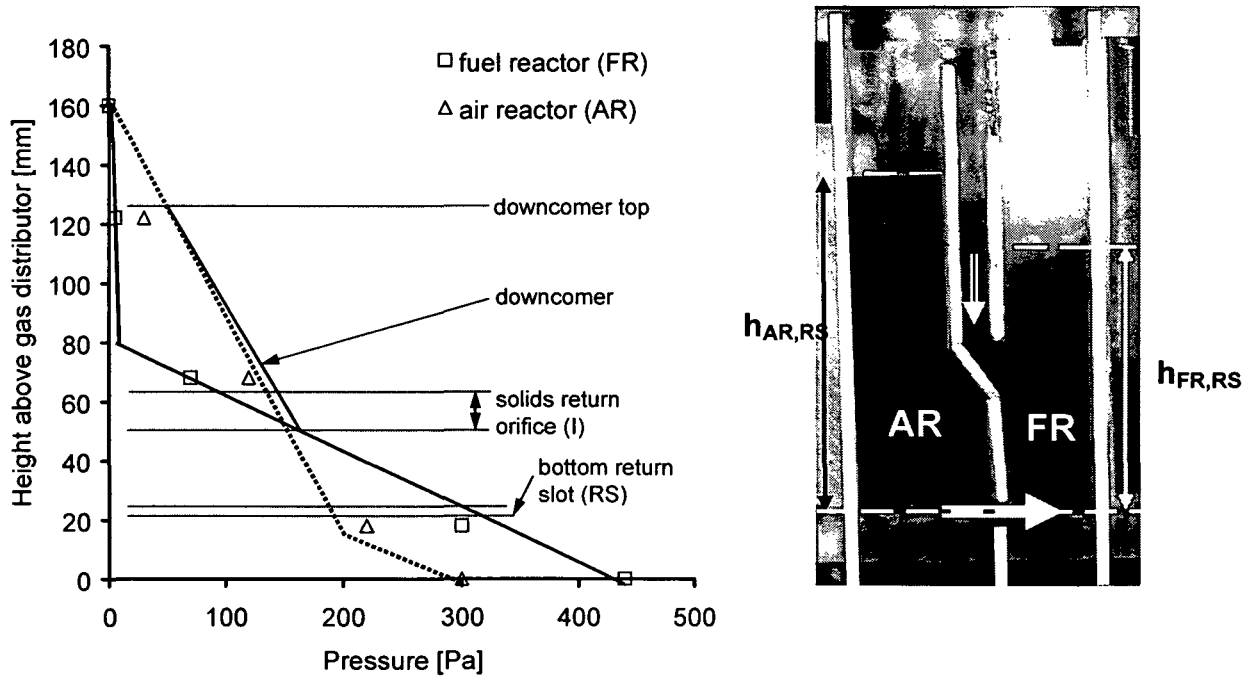


Figure 4-3: Pressure loop of the two-compartment fluidised bed.

It can be observed that as consequence of the different gas velocities in the reactors ($u_{AR} = 1.6 \cdot u_{bt}$ and $u_{FR} = 18 \cdot u_{mf}$) large differences in the bed porosity follow, causing a lower pressure gradient in the “slow-fluidised” bed. The “fast-fluidised” bed, on the other hand, shows a pressure profile, which is similar to typical CFB risers, having a higher pressure drop in the bottom zone followed by a dilute zone. The pressure and the solids flow loops are closed by the downcomer. A particle column balances the pressure differences between the air reactor and the fuel reactor at the height of the particle return orifice (I). The solids column also minimises gas leakage through the downcomer in both directions. At the height of the bottom return slot the pressure is higher in the fuel reactor and a pressure difference appears causing particle flow from the fuel reactor to the air reactor. The pressure difference across the bottom return slot is calculated by:

$$\Delta p_{RS} = p_{FR,RS} - p_{AR,RS} = ((1 - \varepsilon_{FR}) \cdot h_{FR,RS} \cdot \rho_P \cdot g) - (1 - \varepsilon_{AR}) \cdot h_{AR,RS} \cdot \rho_P \cdot g \quad (4-7)$$

where ε_{AR} , ε_{FR} are bed porosities of the two fluidised beds and $h_{AR,RS}$ and $h_{FR,RS}$ are the bed heights at the (mean) level of the return slot (RS).

The bed porosity calculation is based on the determination of the bubble volume fraction according to the modified "Two-Phase Theory" and amplifying the correction factor of Johnsson et al. (1991). Thereby, the minimum fluidisation velocity is derived from the formula of Wu and Bayens (1991) and the voidage at incipient fluidisation from the Ergun equation. The initial bubble size for a porous plate distributor follows the description of Miwa et al., (1972). The bubbling rise velocity (Clift et al., 1978) and the bubble growth are used to determine the bubble size at a certain height (Mori and Wen, 1975).

The lines in Figure 4-3 are calculated using the aforementioned equations and it can be seen that the measurement data can be well reproduced. Deviations are a consequence of the small bed cross-section and the large bed height causing slug formation in the bed. This is confirmed by applying the criteria of Kunii and Levenspiel (1991), which shows that the bubble size exceeds 0.6 times the reactor diameter for the operating conditions.

Solids circulation rate

Figure 4-4 shows the solids circulation rate against the velocity in the air reactor, for the four different designs and FCC as bed material. The velocity in the air reactor (u_{AR}) refers to the velocity in the upper, narrow part, along the downcomer. Since two of the designs, C and D, have a more narrow section, they will have higher velocities for the three volume flows used. The velocity in the fuel reactor (u_{FR}) is held constant at 18 times u_{mf} , which corresponds to 100 W in the hot laboratory unit. In general, it can be seen that the solids circulation rate increases with increasing velocity in the air reactor. The trend for the geometry influence is that the smaller the slot height, the lower the solids flow between the reactors. However, the design with the largest slot, A, did not have the highest recirculation. Similar tests with glass beads gave solids flow rates higher by almost an order of magnitude and an indirect proportionality between the solids flow and the slot height was found.

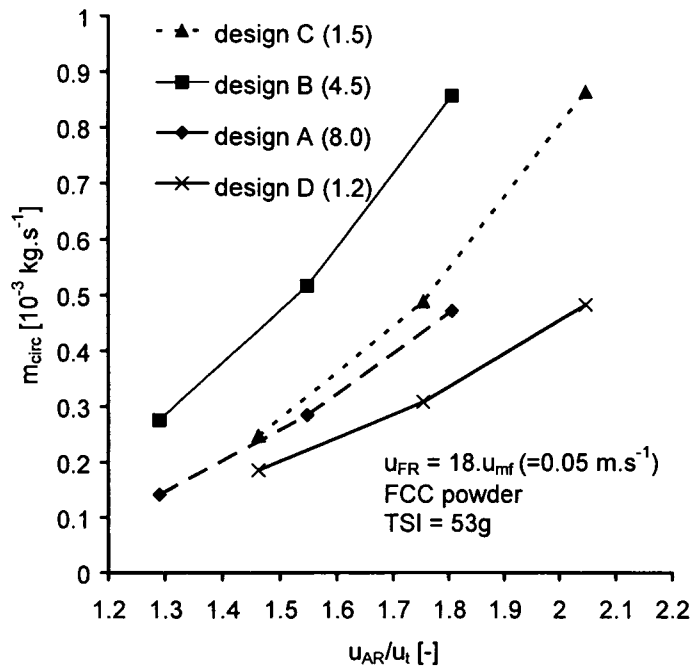


Figure 4-4: Solids circulation rate for all designs (slot height in mm in bracket), and FCC powder. $u_{FR} = 18 \cdot u_{mf} (=0.05 \text{ m}\cdot\text{s}^{-1})$, TSI = 53 g.

The influence of the fuel reactor fluidisation velocity was also examined and it was expected that in case of a lower fluidisation velocity the pressure drop across the slot decreases due to reduced FR bed expansion. As can be seen in Figure 4-5 this was confirmed for the case of FCC and design B and $u_{AR}=0.3 \text{ m}\cdot\text{s}^{-1}$. Another explanation for this is that the stronger fluidisation in the FR will cause a more violent regime at the downcomer return height that supports the solids flow into the reactor. The second approach, however, assumes that the flow conditions in the downcomer outlet are limiting the solids circulation.

For glass beads and other designs a similar tendency was found. The chart also presents the effect of the bed inventory (variations from 43 to 58 g) and thereby it is confirmed that a larger bed mass and the resulting higher bed height causes an increased pressure difference and thus solids flow passing the slot.

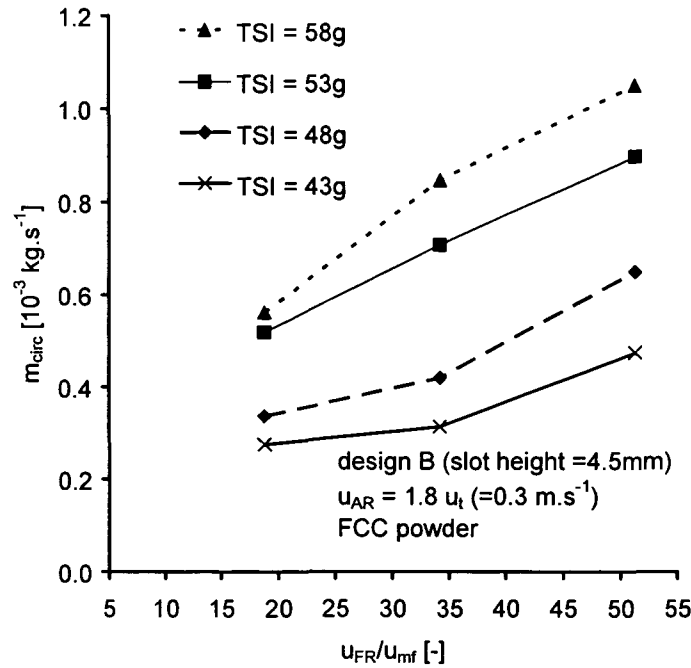


Figure 4-5: Solids circulation rate for design B and different total solids inventory vs. u_{FR} , $u_{AR} = 1.8 \cdot u_t$, FCC powder.

For a flow of solids through an opening (m_{circ}), the solids flow rate is related to pressure drop across the orifice (Δp_{RS}) by applying Bernoulli's equation as:

$$m_{circ} = K_D \cdot A_o \cdot [2 \cdot \rho_p \cdot (1 - \varepsilon_{FR}) \cdot \Delta p_{RS}]^{0.5} \quad (4-8)$$

where A_o is the cross section area of the opening and K_D is the discharge coefficient for the opening. ε_{FR} is the (mean) voidage of the suspension in the slot.

Calculation of the discharge coefficients for both experimental and calculated values according to (4-7) for the pressure drop shows that the approach cannot be applied for the system in question. Numbers for K_D vary strongly due to changing fluidisation conditions at different velocities and no correlation could be determined. As the orifice is located only slightly above the gas distributor the difficulties are attributed to considerable disturbance of the particle movement at the orifice due to the upwards flowing fluidisation gas as bubbles and jets.

The downcomer appears as a further problem in modelling the system. Depending on the operating conditions it was observed that complete filling occurred and it is concluded that in such cases the wall friction resistance of the solids column is limiting the solids flow of the system. To evaluate this effect the flow model was modified and a possibility to introduce fluidisation gas from the sidewall into the downcomer was provided. The results of such tests are presented in Figure 4-6 for design A, FCC powder (58 g) and $u_{FR} = 0.05 \text{ m}\cdot\text{s}^{-1}$. It can be seen that additional fluidisation gas in the downcomer significantly increases the circulation flow.

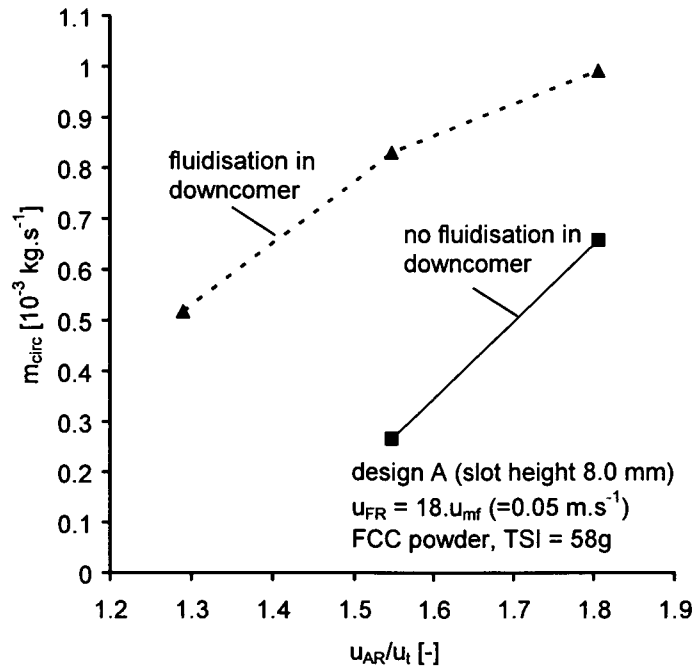


Figure 4-6: Solids circulation rate comparison for additional fluidisation of the downcomer. design B and FCC powder, $u_{FR} = 18 \cdot u_{mf} (= 0.05 \text{ m}\cdot\text{s}^{-1})$, TSI = 58 g.

It is interesting to note that for slightly different bed materials considerably higher or lower solids circulation rates are measured. This is considered to be a consequence of friction effects, both particle to particle and particle to wall. As a consequence the modelling of the results was only possible qualitatively and results show that the required solids circulation rates are fulfilled.

Gas leakage

For large-scale units very low values on gas leakage between the reactors are required, but in the laboratory model, higher leakages can be accepted. The main purpose of the unit is not to demonstrate a very highly effective CO_2 separation but rather to test particles in a continuously operating unit.

In the following charts, Figure 4-7 to Figure 4-10, the gas leakage is defined as the percentage of gas entering one reactor that leaks into the other reactor. Thus, the leakage into the fuel reactor is the leakage flow divided by the flow entering the air reactor. Obtained leakages are based on several test runs and represent mean values.

It can clearly be seen in Figure 4-7 and Figure 4-8 that the gas leakage into the FR is reduced for lower slot heights. Furthermore, a significant reduction is observed for design D. Design D has a slot height of 1.2 mm and an 8 mm wide additional horizontal plate fixed under the slot. For this design the gas leakage into the fuel reactor is about 1%, whereas for design A values of about 5% were determined. As can be seen in Figure 4-7 the gas velocity in the riser does not affect the leakage into the air reactor significantly. Although the leakage in percent is quite constant for each design, in absolute numbers it increases with the velocity since it is based on the volume flow into the air reactor. In Figure 8 the volume flow

in the air reactor is held constant. Since the cross-section area of the riser differs between designs A and B compared to C and D, the velocity in the riser part differs. There is no clear trend in the effect of the velocity in the fuel reactor on the leakage into the fuel reactor.

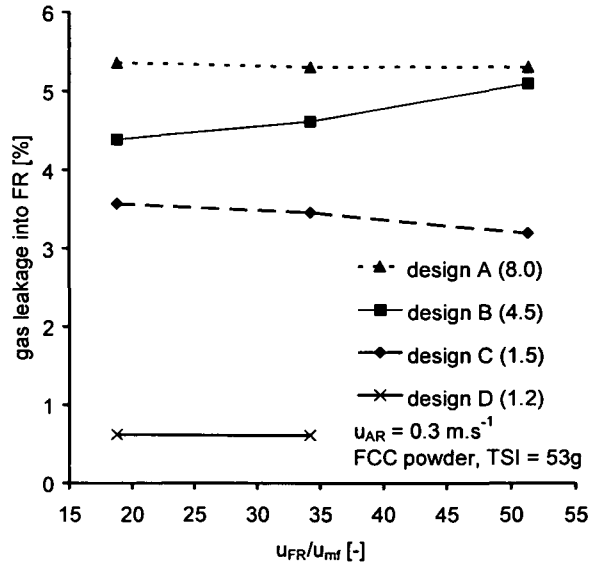
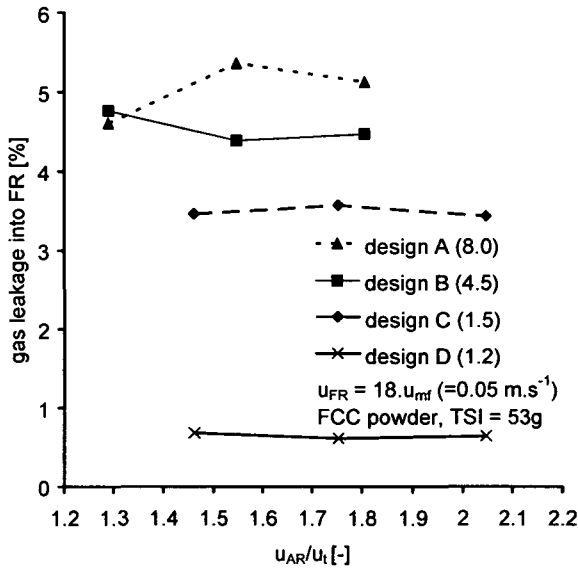


Figure 4-7: Gas leakage into FR for all designs and FCC powder. $u_{FR} = 18 \cdot u_{mf}$ TSI = 53 g.

Figure 4-8: Gas leakage into FR for all designs vs. u_{FR} . $u_{AR}=0.3 \text{ m.s}^{-1}$, FCC powder, TSI=53 g.

Also for the specific gas leakage into the air reactor as depicted in Figure 4-9 and Figure 4-10, a reduction for design D was found. Gas leakage for these cases is about 6% for design D, whereas all other designs lead to a leakage about 11 to 20% based on the incoming fluidisation gas flows.

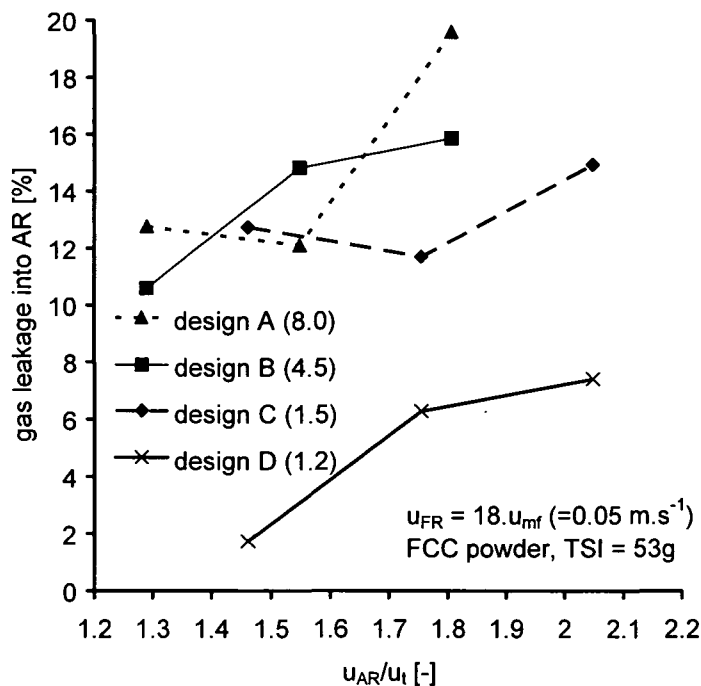


Figure 4-9: Gas leakage into AR for all designs vs. u_{AR} . $u_{FR}=0.05 \text{ m.s}^{-1}$, FCC powder, TSI=53 g

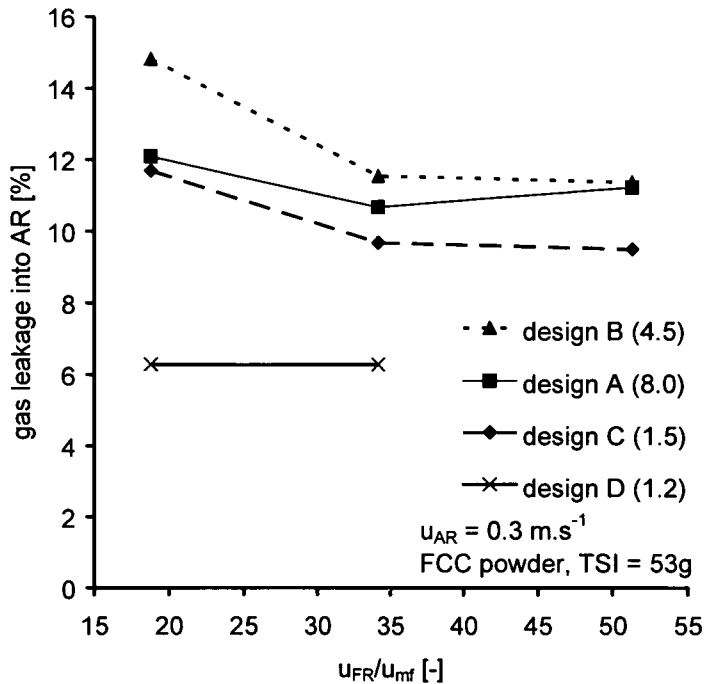


Figure 4-10: Gas leakage into AR for all designs vs. u_{FR} . $u_{AR}=0.3 \text{ m}\cdot\text{s}^{-1}$, FCC powder, TSI=53 g.

When comparing leakages into the air reactor and into the fuel reactor it should be observed that they are based on different incoming flows, and to illustrate this two cases are shown in Table 4-3 (cf. also chapter 4.2.2). Generally, the leakages between the two reactors if measured in $\text{l}\cdot\text{min}^{-1}$ are of the same order. The difference is within a factor of two in almost all cases.

Table 4-3: Comparison of leakage flows for design C and D, $u_{FR} = 0.05 \text{ m}\cdot\text{s}^{-1}$, $u_{AR} = 0.35 \text{ m}\cdot\text{s}^{-1}$

		leakage flow [$\text{l}\cdot\text{min}^{-1}$]	fraction of air flow [-]	fraction of fuel flow [-]
design C	leakage into FR	0.21	3.6%	19.5%
	leakage into AR	0.13	2.1%	11.7%
design D	leakage into FR	0.037	0.6%	3.3%
	leakage into AR	0.069	1.2%	6.3%

In general it was found that gas leakage is directly related to the cross section area of the slot opening. It is likely that the main mechanism of leakage is the exchange of gas bubbles reaching accidentally the other reactor through the opening. This is also suggested by the observation that there is a simultaneous leakage in both directions. Design D gives a lower gas leakage. The horizontal plate reduces this gas exchange and also visual observations support the assumption that fewer gas bubbles cross the orifice and move into the other reactor. When the designs are compared it is seen that an increased solids circulation rate is correlated to a higher gas leakage.

4.3.4 Conclusions and design of the laboratory reactor system

The objective of the present study is the design support for the development of a laboratory scale CLC reactor. A two-compartment fluidised bed system was designed and analysed, and experiments with different flow model designs showed that it is possible to reach sufficient circulation of particles for the oxygen transfer in a model running between 100 and 300 W. As the laboratory system is placed inside heating coils the energy balance of the system does not need to be fulfilled.

The solids circulation of design D (T-slot, 1.2mm slot height), although the lowest, is still higher than the required solids circulation for most oxygen carriers within a power range of 100 to 300 W. The gas velocities in the air reactor correspond to air-to-fuel ratios between 2.5 and 3.5. An overview of operating conditions and main dimensions is given in Table 4-4.

Table 4-4: Operating conditions and main reactor dimensions obtained from flow modelling

Operating parameter and design values		Laboratory CLC unit
Thermal power	W	100 – 300
Fuel type	-	CO/H ₂
Air/fuel ratio	-	2.5 – 3.5
Operating pressure	bar	1
Reactor temperatures	°C	950
Oxygen carrier type		Ni, Fe based
Bed inventory	g	100 - 200
Air reactor dimension (upper narrow part)	m	0.025 x 0.025
Air reactor height	m	0.2
Fuel reactor dimension	m	0.025 x 0.025
Fuel reactor bed height	m	ca. 0.07
Total reactor system height	m	0.4

The fluidisation of the downcomer gave an increase of the solids flow in case of FCC particles, which from their characteristics are likely to be more similar to oxygen carrier particles than glass beads. Further, for a larger system it is expected that friction and inter-particle effects will be less dominant and therefore the measured solids flow from the flow models represent conservative results.

The gas leakage is dependent on the slot design and considered as acceptable for a hot reactor. To reduce the gas leakage further a design with the possibility of fluidisation with inert gas immediately below the slot is considered for the hot unit. It is also expected that this design increases the solids circulation rate.

The final design of the hot unit reactor and a photograph of the manufactured unit are presented in Figure 4-11. The experimental set-up includes particle separators, gas coolers for both exit streams, a water trap for the fuel reactor, and gas analysers for CO, CO₂, CH₄, and O₂. The gases are supplied from gas cylinders and the flows are adjusted by means of mass flow controllers. Pressure measurements are taken along the reactors and

thermocouples are used to determine the reactor temperatures. Further details and results of CLC test runs can be found in Johansson (2005).

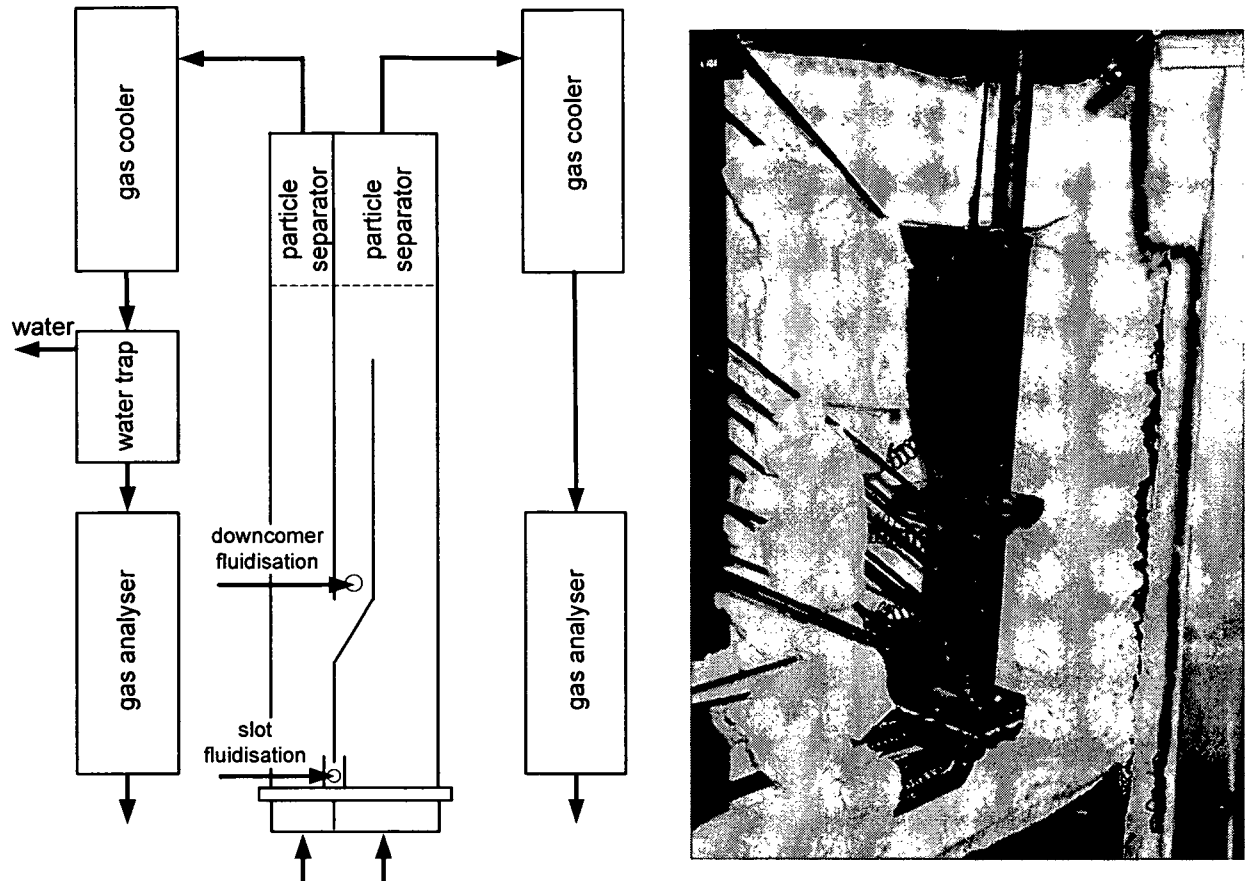


Figure 4-11: Drawing and photograph of CLC laboratory unit set-up. Photograph taken during operation after opening the insulation box.

4.4 Bench scale unit

4.4.1 General design issues

The bench scale unit was designed for analysing the concept for a CLC prototype having a thermal power of 5 to 10 kW operating at atmospheric pressure. The design of the circulating fluidized bed unit is based on the use of natural gas and an operation at 950°C and atmospheric pressure. In the reactor Ni and Fe type carriers are to be tested. The mean diameter of the carrier particles was chosen to be between 100 and 200 μm having a mean density of 2300-5600 $\text{kg}\cdot\text{m}^{-3}$.

The fluid dynamics of the proposed CFB system (Figure 4-13) are predominately determined by the operation conditions of the riser. Velocities similar to typical CFB risers are desired and 4 to 10 times terminal velocity was assumed as superficial gas velocity (Figure 4-12). This is thought to cause, for all particles, sufficient solids entrainment for the required solids circulation rates. The major novelty of the transport reactor is that the bottom section has a wider cross section. The extended volume of the widened section, referred to as the air

reactor, causes a higher mean particle residence time in the oxidation zone. Velocities between 1.2 and 3 times terminal velocity are assumed to be appropriate in this zone.

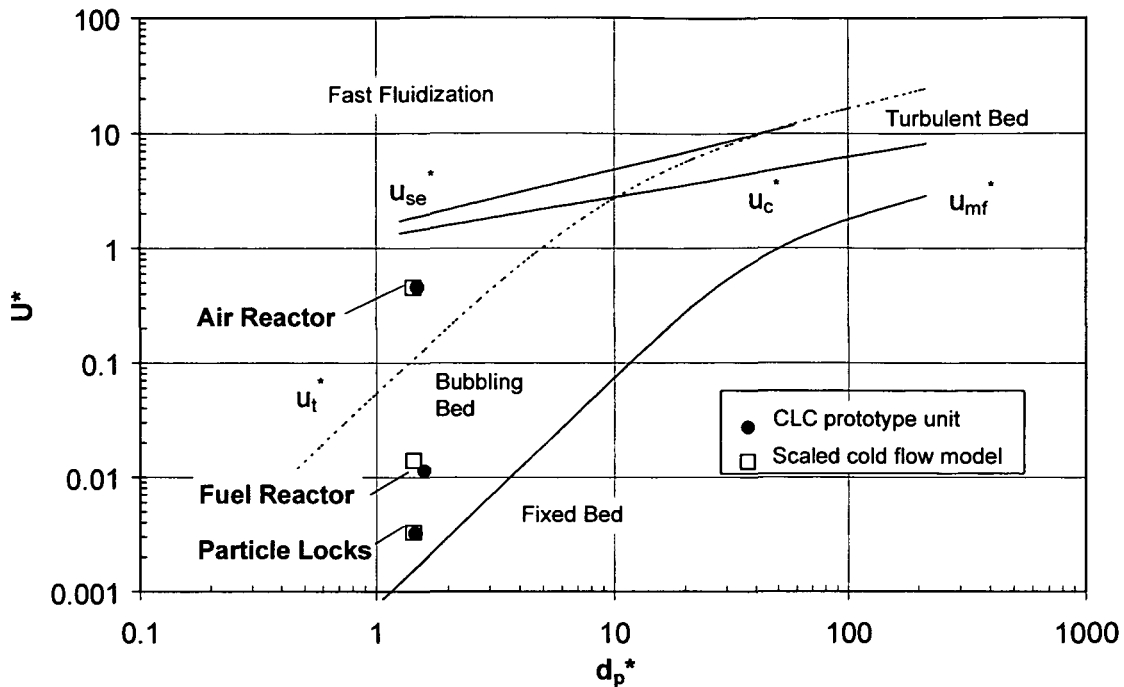


Figure 4-12: Operating regime of the bench scale unit according to Bi and Grace (1995)

The fuel reactor is operating in the bubbling fluidised bed regime. Low gas velocities below 0.7 times u_t and above 2 times u_{mf} , depending on the particle properties and thermal power are design parameters. If methane is used as the fuel, the ratio of fuel molecules to reactant molecules is three, which gives an upper limit of $0.75 \cdot u_t / 3 = 0.25 u_t$ based on the methane flow. No particle separator is planned for simplicity reasons for the fuel reactor although very low solids entrainment is desired. In order to accommodate for the gas volume expansion in the fuel reactor the cross-sectional area increases in the freeboard with height by means of two conical sections.

Gas leakage is difficult to avoid completely in a CFB system. Different types of valves are used to minimize the leakage and in some cases they are simultaneously dedicated to control solids flow. Any gas mixing in a CLC system incurs extra expenditures for separation and an effective valve type, a loop seal, is designed for the concept.

The pressure drop of both fluidised beds is governed by the bed height, which itself follows from required particle residence time. The bed height of the fuel reactor was chosen on the basis of reactivities obtained in previous studies with iron based oxygen carriers. Because reactivity data are different for the various metal oxides and also a safety margin should be included, the bed height can be controlled by an adjustable overflow height. In order to do this, however, the outlet pipe has to be removed. For the freeboard twice the height of the dense bed height (about 0.1 m) is assumed, which results in a total height of about 0.35 m.

Based on the estimated reactivity of most metal oxide particles the required height of the dense bed in the air reactor is small. However, the bed mass in the air reactor and accordingly the bed height are related to the total solids inventory in the unit. This gives the need for a certain bed mass in the air reactor for stable operation. Also, for cooling purpose an adequate surface area must be considered.

The dimensions of the downcomers and the loop seals are based on considerations of required/expected solids flows and allowable particle velocities.

4.4.2 CFB reactor concept of the CLC prototype

The design concept of the CLC prototype (Figure 4-13a) and Figure 4-13a b) shows the air reactor (riser) and the fuel reactor integrated in the return leg. As two different particle separator designs were tested the two graphics show the different concepts. In the case of the standard configuration A (Figure 4-13a) a cyclone is used for solids separation of the air reactor exit flow. Fuel reactor and air reactors are separated by L-type loop seals. The fuel reactor gas exit is designed to have a large cross-section as high gas velocities would cause high particle loss due to entrainment. The solids flow leaving the fuel reactor by an overflow standpipe is returned into the air reactor at a height corresponding to an appropriate pressure level in the transport reactor.

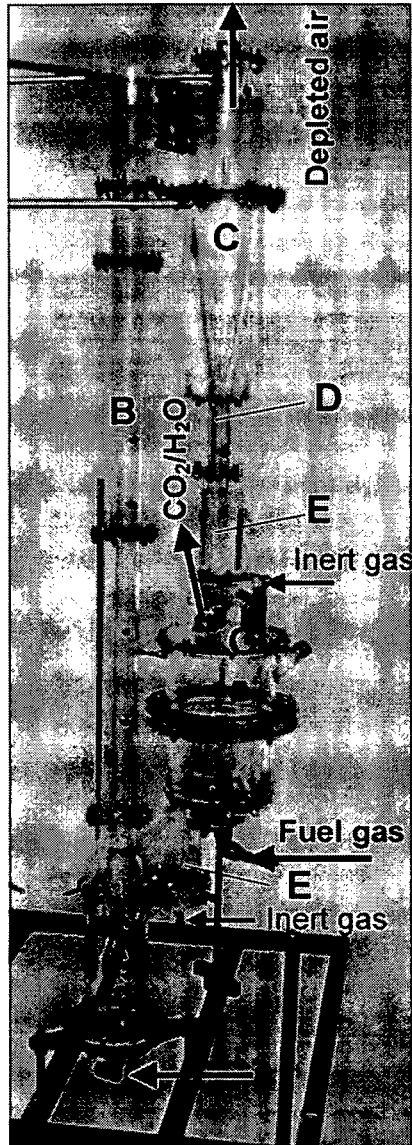


Figure 4-13a: configuration A

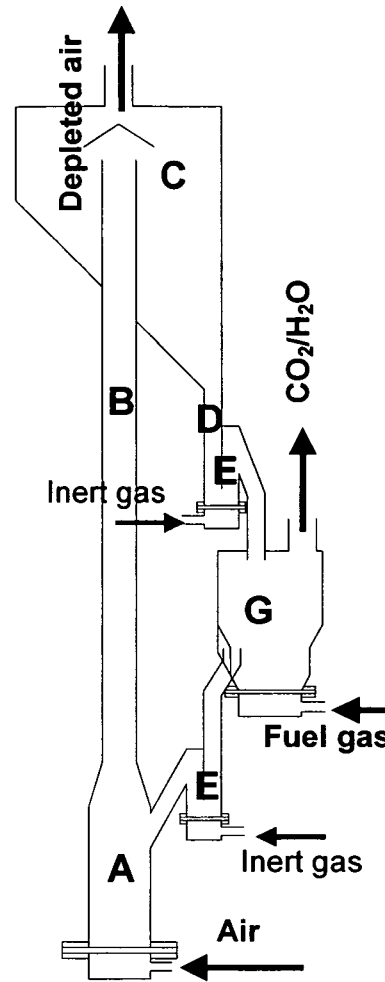


Figure 4-13b: configuration B

Design layout of dual fluidised bed system (10 kW CLC prototype) with (A) air reactor , (B) riser, (C) particle separator, (D) downcomer, (E) loop seal, (G) fuel reactor with standpipe overflow.

The advanced design, configuration B, (Figure 4-13b) is identical to the aforementioned configuration but includes an alternative particle separator design. The “hat” separator is based on the settling chamber principle and is intended to decrease exit effects on the solids flow. The particle back-flow in the riser is lower for such a concept, which increases the solids flow and leads to smaller pressure drops for a given solids flow. The particle/wall friction is minimised because of lower velocities, which compared to the cyclone has a positive effect on undesirable attrition of the oxygen carrier particles. Further, because of a smaller pressure drop of the separator it leads to reduced energy consumption of the gas fans. A negative effect is expected on the particle separation efficiency. However, the

synthetically produced metal oxide particles can be produced in a narrow particle size range with very low fines content that should be easily separated.

In addition to tests with the standard design of the prototype reactor geometry, tests with different riser heights and the alternative type of particle separator system were made. The riser height variations are aimed at giving more detailed information on the effect of riser height scaling for transferring the results to larger scale CLC units. The design configurations used in these tests are given in Table 4-5.

Table 4-5: Configurations used

Configuration	Specification
configuration A (standard configuration)	cyclone with standard riser (Figure 4-13a)
configuration B	alternative particle separator with standard riser (Figure 4-13b)
configuration AS, BS	configuration A or B with short riser

For larger particle sizes the thermal power of the unit is raised up to 10 kW and with the increased gas velocities the fluidisation regimes of the riser and the stationary bed are still in a range that is considered appropriate for operation of the combustor. The air ratio in that case increases up to about 2.5. Although, the heat balance has to be fulfilled for all particle types, it is not required to keep the air ratio low as the unit is not designed to represent a large-scale boiler. A summary of the design values chosen for the CLC laboratory unit is given in Table 4-6.

Table 4-6 : Design values of the CLC bench scale unit

Operating parameter and design values		Bench scale unit
Thermal power	kW	5÷10
Fuel type	-	methane
Reactor temperatures	°C	950
Air to Fuel Ratio	-	1.2 - 2.6
Operating pressure	Pa	$1 \cdot 10^5$
Particle density	$\text{kg} \cdot \text{m}^{-3}$	2500 - 5400
Mean particle diameter	m	$100 \cdot 10^{-6}$ - $200 \cdot 10^{-6}$
Gas fluidisation velocity in the riser $=u/u_t$	-	4 - 10
Gas fluidisation velocity in the air reactor $=u/u_t$	-	1.2 - 3
Gas fluidisation velocity in the fuel reactor $=u/u_{mf}$	-	5 - 15
Loop-seal gas fluidisation velocity $=u/u_{mf}$	-	1.2 - 4
Riser diameter	m	0.072
Riser height	m	1.85
Air reactor diameter	m	0.14
Air reactor height	m	0.53
Fuel reactor (maximum) diameter	m	0.25
Fuel reactor bed height	m	0.13
Fuel reactor total height	m	0.34
Total reactor system height	m	2.2

4.4.3 Design aspects specific to the cold flow model

Application of the scaling laws (chapter 4.2.1) showed that for the selected material properties it is difficult to develop reasonable scaling factors using ambient air. Therefore a gas mixture of e.g. helium/nitrogen is required and as bed material glass beads with a mean particle diameter of 67 μm and a particle density of 2550 $\text{kg} \cdot \text{m}^{-3}$ was used.

The cold flow model was built from acrylic glass and the gas distributor plates of the two reactors were of perforated plate type whereas for the particle locks porous glass plates were used. The cyclone is designed according to design formulae by Barth-Muschelknautz (Stiess, 1992) and on data from Hugi (1997). An anti-static powder (Larostat®) was added to the bed material to reduce electrostatic charges. The gas mixture for the cold flow model is provided by a gas recirculation system. After passing a filter the exit gas flows are collected in a large gas bag, which ensures atmospheric working pressure in the system. A gas compressor pumps the gas from the bag and raises the gas to the operating pressure of the mass flow controllers. A gas cooler ensures ambient temperature and safety valves protect the Perspex flow model from any overpressure (further details see Tagwerker, 2003).

The cold flow model was operated with a total bed material inventory between 1.1 and 2.2 kg. Further, gas velocities in the reactors and also in the loop seals were varied. Their effect on the CFB pressure balance and solids circulation rate, (mean) gas and particle

residence time, and gas leakage were tested. An additional pressure relief valve was installed at the fuel reactor exit and variations were carried out to study the effect of the fuel reactor pressure on the pressure balance of the system, in particular the gas leakage.

4.4.4 Pressure loop analysis

From start-up of the unit it could already be seen that the system was working without any difficulties. Nonetheless, a few design variations were indicated and realised before the main test programme was carried out.

- The fuel reactor geometry was modified as observations suggested that particle mixing was not satisfactory.
- The cyclone inlet duct geometry was modified in order to reduce the particle accumulation. Due to the high operating temperatures in the prototype particle softening cannot be excluded totally and that might cause agglomeration and total blocking of the system.

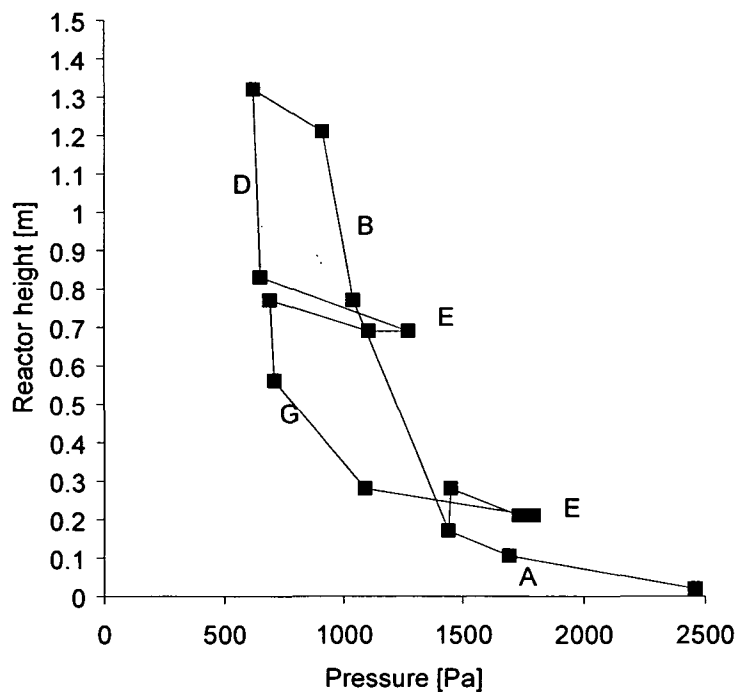


Figure 4-14: Pressure loop of the cold flow model (configuration A, total solids inventory = 1.9 kg, $u_{AR}=0.45 \text{ m}\cdot\text{s}^{-1}$; letters refer to Figure 4-13a).

The static pressure loop in the unit (Figure 4-14) for configuration A shows that the loop seals can balance the pressure differences between the reactors. The absolute pressure in the fuel reactor should be between the air reactor and the cyclone-downcomer pressure. Preferably, the latter is lower than the fuel reactor pressure because then the fuel reactor exit flow, i.e. CO_2 , is not diluted. For similar reasons the pressure in the fuel reactor should be lower than that of the air reactor to avoid leakage of CO_2 into the air reactor.

4.4.5 Solids circulation rate measurements

In this section measurement results are presented for the “hot” reactor. This means that data from the cold flow modelling were already converted by using the scaling laws according as presented in section 4.2.1.

Variation of air reactor fluidisation velocity and total solids inventory

In the parameter plot in Figure 4-15 the specific solids circulation rate is presented vs. the total solids inventory, the reactor masses, the air/fuel ratio, and the air reactor velocity. It can be observed that for the standard configuration (configuration A) a wide range of values for the specific solids circulation rate above the minimum required solids flow (about $12 \text{ kg}\cdot\text{m}^{-2}\cdot\text{s}^{-1}$ for 10kW_{th}) can be achieved. The solids circulation rate values were determined up to $90 \text{ kg}\cdot\text{m}^{-2}\cdot\text{s}^{-1}$, where the system becomes unstable. In such case the fuel reactor is filled up higher than the overflow level, which can be attributed to the flow limitation of the downcomers and loop seals. Due to the resulting higher pressure on the particle column in the downcomer, however, it is possible to further increase the solids circulation but this is considered not to be a desired operation point for the current CFB system.

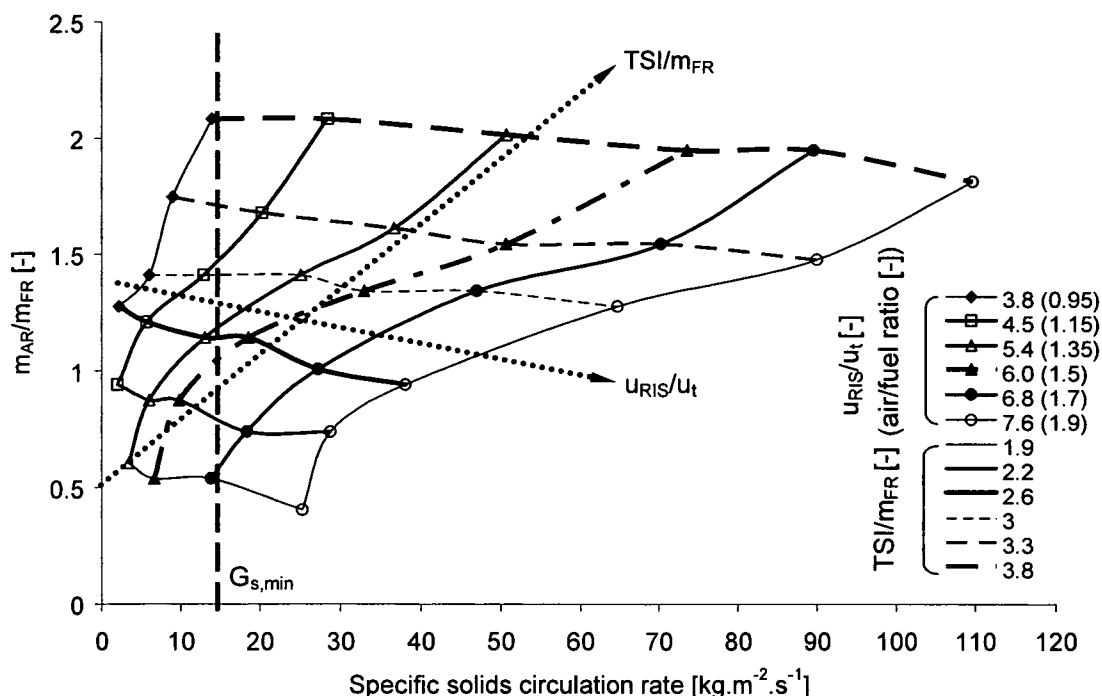


Figure 4-15: Specific solids circulation rate design chart of configuration A. Parameters: total solid inventory (TSI) and bed mass distribution, riser velocity, air/fuel ratio. $G_{s,min}$ gives the minimum required solid flow from mass and energy balance.

Variation of TSI for standard configuration and reduced riser length

Variation of the riser height was carried out throughout the experimental programme and it was found that a riser length reduction of 0.1 m (about 10%) results in an increase of the solids circulation rate up to 20% (Figure 4-16). The graph shows a comparison for two different solids inventories of the system.

The increasing solids flow is a consequence of the fact that the riser height in all design configurations is well below the transport disengagement height (TDH). The TDH is defined, according to Geldart (1985), as the height above which the elutriation rate remains constant. In our case the TDH was calculated according to Fournol et al. (1973), as being at least an order of magnitude higher than the actual riser height.

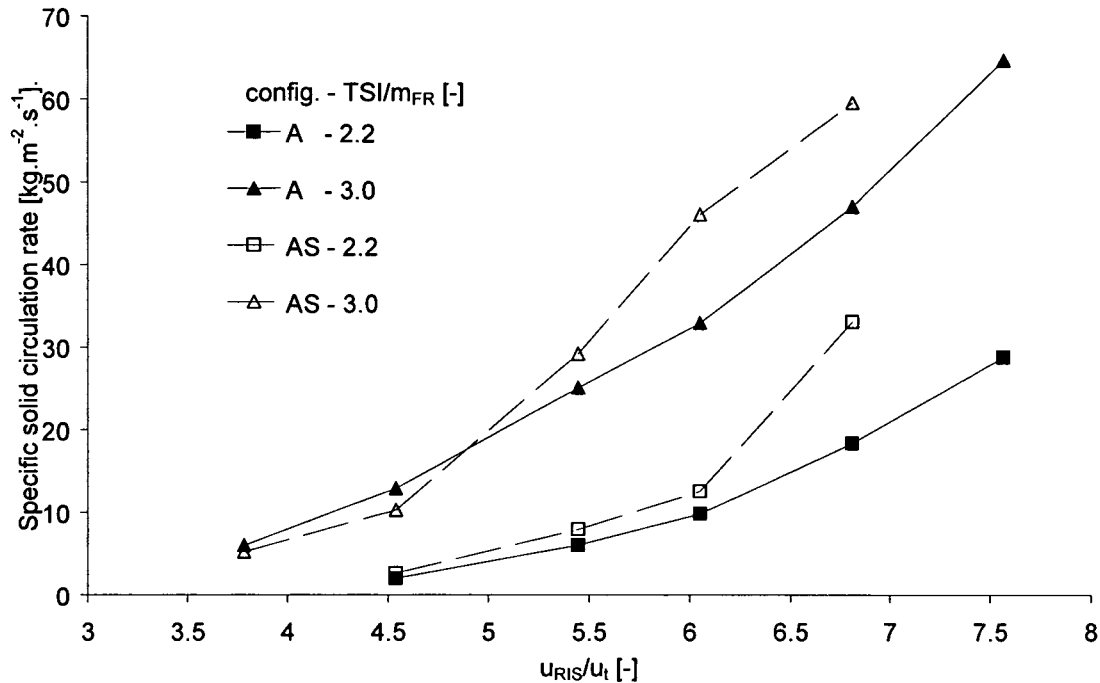


Figure 4-16: Comparison of specific solids circulation rate vs. riser velocity for riser height variation of configuration A (standard conf.) and AS (A with short riser), TSI/m_{FR} of 2.2 and 3.3.

Comparison of system design A and B

Experimental test results obtained with the alternative particle separator, but for equal riser length, are given in Figure 4-17. It appears that a significant increase of the circulation rate is achieved with the “hat” separator (B) for identical mass distribution in the system. The reason for this is the reduced particle reflux at the exit of the riser - the bend into the cyclone inlet duct. For the alternative particle separator the riser top exit is entirely open and presents less resistance to the suspension flow.

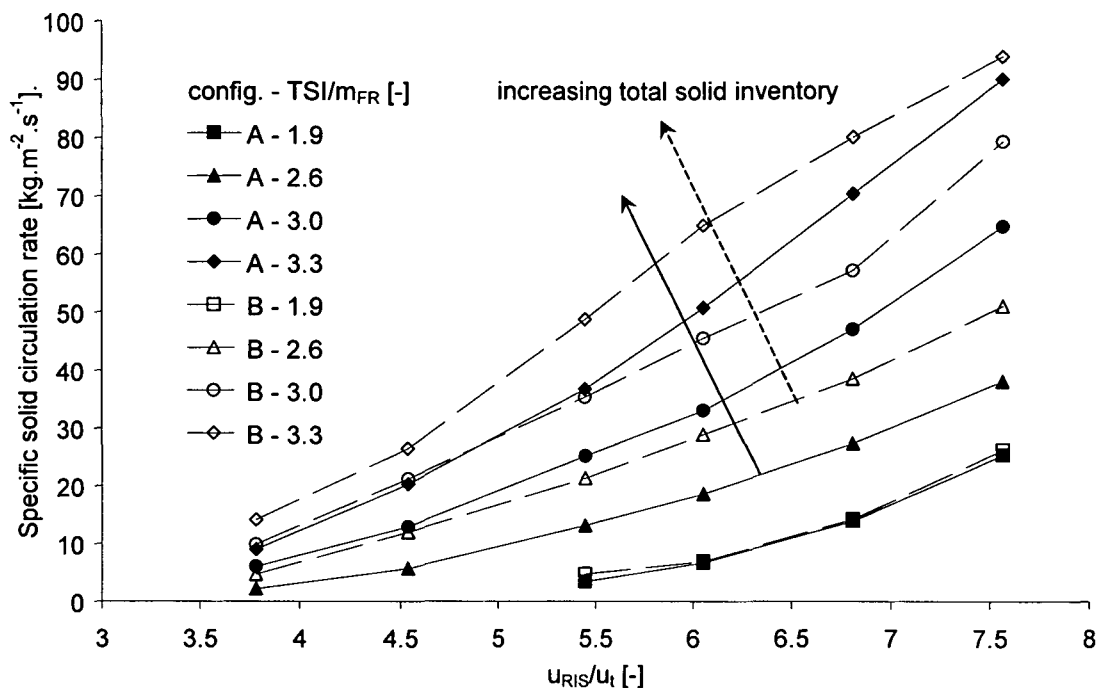


Figure 4-17: Comparison of specific solids circulation rate vs. riser velocity for variation of the particle separator type A (standard conf.) and B (alternative particle separator) and TSI.

For all design configurations the particle separation (cyclone) efficiency of the gas solids separators was determined. In long-term measurements the particle separation efficiency for both types was above 99.93% and up to 99.97% per cycle. Certainly, this is sufficient for the CLC prototype unit and allows operation with very low loss of precious oxygen carrier in the laboratory.

Dimensionless solids circulation vs. solids hold-up

The pressures measured along the riser height can be converted into solids hold-up values. At first, this gives the solids distribution along the riser. Although not presented in this work the examination confirms the effectiveness of the bottom widening for increasing the solids hold-up and thus, mean particle residence time in the riser. Another important result of this analysis is a comparison of the solids hold-up detected in the upper portion of the riser with the dimensionless specific circulation rate according to the estimation of (4-9). The acceptability of this approach was examined by Johnsson et al., (1999). A successful comparison gives a basis for a mathematical riser model but, more importantly, the verification allows the determination of the solids circulation rate in the prototype reactor from pressure measurement along the riser. This is of relevance since no test method presented in section 4.2.2 can be applied in the hot reactor and other methods are often complicated or somewhat inaccurate.

$$(1 - \varepsilon) = \frac{G_s}{(u - u_t) \cdot \rho_p} \quad (4-9)$$

Although the pressure drop at the top of the riser is very low, which causes higher measurement inaccuracy and also some uncertainty exists on the actual value of the terminal velocity at the top of the riser, the results are satisfactory. The solids hold-up used for this chart is not determined at the very top of the riser but about 0.1 m lower in order to eliminate the effects of slightly higher solids density due to particle reflux from the riser exit bending.

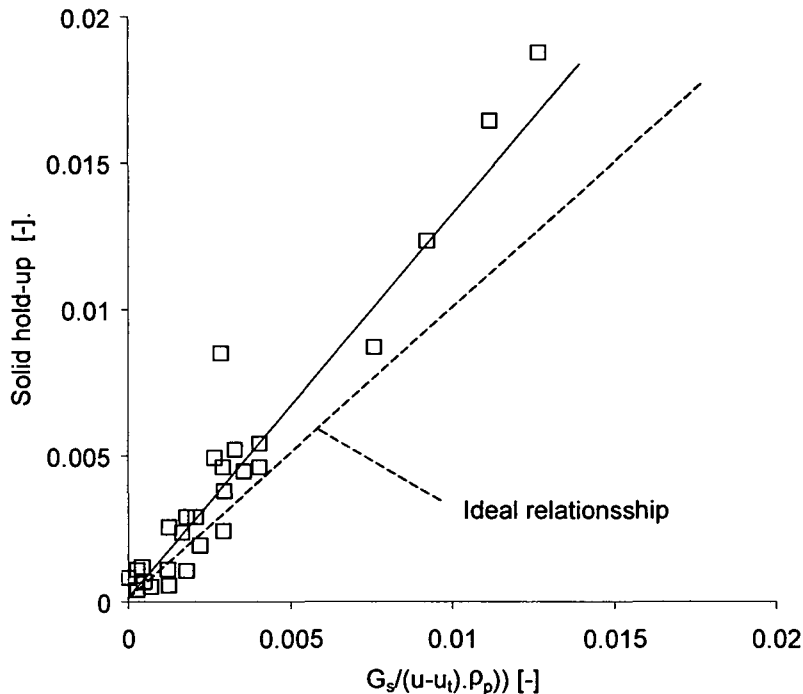


Figure 4-18: Solids hold-up vs. dimensionless specific solids circulation rate for standard configuration (A), Dashed line gives ideal relationship according equation (4-9).

The results of this study are presented in Figure 4-18. It can be seen that the estimation according to (4-9), which ideally gives the dashed line, agrees well with most measurements data. It is therefore concluded that this analysis can be applied in the laboratory prototype.

4.4.6 Gas leakage

The gas leakage rates have been studied since they are important for the CO₂ capture performance of the CLC process. Total solids inventory, reactor fluidisation velocities, loop seal fluidisation and the pressure balance between fuel and air reactor were varied in these tests. The description of the measurement method can be found in section 4.2.2.

In Figure 4-19, a correlation of the measured gas leakage flow to the gas volume (flow) in the void between the particles of the solids flux is presented. The latter (solid line) is the gas leakage that can be expected if the leakage is equivalent to the gas volume that is carried in the inter-particle void fraction of the moving solids flux. Thereby, the bed voidage in the solids bulk was calculated assuming minimum fluidisation conditions. The effective gas velocity results such as difference between the particle velocity and the loop seal fluidisation

gas velocity and was kept constant for the presented line. Results in Figure 4-19 show gas leakage flows into the air and the fuel reactor, for measurements at different solids circulation rates as well as different pressure differences between the fuel reactor exit and the cyclone downcomer.

The basic correlation that can be seen in this figure is the proportionality between the two parameters. The gas flow in the inter-particle void is also proportional to the solids circulation rate. Furthermore, it can be observed that there is no dependency of gas leakage on the pressure drop across the loop seals and on the total solids inventory.

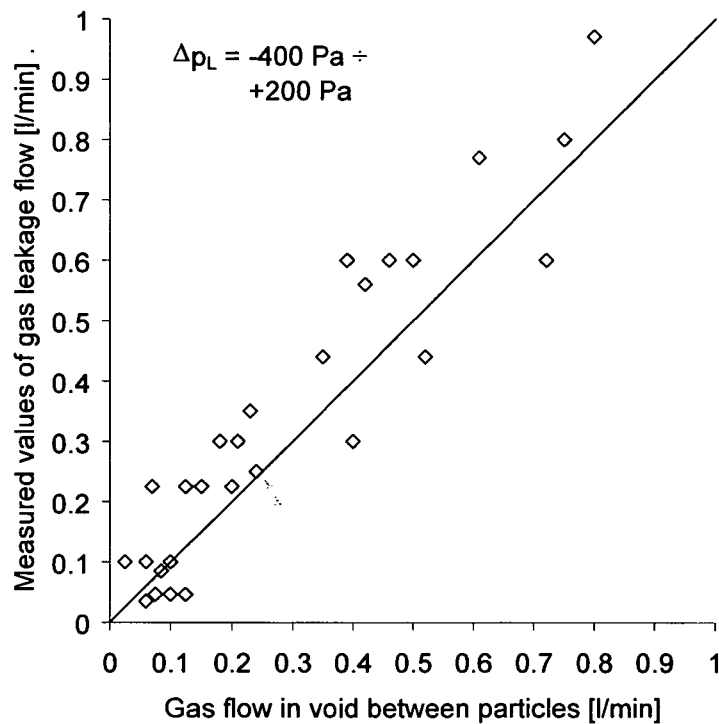


Figure 4-19: Correlation of gas flow in the void between particles and measured gas leakage for variation of solids circulation rate and pressure difference between FR and downcomer Δp_L . Positive values give overpressure of the FR in comparison to the pressure in downcomer of the cyclone.

The understanding of the gas leakage mechanism, i.e. the proportionality of the gas leakage and the solids circulation rate, makes a possible countermeasure obvious. An increase of the siphon fluidisation reduces the gas leakage by a stripping effect of the loop seal fluidisation gas.

An analysis of this can be seen in Figure 4-19. The leakage rates in Figure 4-20 represent the dilution of the CO_2 stream. As can be seen this would be low, 0.1-0.6%.

It can be seen in Figure 4-20 that increasing the velocity in the loop seals causes a significant decrease of the gas leakage, which theoretically gives the possibility to totally prevent gas leakage by completely stripping the solids flow. Another possibility for this is the injection of fluidisation gas into the downcomer.

From the measurements also the flow of the particle lock fluidisation gas (steam or inert gas in case of hot CLC process) could be tracked precisely and it was found out that for siphon velocities up to about $3 \cdot u_{mf}$ almost the entire gas flow (>97%) is following the solids flow. This result is valuable as it allows also the calculation of the dilution of the gas streams with loop seal fluidisation agent.

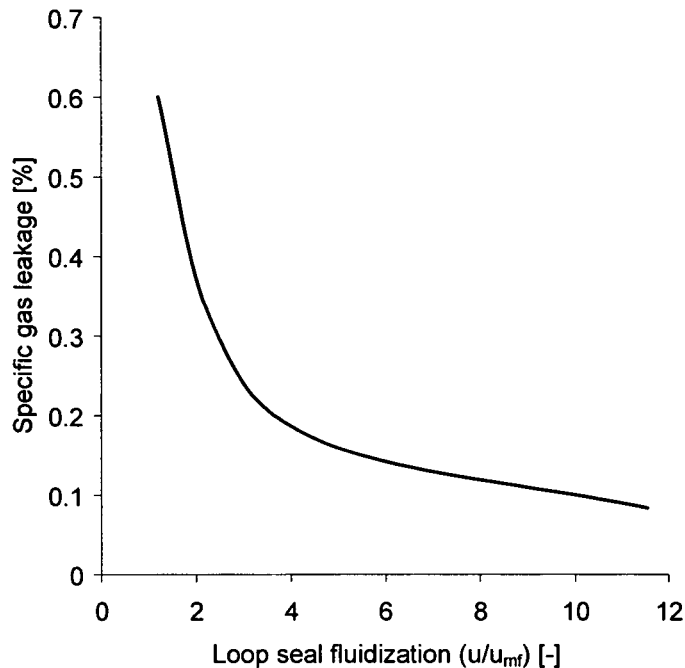


Figure 4-20: Specific gas leakage vs. loop seal fluidisation velocity for zero pressure difference between air and fuel reactor and standard operating conditions.

From these observations it can be concluded that increasing the siphon fluidisation velocity is an appropriate measure to decrease the gas leakage into both reactors. The transfer of the specific gas leakage results can be pursued directly but attention must be given to gas mixing between fluidised bed reactors caused by porous particles. Because of the required reactivity the oxygen carrier particles comprise a porous structure. Franke et al. (2001) reported an effect of the capture of heavy oils in pores on fluidised bed incineration quality and, similarly, also in this case an effect is expected in the prototype. An exact analysis can be carried out easily once test data of the prototype and particle porosity and mass flow are available but estimation of the oxygen carrier porosity shows that an additional specific gas leakage up to one per cent must be taken into consideration.

4.4.7 Residence time distribution of solids in the CLC prototype fuel reactor

High fuel conversion is crucial not only for high thermal efficiency but also environmental standards may require recycling of combustibles in the flue gas. The residence time distribution in the fuel reactor influences the kinetics of the fuel oxidation and thus, the conversion. In this section, the results of residence time distribution (RTD)

measurements in the fuel reactor under continuous operation and a phenomenological modelling approach are presented.

Methodology and experimental procedure

The range of experimental techniques for measuring RTD in fluidised beds is extensive and in general the methods are all based on tracer techniques. Harris et al., (2002) give an overview on different techniques for particulate systems and group them, in view of the flow conditions in the system, into disruptive or non-disruptive methods and, in respect to the solids inventory into contaminating or non-contaminating techniques. For an experimental test program the method should be easy and safe to apply, minimize the cost involved, and provide reliable results. The following Table 4-7 gives an overview on different classes of tracer techniques and their main characteristics with respect to their application to stationary fluidised beds.

Table 4-7: Experimental RTD techniques modified acc. to Harris et al. (2002), Riviere et al, (1996), Habermann et al., (1998), Valenciano (2003), Grace et al., (1997).

	Tracer/detection method	Benefits/limitations
Disruptive tracers		
Chemically different tracers	Sodium chloride particles or saturated catalysts Strongly acidic cat-ion exchange resin Particles marked with an organic substance	Easy and cheap method Low resolution due to handling of sampling (resolution ca. 0.5s) Time/labour intensive
Radioisotope tracers	Short half-life radioisotope and low ion tracers	Fast response, applicable to large-scale systems. Health risk, disposal of tracer after tests, long leg time because of contamination of the bed material.
Magnetic tracers	Ferromagnetic tracers (Fe, Ni, Co)	Easy method, low resolution
Subliming tracer particles	CO ₂ "pellets": measuring either temperature or the gaseous sublimation concentration product	Non-ideal tracer injection, different motion of gas and solids causes uncertainties, difficulties in matching tracer and bed material properties
Particle sampling	Bed sampling to determine tracer concentrations and mixing parameters	Inaccurate measurement of particle velocity. For single particle tracing.
Particle sizing techniques	Tracer of a narrow size interval separated from the main solids	
Coloured tracer techniques	Coloured glass beads or base material	Easy and cheap method

Table 4-7: Experimental RTD techniques (continued)

Non - disruptive tracers		
Optical methods	Injection of porous particles labelled with fluorescent dye, Excitation of light emissions of fine phosphor particles	Can be used to determine particle velocity, difficulties in depth analysis
Thermal methods	Heated particles as tracer and recording of bed temperature	Difficulties and inaccuracies to determine experimental results.
Single particle tracers	Measurement of trajectories of single particles, averaged values result in RTD	

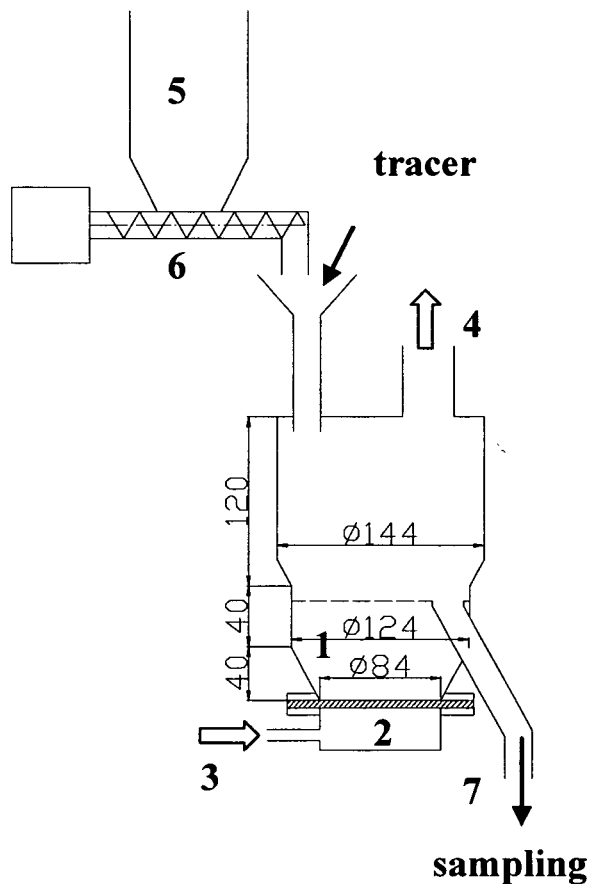
Experimental set-up

Figure 4-21: Experimental set-up (measures in mm) 1 fluidisation section, 2 wind box, 3 gas inlet, 4 gas outlet, 5 feed hopper, 6 screw feeder, 7 solids outlet.

Continuous measurement of the RTD in the closed CFB loop was found to be very difficult as the results were significantly influenced by the second response of the reactor system on the impulse injection. Therefore, the experimental set-up (Figure 4-21) consisted

of the stationary fluidised bed, the fuel reactor, and the solids flow was simulated by an adjustable screw feeder and a feed hopper arrangement similar to Babu et al. (2003).

To investigate the RTD of the CLC prototype a sodium chloride tracer, (chemically different tracer type) as applied by Bader et al. (1986) and Rhodes et al. (1991) was selected. The material was ground to a size similar to the beds solids for impulse injection experiments in the bed. The tracer particles are characterised by a density similar to that of the tracer particles ($2250 \text{ kg}\cdot\text{m}^{-3}$) and the only characteristic difference to the base material is given by the sphericity. A known amount of tracer was injected as a pulse at steady state into the feed inlet and sampling was performed at the overflow of the reactor. Individual samples of known weight were washed and the salt concentration $c(t)$ was determined by the conductivity of the wash solution.

Experiments were carried out to measure the residence time distribution of solids for different experimental conditions by varying the solids flow rate, gas flow rate and solids characteristics. Additional experiments were conducted to confirm the suitability of the measurement technique.

Experiments were carried out to measure the residence time distribution of solids for different experimental conditions by varying the solids flow rate, gas flow rate and solids characteristics. Additional experiments were conducted to confirm the suitability of the measurement technique. An overview on the test program is given in Table 4-8.

Table 4-8: RTD test matrix

	G_s [$\text{kg}\cdot\text{m}^{-2}\cdot\text{s}^{-1}$]	u/u_{mf} [-]	$d_{p,bed}$ [μm]	$d_{p,tracer}$ [μm]
A	0.011	7	67	70
B	0.015	7	67	70
C	0.015	10	67	70
D	0.015	15	67	70
E	0.015	5	67	70
F	0.02	15	67	70
G	0.02	15	67	90
H	0.02	7	120	70

Experimental results

The experimental curve $c(t)$ vs. time t was used to evaluate the residence times of solid particles. The space time is obtained as:

$$\tau = \frac{m_{FR}}{m_{circ}} \quad (4-10)$$

and the RTD function (= exit age distribution, for dimensionless time (4-13) as:

$$E(\theta) = \frac{c(\theta)}{c_0} \quad (4-11)$$

$$\theta = \frac{t}{\tau} \quad (4-12)$$

The cumulative age distribution function $F(\theta)$ can be derived by integrating $E(\theta)$. $F(\theta)$ provides the fraction of molecules exiting the reactor that have spent a time t or θ or less in the reactor and is the integral of the age distribution function $E(\theta)$.

$$F(\theta) = \int E(\theta) d\theta \quad (4-13)$$

The effect of variations of the solids mass flow and the fluidisation velocity on the cumulative residence time distribution of the reactor vs. dimensionless time is shown in Figure 4-22.

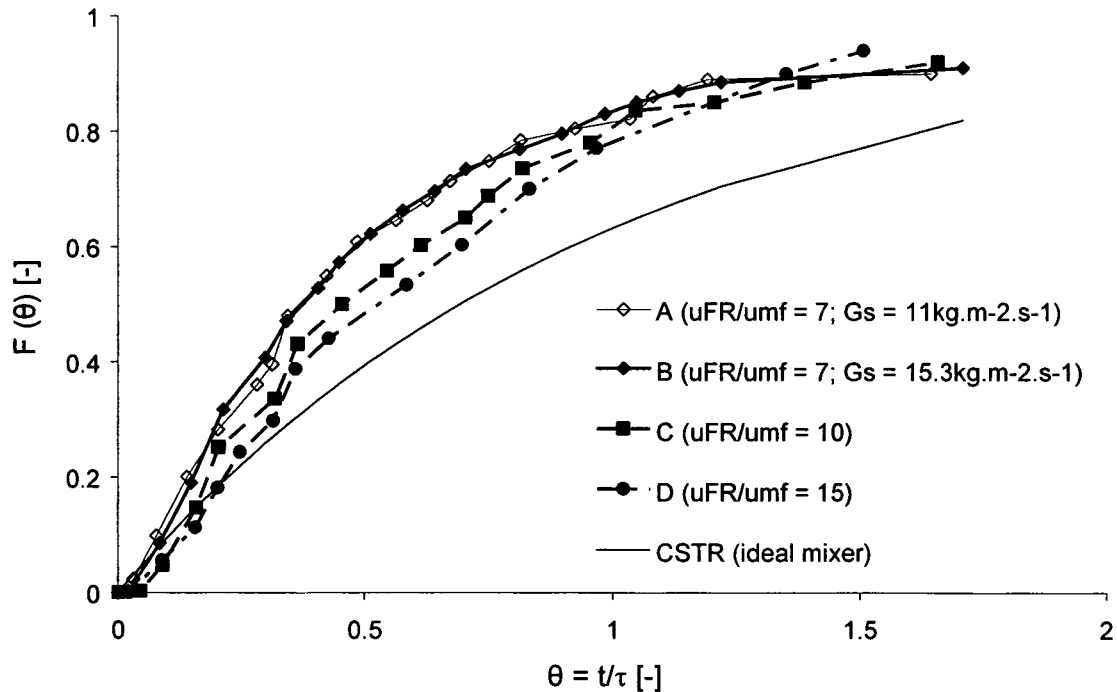


Figure 4-22: Effect of fluidisation velocity (and solids circulation rate) on cumulative RTD function ($F(\theta)$) vs. θ . CSTR gives comparison with an ideal continuous stirred tank reactor (CSTR).

All experimental data were taken only to about twice the space time but it is clear that the curves must reach the value one for $F(\theta)$ at infinite time. Despite this lack the main information on the RTD can be obtained from the experiments. A comparison of the general trend of the RTD curves A to D shows a considerable deviation from the common assumption of ideal mixing of an ideal continuous stirred tank reactor (CSTR) as proposed e.g. by Geldart (1986).

Curves A and B differ only in the solids mass flow but show an identical behaviour for $F(\theta)$, the dimensionless time scale. This confirms the expectation of a solids-flow-independent bed mixing process. Curves B, C, D are experimental results at different reactor fluidisation velocities. Although the differences appear small in the cumulative RTD

presentation it can be seen that a higher velocity causes a decrease of the median residence time (the time required for half the bed mass leaving the reactor). A more detailed analysis in a later section confirms the improved mixing.

In addition to the variation of the operating conditions, the solids characteristics of the bed material and the tracer were analysed. When using bed material with a larger mean particle diameter (test H) at similar flow conditions (u_{FR}/u_{mf} was kept constant) and equal solids flow no difference was encountered. Equally, a change of the mean particle diameter of the tracer particles (test G) did not lead to a change in the response of the reactor on the pulse injection.

A detailed analysis of the RTD function $E(\theta)$ results in further parameter variations, confirming the observation of non-ideal mixing of the bed at low fluidisation velocities. It can be concluded that dead or less active regions in the bed exist at the low fluidisation velocities considered for the prototype. These are most likely located close to the distributor plate in between the gas discharge holes but primarily in the annulus of the conical sections. The latter is also consistent with visual observations made during the test program. In the case of increasing the fluidisation velocity and decreasing the particle diameter, similar to that reported by Rivière et al., (1996), the particle mixing improved and the stagnant zones reduced.

Mathematical modelling of the residence time distribution

Based on the experimental findings a mathematical model of the mixing process within the fuel reactor was developed. It was found that with typical one or two parameter models (e.g. completely stirred tank reactor, fractional tanks in series with and without bypass (Stokes and Nauman, 1970) the experimental curves could not be reproduced. Instead, an approach was chosen to develop a phenomenological model including a split into several zones and mass transfer mechanisms based on empirical correlations for fluidised beds.

The model (Figure 4-23) comprises a split of the reactor into three zones. The actual fluidised bed is divided into a bubbling bed, a stagnant zone, and a freeboard section located above. Each zone is modelled as continuous stirred tank reactor and the solids flux is divided into two flows passing the freeboard and the fluidised bed respectively. The existence of the stagnant zone is justified by visual observations and pressure measurements. The conical sections in the reactor lead, at the low fluidisation velocities, to an uneven velocity profile (Olazar et al., 1995) and thus, the fluidisation gas is passing the conical region equal to a fixed bed. The good solids mixing caused by the upward movement of bubbles, which is typical for fluidised beds, is absent in this zone. Also, the general flow pattern of the emulsion movement of the bubbling bed is very weak and cannot agitate an intensive solids movement of the conical section.

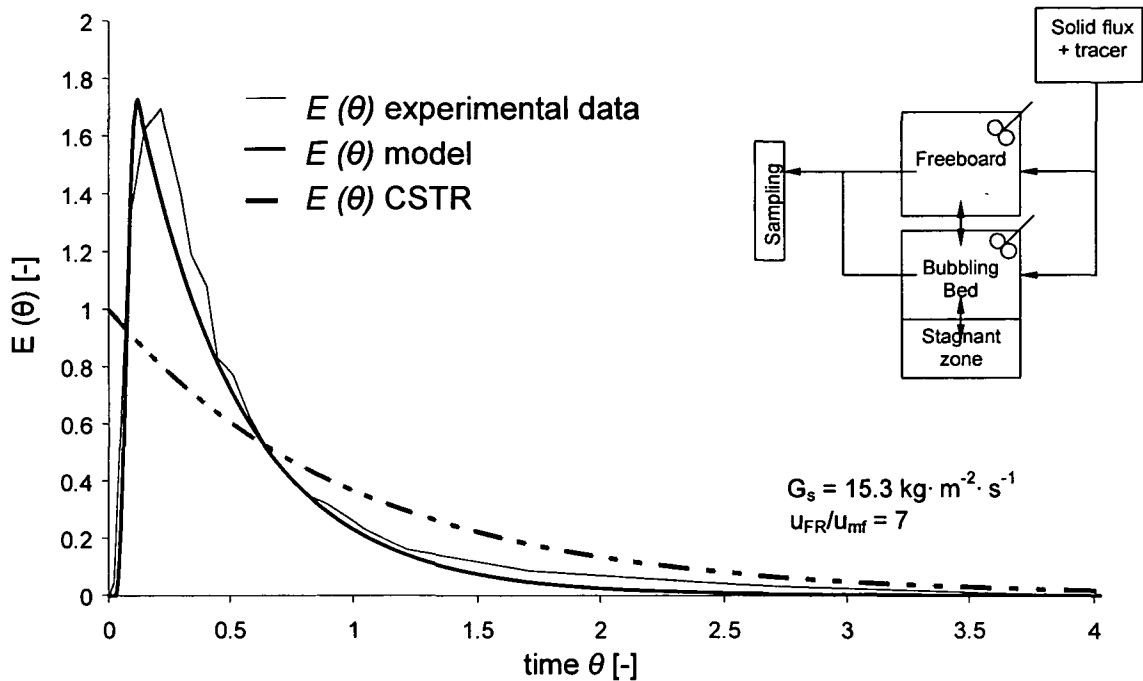


Figure 4-23. Comparison for RTD between of experimental results and model for run B.

Mass transfer between different zones is included in the model. The solids exchange between the freeboard and the bubbling bed is modelled as the particle entrainment. As the solids are ejected by the bursting bubbles, it is reasonable to assume the ejection flux to be proportional to the bubble flow. According to George and Grace (1978 this gives:

$$E_0 = \xi \cdot \rho_p \cdot (1 - \varepsilon_{mf}) \cdot Y \cdot (u - u_{mf}) \quad (4-14)$$

where the factor ξ is the volume of ejected particle to the bubble volume, which Geldart (1985) recommends to be 0.1. Y is the correction factor for the two-phase theory. The mass transfer between the freeboard and the bubbling bed resulting from (4-14) is in the range of the solids circulation rate between 10 to 30g·s⁻¹.

In addition to the physical phenomena involved, influences from the measurement procedure were also considered. A significant effect was expected for the injection pulse duration and the time delay and duration of sampling. Reasonable estimations were based on the experience during the experimental phase.

The resulting number of parameters allows the determination of meaningful values for modelling the behaviour of the reactor. The three undetermined model parameters, i.e. the fractions of each zone, the mass transfer between the stagnant zone and the bubbling bed, and the solids flux split were fitted to the experimental values by minimizing the RMS (root mean square) deviation between experimental and model values of $F(\theta)$ at each interval of time. The RMS deviation σ is given by (4-15) and the deviation is minimised with respect to the undetermined parameters.

$$\sigma = \left[\frac{1}{M} \sum \{F(\theta)_{\text{exp}} - F(\theta)_{\text{model}}\}^2 \right]^{\frac{1}{2}} \quad (4-15)$$

Good agreement between model predictions and test results could be found for the RTD function as presented for test run B in Figure 4-23. For comparison purposes the RTD curve of the CSTR is also given. In all test runs an exponential function was used to add data for response times greater than θ to the experimental value. It is assumed that the approximation by an ideal mixer does not insert a big error. Mass fractions and solids flux in each reaction zone were determined and sensitivities on operating conditions established.

The most interesting outcome of this analysis is that a significant mass fraction is not involved in the mixing process in the reactor. Figure 4-24 shows model results for the variation of the reactor fluidisation and a clear tendency towards a decreasing stagnant zone with increasing gas flow rate. Also, the bed mass in the freeboard zone was identified as significant and in average between 50 and 90% of the bed mass is ideally mixed in the bubbling bed or freeboard for the considered operation range. No dependency on other operating conditions such as the solids flow could be determined and it is concluded that solely the fluidisation velocity is determining the fractions of the zones.

The mass transfer between the bubbling bed and the stagnant zones was found to be small, in the range of the elutriation of the bubbling bed into the freeboard. For the solids flux split between freeboard and dense zone no clear tendency was observed but it was determined to be about 10% of the total solids circulation.

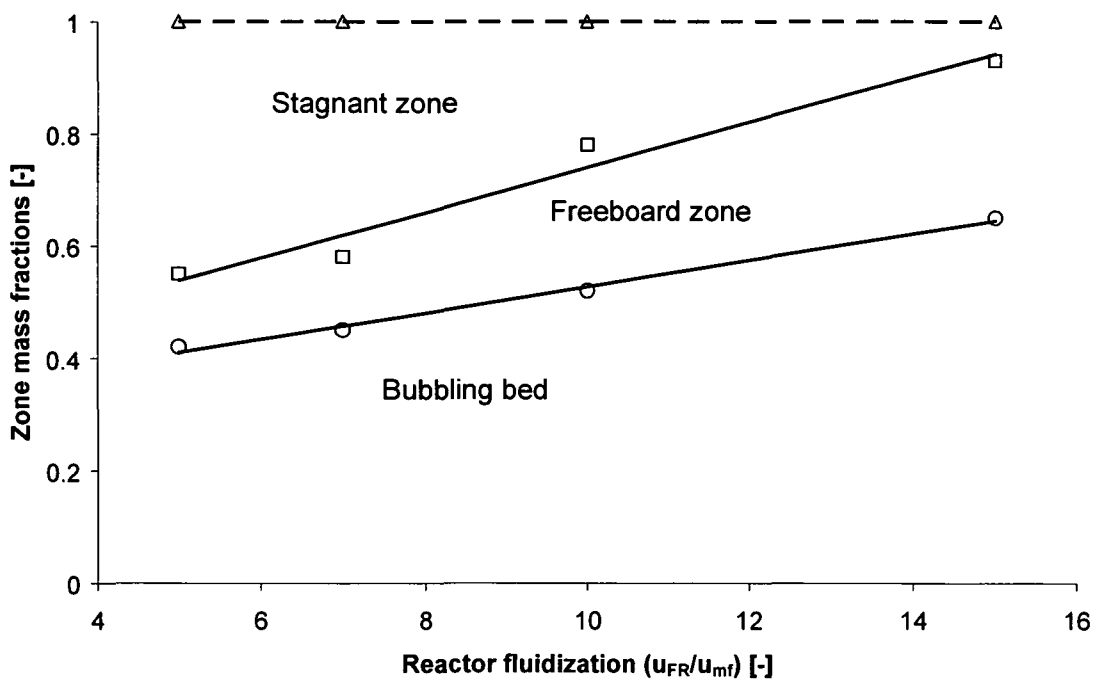


Figure 4-24: Mass fractions of reactor zones vs. reactor fluidisation for different solids circulation rate

Conclusions of RTD transfer into hot modelling tests

Although appropriate scaling criteria for fluid dynamic similarity were used for the design of the model it is clear that the volume increase occurring during CH₄ combustion could not be represented. Also, the gas properties change across height in the prototype fuel reactor hinders the direct transfer of the flow model results to the prototype unit.

Kinetic modelling results of Adanez et al., (2003) and Kronberger et al. (2004) show that about half of the gas conversion in the bubbling bed occurs close above the gas distributor plate because of the highest rates of reaction and high gas-solid mass transfer in this region. Therefore it is suggested that as approximation the ratio u/u_{mf} is twice for equivalent conditions in the fuel reactor of the hot unit, which gives a stagnant zone fraction of up to 20%.

The measurement and modelling of the solids residence time distribution in the flow model of a chemical-looping fuel reactor showed significant stagnant zones in the conical sections. It is important for the evaluation of the prototype test runs to know the actual solids conversion and together with the kinetics this information is used for validating kinetic fuel reactor models and for analysing further operating parameter variations of the chemical-looping combustor.

4.4.8 Design of bench-scale unit and operation results

The entire CLC prototype unit installation scheme is presented in Figure 4-25. The set-up is equipped with measurement instrumentation, monitoring and data collection with pressure transducers, thermocouples, and mass flow controllers. The following gases are supplied to the unit: inert gases for the loop seals (2, 4), methane as fuel gas (3) and air (5) for the oxidation reactor where the latter is preheated by an electrical heater (6). The gas exit flows are passing a free convection cooling section (8). Additionally, the air reactor temperature can be automatically controlled by cooling air, which is fed to a jacket surrounding the air reactor. The fuel reactor temperature can be adjusted with the heating coils (7). Two large filters (9) are installed to achieve a low pressure drop of the air reactor exit train to the chimney (10). Manual switching during operation enables the measurement of elutriation over a chosen time period. A water trap (1) with adjustable water level is used to control the pressure balance between the reactors (air reactor and cyclone vs. fuel reactor). The water seal has an overflow exit and also acts as a condensate trap for the humid gas from the fuel reactor, as well as a particle trap.

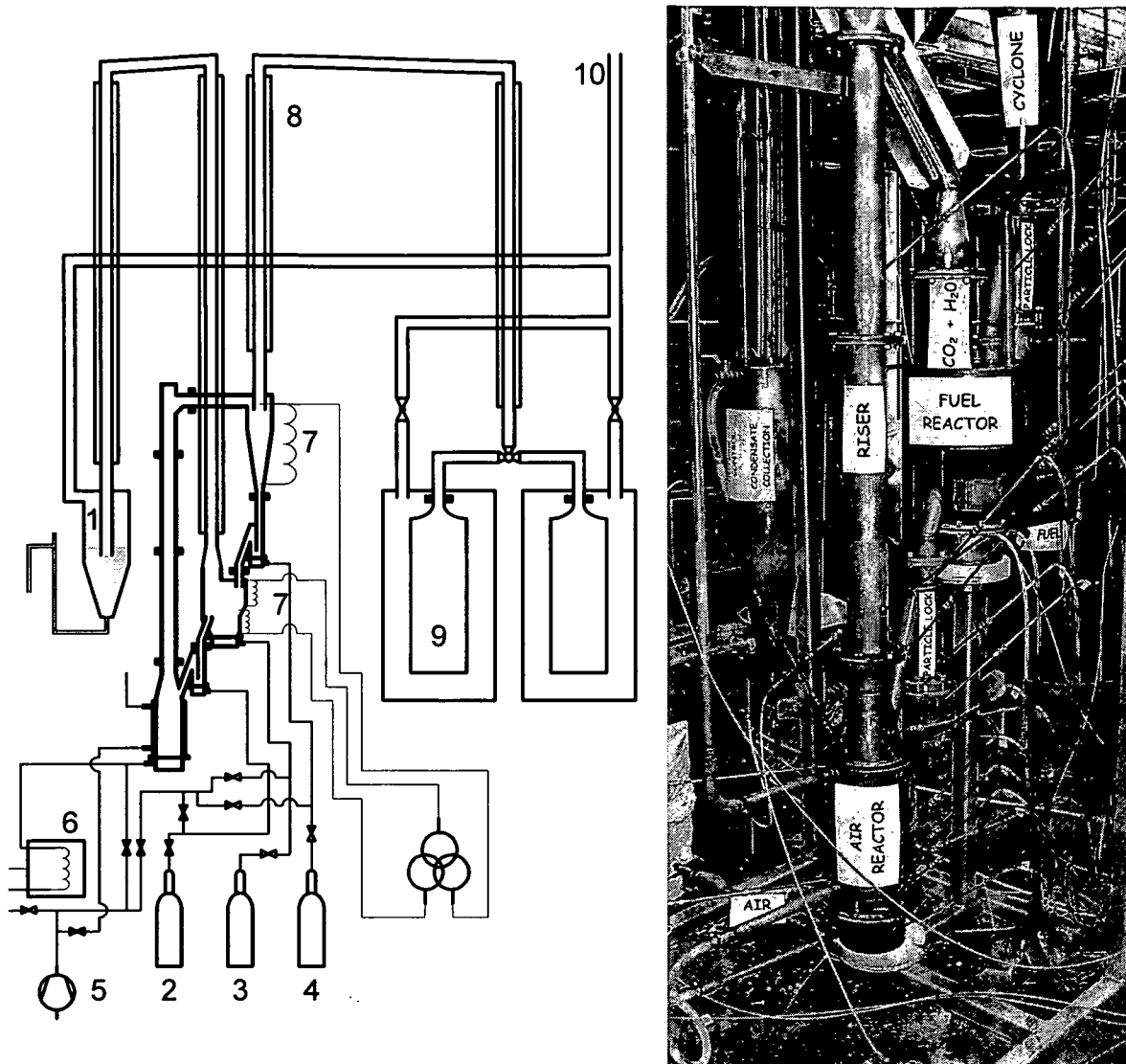


Figure 4-25: Drawing and photograph (Lyngfelt et al.,2004b) of prototype reactor test set-up (1) water trap, (2) nitrogen (3) fuel gas, (4) argon, (5) air, (6) preheater, (7) heating coils, (8) finned tubes for cooling of gas streams, (9) filters and (10) connection to chimney.

Operation of the bench scale unit over several hundred hours at Chalmers University by Lyngfelt et al. (2004) proofed the concept of chemical-looping combustion at continuous operation mode. In Figure 4-26 it can be seen that at the start of the process (at time 12200s) immediately almost complete conversion of the fuel gas (CH_4) is achieved. Simultaneously, the oxygen concentration at the AR outlet decreases to about 8% and small concentrations of CO (and H_2 , not shown in Figure 4-26) are measured at the FR outlet. The latter is mainly a consequence of the thermodynamic equilibrium as shown in section 3. The most important findings of the bench scale operation can be summarised as follows:

- no significant coke formation observed
- very low gas mixing between air and fuel reactor
- 99.5% fuel conversion (LHV based)

- almost 100% CO₂ capture

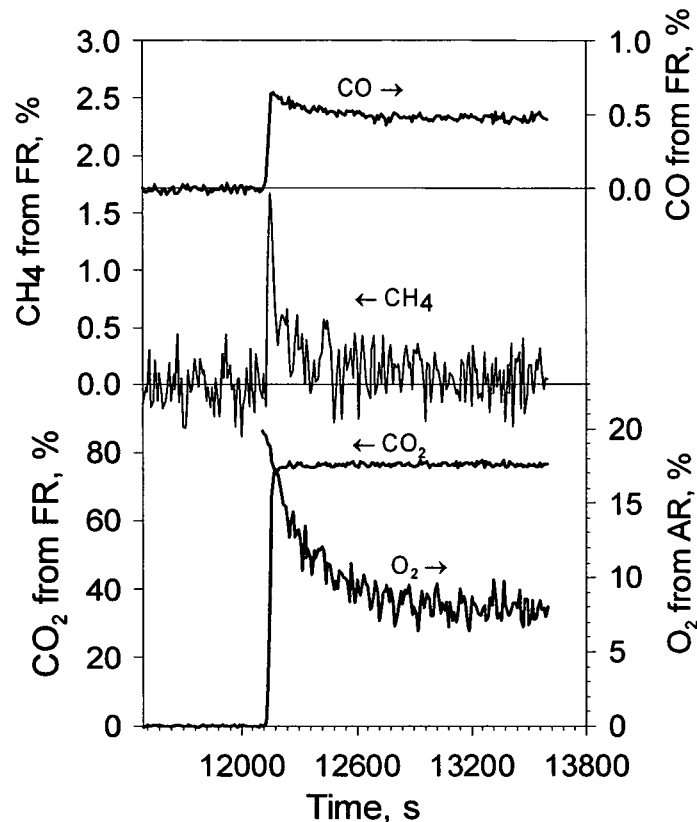


Figure 4-26: Gas concentrations at AR and FR outlet during chemical-looping combustion mode (Lyngfelt et al.,2004b)

4.5 Pilot and large-scale unit

4.5.1 CFB system description

The CFB experimental rig used in the present work is (see Figure 4-27) a cold flow model of a demonstration scale CLC plant. It consists of a 1.18 m high rectangular riser with inner dimensions of 0.105 m by 0.160 m. Experiments were conducted at ambient temperature and pressure. The fluidisation gas used in all experiments was air, and bronze powder with 54 μm mean particle diameter and 8750 $\text{kg}\cdot\text{m}^{-3}$ density was used as bed material. This gas/bed material combination resulted from downscaling of a pre-demonstration scale CLC power plant (2 MW_{th}) applying scaling criteria of Glicksman (1993). In general the design in Figure 4-27 follows a “close to real system” approach. It includes for the large-scale CFB unit specific features like air staging (secondary air injection) for better control of the solids circulation rate and advanced loop seal designs for the prevention of gas mixing between the two reactors. The solids return into the riser is designed such that it can be used to increase the solids residence time in the air reactor and is therefore referred as air reactor in Figure 4-27. The fuel reactor design is simplified as in a large scale unit an internal solids circulation system should be applied to allow high gas velocities. This is not influencing the overall fluid dynamic behaviour of the flow model. A detailed discussion of this

issue can be found in section 7. A summary of property data and dimensions of the cold flow model is given in Table 4-9.

Table 4-9: Data of cold flow model and pilot scale plant

	cold flow model	pilot scale plant	unit
riser dimension (L x W x H)	0.105 x 0.16 x 1.18	0.7 x 0.45 x 5	m
FR dimension ((L x W x H)	0.09 x 0.11 x 0.15	0.43 x 0.5 x 0.65	m
AR dimension (L x W x H)	0.09 x 0.08 x 0.15	0.43 x 0.4 x 0.4	m
bed-material	bronze powder	oxygen carrier	
d_p	54	119	μm
ρ_p	8750	2250	$\text{kg}\cdot\text{m}^{-3}$
ρ_g	1.28	0.3	$\text{kg}\cdot\text{m}^{-3}$

The operating superficial gas velocity of the riser, u_{RIS} , and mean solids flux, G_s , are $1.6 - 3 \text{ m}\cdot\text{s}^{-1}$ and up to $100 \text{ kg}\cdot\text{m}^{-2}\cdot\text{s}^{-1}$, respectively. The fuel reactor operating regime for the pre-demonstration at 2MW_{th} scale was selected to follow a turbulent regime u_{FR} about $1\text{m}\cdot\text{s}^{-1}$. Because of simplicity reasons, however, this was not directly scaled to the flow model but a lower velocity was chosen. Omission of particle separator at the fuel reactor exit was compensated by installation of a valve for simulation of the gas-solid separator pressure drop and its effect on the system behaviour. The loop seal fluidisations were all set to 1.5 times u_{mf} but variations were carried out for optimisation of the gas leakage. For the gas distribution in the riser a perforated plate with 30 holes (6 mm in diameter) was used. The loop seals, air reactor, fuel reactor, and loop seals were fluidised through porous glass plates.

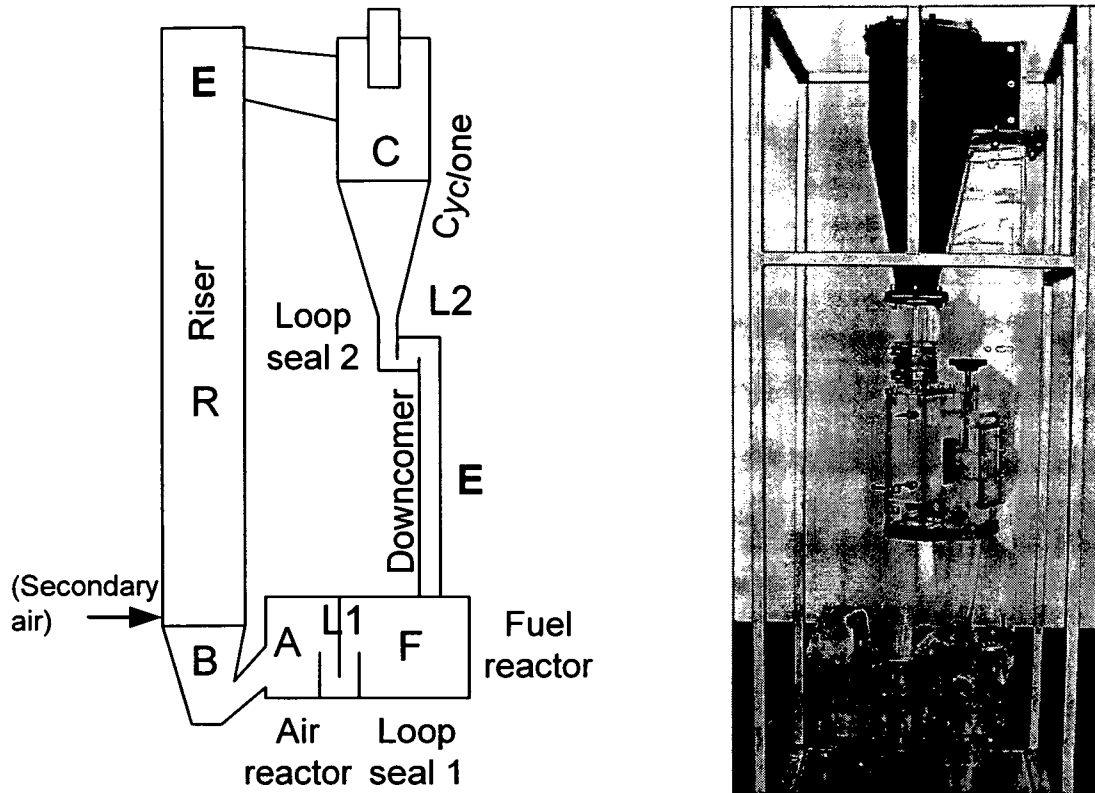


Figure 4-27. Schematic diagram of flow model.

4.5.2 Experimental programme

Experiments were carried out by variation of the total riser fluidisation flow and the air staging at the bottom and secondary gas inlets. Additional variations were done with the solids inventory of the fluidised bed system (Table 4-10). Variations on the fuel reactor velocity and the geometry and fluidisation of the loop seals between stationary bed and the riser were carried out for detailed analysis of the component fluid dynamics as presented in the modelling section. For the results presented in this study they were kept constant at the values mentioned earlier.

Table 4-10: Experimental programme

Parameter	Variaton range	Unit
Superficial riser velocity (transport zone) (u_{RIS})	1.66 – 2.74	$m.s^{-1}$
Secondary air fraction	0 – 85	[%]
Total solids inventory (TSI)	14- 20	[kg]

4.5.3 Experimental results for solids circulation and gas leakage

Solids circulation rate

In the current CFB system adjustment of the solids flux for part load behaviour can be achieved by variations of the air staging, i.e. the ratio of bottom air to secondary air flows.

Since the superficial velocity in the riser section above the secondary air injection is significantly higher than the terminal velocity of particles in all test series, conditions in the riser are assessed as being fast fluidised (Bi and Grace, 1995). Therefore, a strong influence of the riser superficial fluidisation gas velocity on the solids circulation rate can be expected.

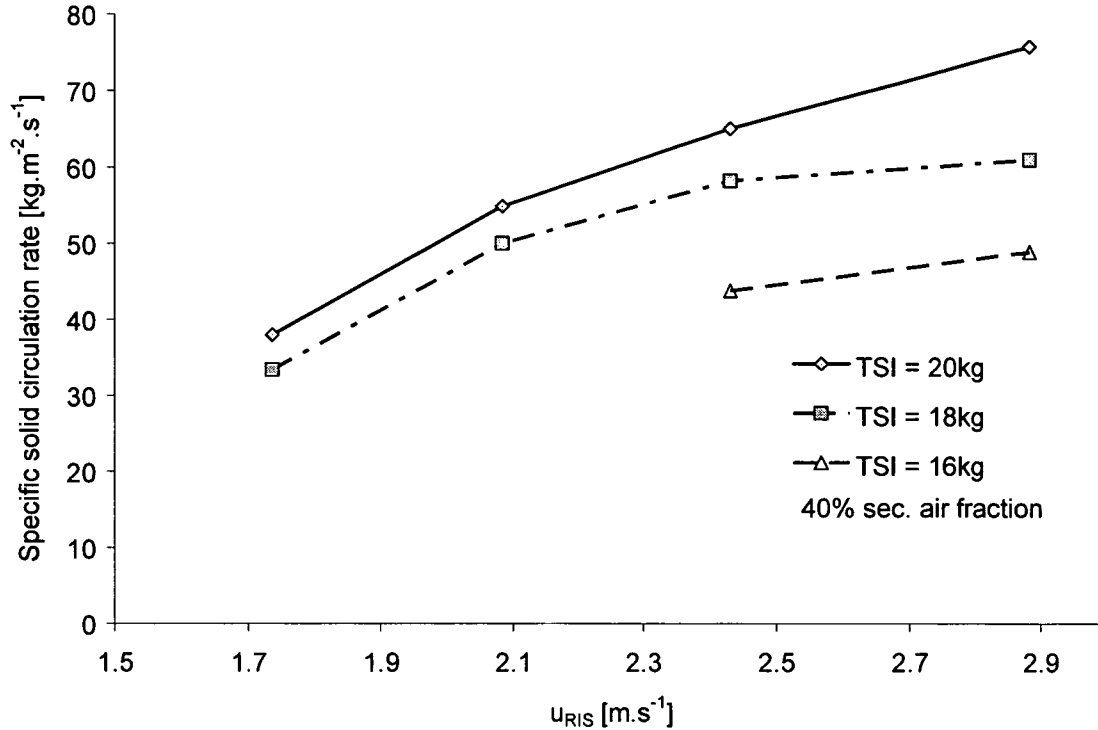


Figure 4-28: Specific solids circulation rate vs. fluidisation gas velocity in the riser for different total solid inventories (TSI)

The graph in Figure 4-28 shows that the solids circulation rate is influenced by both the gas velocity in the riser and the total solids inventory. However, the increase was lower than expected and this can be explained by the fact that due to higher solids flux bed material is accumulated in other components of the CFB-system. In the downcomer of the cyclone it is caused by higher flow resistance of the loop seal at higher solids flow rates. Therefore, the material inventory and the return flow at the bottom of the riser are reduced and the solids circulation rate is limited. This tendency is also confirmed by the results of Figure 4-29 where the enhancement of total solids inventory at constant gas velocity is represented.

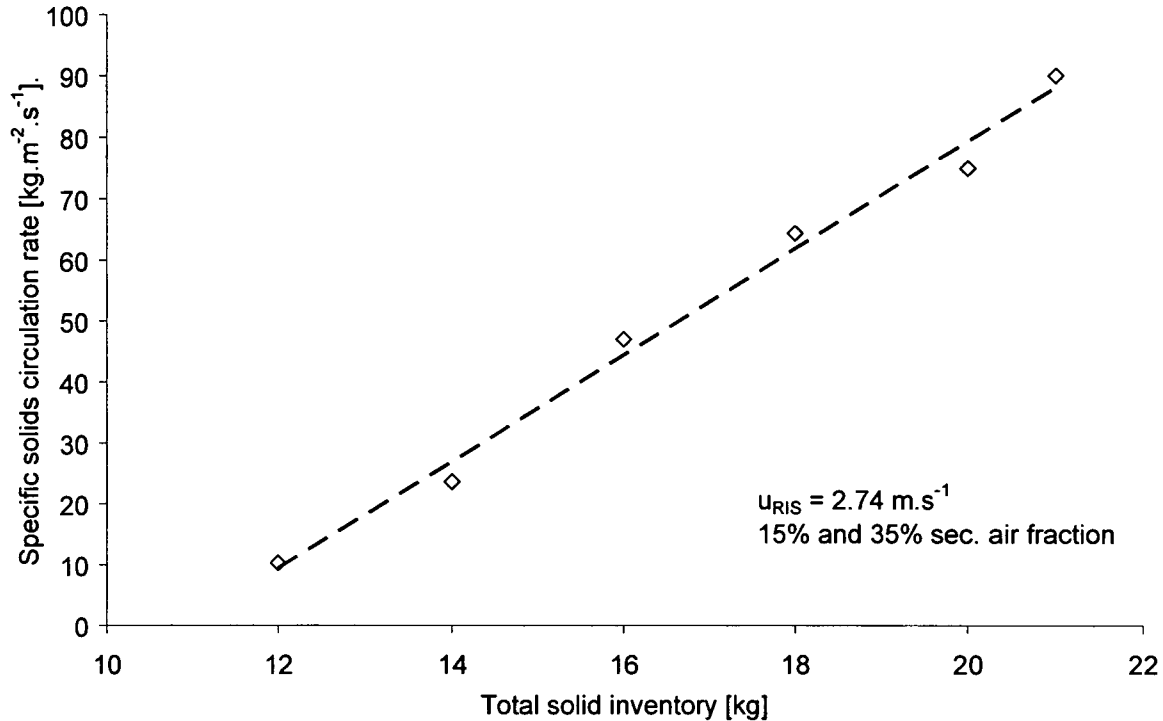


Figure 4-29: Specific solids circulation vs. total solid inventory (TSI)

The use of secondary air is essential for process control and adjusting the fluidisation to changed conditions given by part load behaviour or off-design operation e.g. for control of the heat transfer (Morin and Beal, 2004). The influence of this parameter must be well understood and the experimental results of the correlation of solids circulation rate and secondary air fraction are represented in Figure 4-30 for different TSI-values. Up to a secondary air fraction of about 45% the solids circulation rate is nearly constant and then decreases rapidly until the solids flow reaches zero at about 90% secondary air fraction. During experimental work it was visually observed that the latter occurs when material accumulation happens at the bottom zone at low bottom gas velocities close to terminal velocity. Material accumulation in the bottom part reduces the solids mass in the transport zone of the riser, which in turn also reduces the solids circulation rate.

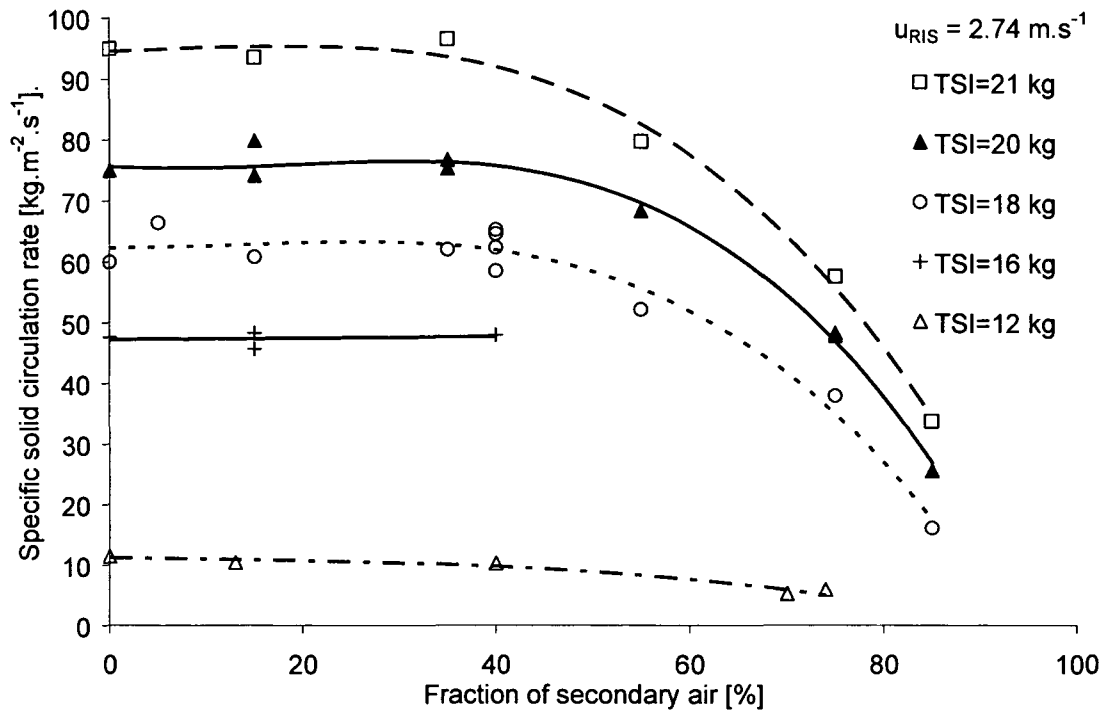


Figure 4-30: Specific solids circulation rate for various secondary air fractions and total solid inventories (TSI)

In addition to the riser velocity and the split into bottom and secondary air, the effect of variations of the fuel reactor and loop seal fluidisations in the CFB system were analysed. A small rise of solids flux with increasing fluidisation (velocities) of FR and loop seals was expected, which would lead to a higher voidage in these units, a larger amount of solids in the riser and thus, a higher circulation rate. However, the small changes are within the measurement accuracy of the experiments.

Gas leakage and split factor measurement

The study of gas mixing is more important for large-scale concepts than for the laboratory systems. To this end, two criteria are used for quantitative assessment:

- Since gas mixing and dilution in particular of the fuel reactor exit stream should be prevented, it is important to know the flow direction of the fluidising gas of the loop seal. The split of loop seal fluidisation volume flow in and against the flow direction of the solids into the fuel reactor is termed "split factor" (4-16).

$$SF = \frac{\dot{V}_{LS,FR}}{\dot{V}_{LS}} \quad (4-16)$$

- The gas-leakage is the amount of fluidisation gas of one reactor that leaves the system, mixed with the other gas flow through a second reactor exit. In the current work, the gas leakage is expressed in terms of absolute volume flow values.

Acceptable operation can only be obtained as long as the pressure difference is below a value determined by the solids column in the bed of the loop seal. This can be guaranteed by adjustment of a valve mounted at the FR-exit, which also simulates the pressure drop of a particle separator that is required for a hot unit. Variations of solids flow and fluidisation velocities (of both loop seals and the fuel reactor) have been carried out. Information about measurement methods have already been given in chapter 4.2. and the results are presented below.

Split factors of the loop seals

Although the volume flow in the loop seal is low compared to the total volume flow in the fuel-reactor, split factors have an effect on the systems efficiency. Any dilution of the "product" stream CO_2 causes an extra effort for the CO_2 separation step downstream of CLC. For this reason it is important to know the influencing factors and the extent of dilution of the flue gases.

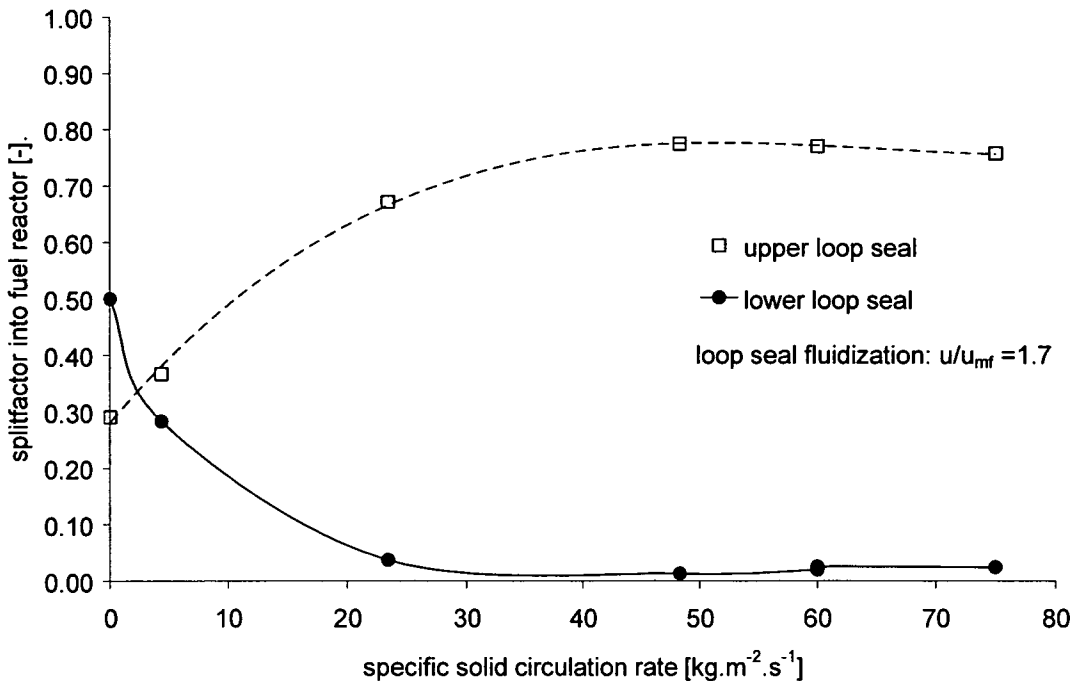


Figure 4-31: Split factors of the loop seals into the fuel reactor

In Figure 4-31 the split factors of both loop seals are represented as a function of solids circulation rate. For the lower loop seal, a split factor of 0.5 is determined at zero solids circulation, which means that equal amounts of gas leave the seal through the standpipe and the downcomer. It is decreasing with increasing solids flow down to an almost constant value of about 0.02. The main reason for this is that gas is carried with the solids and also the higher solids column in the downcomer reduces the gas flow passing it. The upper loop seal shows reverse behaviour and only reaches a value of 0.3 at zero flux, which is due to the construction of the upper loop seal. Since there is a short circuit to the bottom of the riser

part of the gas is leaving the loop seal this way and in the entire range of operating conditions only about 75% to 80% is entering the fuel reactor.

It can be seen from the results for the lower loop seal that starting at a solids circulation rate of about $30 \text{ kg}\cdot\text{m}^{-2}\cdot\text{s}^{-1}$, the function of the loop seal reaches nearly 100% and thus it might not be necessary to use a specific inert fluidisation gas for this unit.

Generally speaking both loop seals show very similar behaviour and under these operating conditions, the graphs can be used for optimising the loop seal fluidisation velocities and finally the CO_2 -capture efficiency.

It is primarily assumed that gas leakage is proportional to the interstitial gas flow and therefore to the solids circulation rate. In Figure 4-32 the gas leakage is shown as a function of solids circulation rate. Evaluations are made for one loop seal and no significant difference between the two loop seals is assumed. The data points are mean values of two measurements.

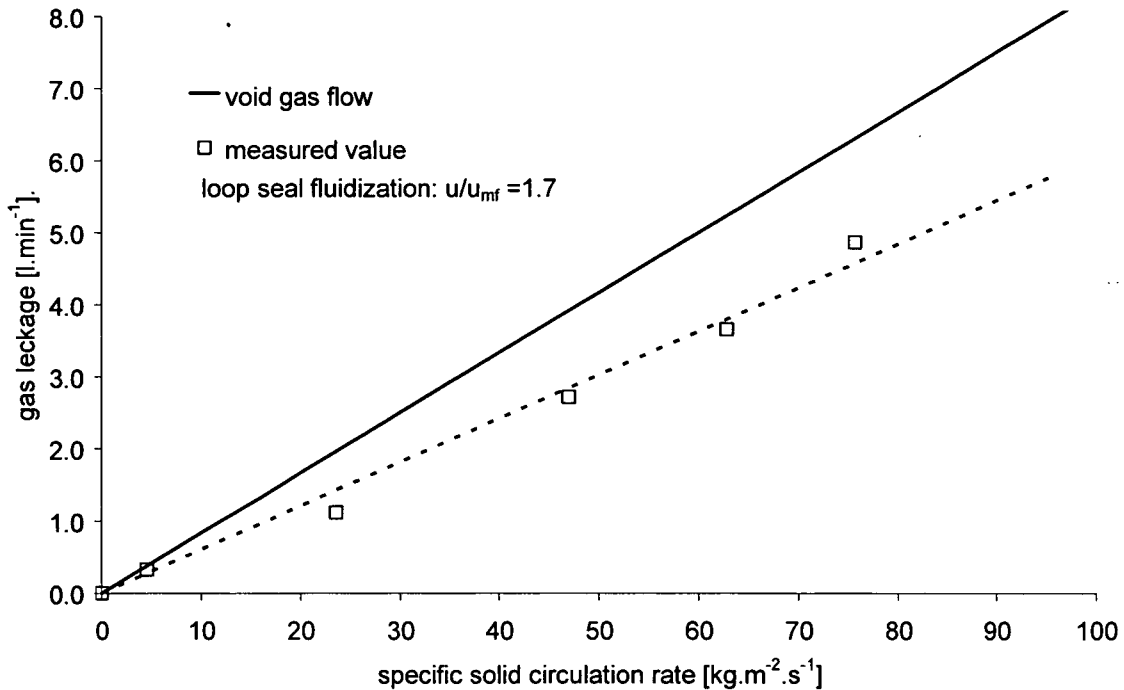


Figure 4-32: Gas leakage for the fuel reactor vs. specific solids circulation rate

The upper line shows the computed leakage, assuming that the entire interstitial volume consists of gas from the fuel reactor and therefore represents a maximum value. For this calculation a voidage at minimum fluidisation conditions is assumed. The gas leakage is lower than the interstitial gas flow and the strong correlation with the solids circulation rate can be verified. The reason for the proportional factor between the prediction and the measurement values is most likely a stripping effect of the upstream gas flow.

5 Mathematical modelling of fluid dynamics of CLC reactor systems

In this study the CFB fluid dynamics of the large-scale concept unit described in chapter 4.5 are presented. For the riser a type ii)-model (axial and radial variations by assuming two or more regions) is applied because, as mentioned by Pugsley and Berruti (1996), these are best suited as design tools and they can easily be coupled with reaction kinetics to study the performance of the reactor. For the global CFB loop a type i)-model (based on experimental data) was chosen. For the intended application as an instrument supporting design and scale-up the reduction of generality is less disadvantageous. In this chapter details of the mathematical model and the simulation results are presented.

5.1 Global model description

Input parameters for the global model are fluidisation conditions (volume flows, temperature, total mass load, secondary air injection etc.), physical material properties, and geometry data of the system. After calculation of the riser solids flow and pressure drop these values are used to calculate pressure drop and solids inventory consequentially for each CFB loop component. Mass and pressure balances are used to connect the components of the system to each other and therefore adjust the values in an iterative procedure. This loop calculation (Figure 5-1) is stopped when mass and pressure balances for the loop are converged and deviation is within a given increment.

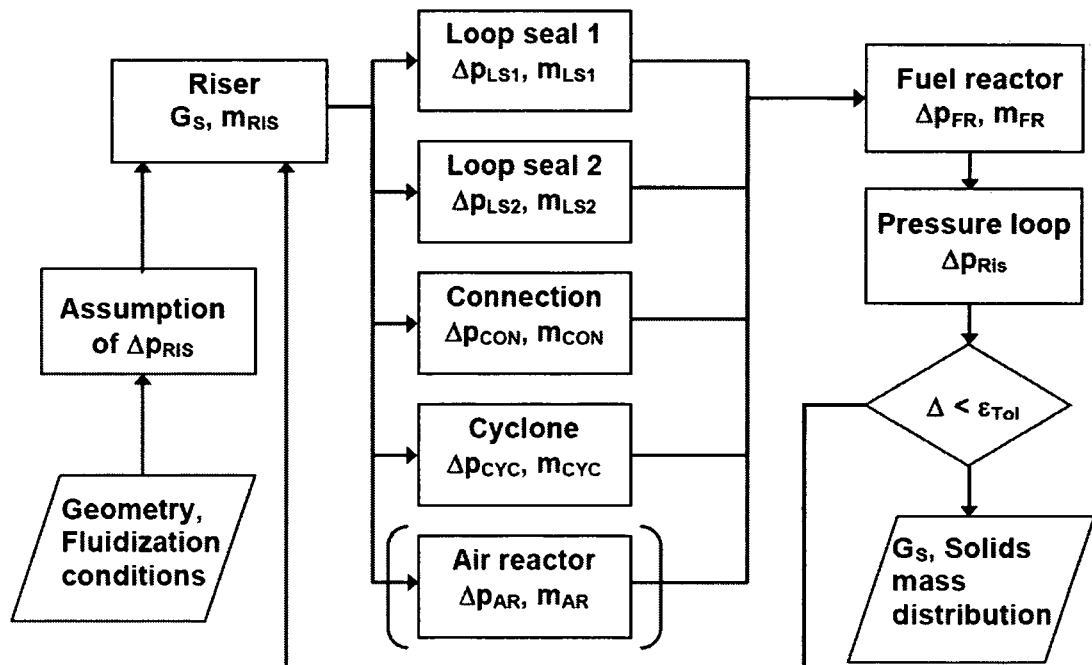


Figure 5-1: Structure of the program

5.2 CFB-components models

5.2.1 The riser model

Transport zone

The fluid dynamic model for the riser used in this study was developed based on the assumption of a core-annulus flow structure as e.g. proposed by Pugsley and Berruti (1995) and Bader, Findlay and Knowlton (1988). The solids flow structure of the transport zone is formed by a dilute core zone, an upward solids flow, and a dense annulus (a downward solids flow at the riser walls). The gas is assumed to flow upward only in the core region.

The downward solids velocity in the annulus was assumed constant, similarly to Adanez et al. (1994, 1995a, b). Its influence on the overall model is small, as demonstrated by Kaiser et al., (2003). By equal reasoning the voidage in the annulus was kept constant for all conditions and heights at the minimum fluidisation voidage.

The upwards solids flow velocity in the riser was determined on the basis of a force balance of a single particle. In comparison to the common assumption of a constant velocity formed by the difference of gas velocity and a slip velocity - often the terminal velocity - this allows a physically meaningful calculation in acceleration regions due to secondary gas injection or changes in cross section. According to Pugsley and Berruti (1996) the drag coefficient determined by the standard drag for particles can be an overestimation. Therefore for particle Reynolds numbers in the range of $0.3 < Re_p < 1000$ the calculation of C_D is based on previously calculated results in the transport zone according to (5-1):

$$C_D = \frac{K}{Re_p^{0.6}} \quad (5-1)$$

whereby K follows from the force balance of the single particle at constant velocity as:

$$K = \frac{4 \cdot g \cdot (\rho_g - \rho_p) \cdot d_p \cdot Re_p^{0.6}}{3 \cdot \rho_g \cdot \left[\left(u_g / \frac{C_D}{\varepsilon^n} \right) - u_{s,c} \right]^2} \quad (5-2)$$

The axial mean voidage profile in the transport zone is calculated according to the exponential voidage profile correlation as proposed by Zenz and Weil (1958) and Johnsson (1991) and Wein (1992) have been adopted.

$$\frac{\varepsilon(h_i) - \varepsilon_\infty}{\varepsilon_0 - \varepsilon_\infty} = \exp[-a \cdot (h_i - h_0)] \quad (5-3)$$

The decay factor "a" in equation (5-3) varies widely in literature. Löffler et al. (2003a) have compiled values between 2 and $6.4m^{-1}$. Kunii and Levenspiel (1991) suggest that the product of "a" and "u" is constant and only a function of particle size (5-4).

$$a \cdot u = \text{const.} = \begin{cases} 2 \sim 5 \text{ s}^{-1} & \text{for } d_p < 70 \mu\text{m} \\ 4 \sim 12 \text{ s}^{-1} & \text{for } d_p > 88 \mu\text{m} \end{cases} \quad (5-4)$$

This assumption was found to cover well the experimental results of this study and the value of 4 s^{-1} for a mean particle diameter of $54 \mu\text{m}$ also follows their suggestion.

The second parameter for determining the axial voidage profile according to (5-3) is the voidage above TDH ε_∞ . The value can be determined from the particle elutriation rate constant $K_{i,\infty}$ for a mono-sized bed material according to (5-5).

$$\varepsilon_\infty = \frac{K_{i,\infty}}{\rho_p \cdot (u_g - u_t)} \quad (5-5)$$

In literature numerous correlations for $K_{i,\infty}$ can be found with wide deviations. The evaluation of the experimental results of this study showed that the correlation of Geldart et al. (1979) (5-6) best fits this model.

$$\frac{K_{i,\infty}}{\rho_g \cdot u} = 23.7 \cdot \exp\left(\frac{-5.4 \cdot u_{t,i}}{u}\right) \quad (5-6)$$

The momentum balance for gas and solids in the transport zone (5-7), (Leretaille, 1999), was used to determine the pressure at each riser height. The terms on the right side of the equation are covering the solids acceleration, the hydrostatic head of solids and the wall friction of the two-phase flow.

$$-\frac{dp}{dh} = \left(\frac{d(m_{s,up} \cdot u_{c,s})}{dh} + \frac{d(m_{s,down} \cdot u_{a,s})}{dh} \right) + (1 - \varepsilon) \cdot (\rho_p - \rho_g) \cdot g + \frac{dp_{fric}}{dh} \quad (5-7)$$

The wall friction, covered by the term dp_{fric}/dh , was considered in the form presented in equation (5-8). The recommendation of Capes and Nakamura (1973) is applied for the friction coefficient f_s .

$$\Delta p_{fric} = \int_h^{h+dh} f_s \cdot \frac{u_{a,s}^2}{2} \cdot \frac{4}{D_h} \cdot \rho_p [1 - \varepsilon(h)] dh \quad (5-8)$$

Solving of the momentum balance (5-8) and consideration of the special situation in the section of enlarging cross section area results for given bottom solids concentration in a pressure profile of the riser. It was found that the momentum balance leads to high pressure drop recovery above the acceleration zone in the riser because the upward mass flow in the core diminishes. The resulting values are high and lead to significant differences between the predicted pressure profile and the model results. Therefore, pressure recovery has been eliminated justified by the assumption that a large momentum is transmitted to the riser wall and in particular to the hat-shaped exit

Exit zone

The T-shaped exit of the riser severely influences the solids hold-up. As Zheng and Zhang (1994, 1995) showed, exits can affect the fluid dynamics of the gas-solid two-phase flow not only in the vicinity of the exit but also for a considerable distance down the column. As the riser of the demo unit is very short this is even more important. The separation effect of the riser was implemented by using the approach of from Gupta and Berruti (2000). The concept is based on the definition of a reflection coefficient for the correction of the slip factor. The corrected slip factor (5-9) then allows the calculation of a corrected particle velocity at the exit zone, giving the net solids flux.

$$\psi_{corr} = \psi \cdot (1 + \eta_B) = \frac{u_{g,c}}{u_{s,c}} \cdot (1 + \eta_B) \quad (5-9)$$

The coefficient for the separation efficiency in equation (5-9) includes terms for the riser and exit geometry, the net solids flux, and the height at which the exit is located.

$$\eta_B = 0,00091 \cdot N_{Gs}^{-2,43} \cdot N_{Gst}^{2,02} \cdot N_{De}^{-1,54} \cdot N_{He}^{-2,8} \cdot N_{\alpha} \quad (5-10)$$

$$N_{Gs} = \frac{G_s}{(\rho_p \cdot u_0)}; N_{Gst} = \frac{G_s}{(\rho_p \cdot u_t)}; N_{De} = \frac{D_e}{D}; N_{He} = \frac{H - H_e}{H}; N_{\alpha} = \frac{\alpha - 45^\circ}{45^\circ} \quad (5-11)$$

Bottom bed

The momentum balance as given in (5-7) causes a situation where the entire upwards solids mass flux is accelerated at the height of the solids return, which results in a drastic overestimation of the dynamic gas pressure drop. Because of this and following the geometric situation of the riser a bottom zone was included. This allows a gradual increase of the mass flow to be accelerated at the bottom area of the riser. The model is based on work by Schlichthaerle et al. (1999).

The height of the bottom zone is assumed as equal to the height from the gas distributor to the solids return line. The flow structure in the bottom zone is assumed as core-annulus model with constant solids concentrations of annulus and core, respectively. The voidage profile decreases linearly between the conditions at the height of the solids return line to the bottom where no annulus exists. From this and equal assumptions for the solids velocities as stated above for the riser transport zone the mass fluxes for the bottom zone result.

Industrial CFB risers are often designed to have a bottom section with an increase of the cross section area. It has been observed during flow modelling that a solids accumulation occurs in this region. Few attempts exist in literature on such configurations, presumably because the effect is negligible in large-scale systems. It was shown by Schut et al. (2000) that such an increase in cross section strongly enhances the particle reflux and increases the thickness of the wall layer of down-flowing solids. Löffler et al. (2004a) conclude that the

reason for this behaviour is that particles are not able to follow the gas stream lines along the walls. Also visual observations of this study confirm that the region behind a certain angle consists of the downward solids flow of the annulus. In the present configuration the geometric angle of the inclined walls is 20° and the maximum angle where particles can follow the gas flow is determined by fitting the model to experimental data as 10° .

Results of riser model

The riser model described in the preceding section allows a complete calculation of the fluid dynamics of the riser from operating conditions and geometry data. The only input required is the total riser pressure drop, or the total riser solids inventory respectively, which is calculated from the solids hold up. All results presented are calculated without the change of any fitting parameter, and thus the model is characterised by full predictivity.

In Figure 5-2a) detailed results of the solids concentrations and the total pressure drop for the standard case of 35% secondary air fraction and a superficial riser velocity of $2.74 \text{ m}\cdot\text{s}^{-1}$ are shown and compared to experimental results. In Figure 5-2b) it is seen that the pressure profile can well be reproduced, which results also in agreement of the apparent solids concentration values in Figure 5-2a). The pressure profiles shown in this study are levelled to the measured pressure of the top experimental value, which is located at the height of the riser exit. In Figure 5-2a) the solids concentration of apparent, core, and annulus are depicted. It is remarkable that the apparent solids concentration and the mean solids concentration are equal already at a height of about 0.2 m. An analysis of the particle acceleration showed that the change of the cross section at the bottom zone gives very high gas velocities, resulting in a very high particle drag. The core concentration is lower than the mean solids concentration, which is a consequence of the exit effect. The annulus at the riser exit is not zero but equivalent to a flow predicted from the exit coefficient. Because the model is intended to be used as scale-up tool it should be mentioned here that scale-up of the exit effects needs to be done carefully as some authors (Lackermeier et al., 2002, Pugsley et al. 1997) conclude that the increase of the solids concentration near the exit is a scale effect only.

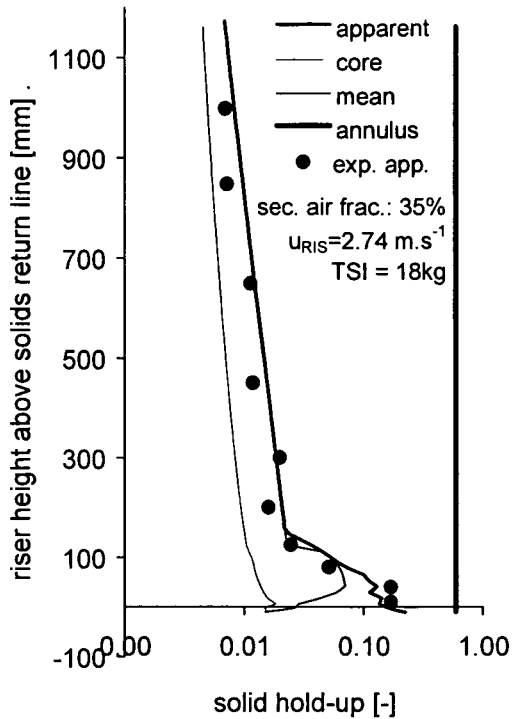


Figure 5-2 a)

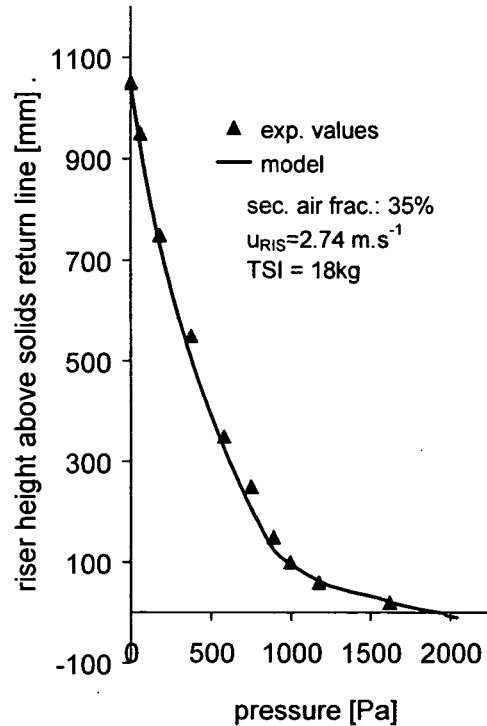


Figure 5-2 b)

Solids hold-up (a) and static pressure (b) vs. height for reference case ($u_{RIS} = 2.74 \text{ m.s}^{-1}$, 35% sec. air fraction, TSI = 18kg)

Figure 5-3a) and b) show comparison of model prediction and experimental values for variation of the riser velocity and secondary air fraction. For both figures, also the measured and predicted specific solids flow rates are given and it can be seen that all results agree. More deviation can be seen for the solids flow rates for variation of the secondary air fraction of the total riser fluidisation. The reason for this is the interaction between the secondary air injection and the change in cross section, which are located almost at the same height.

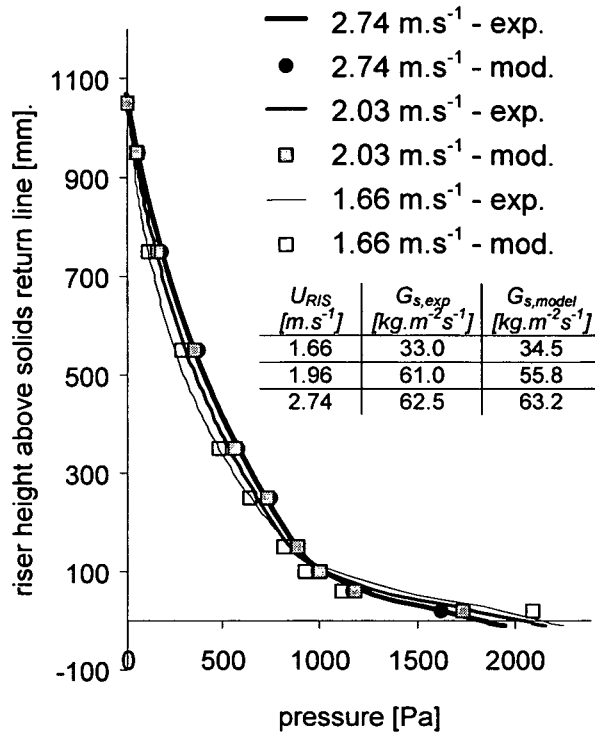


Figure 5-3: Riser pressure profiles for variation of u_{RIS} . (sec. air fraction = 35%, TSI = 18kg)

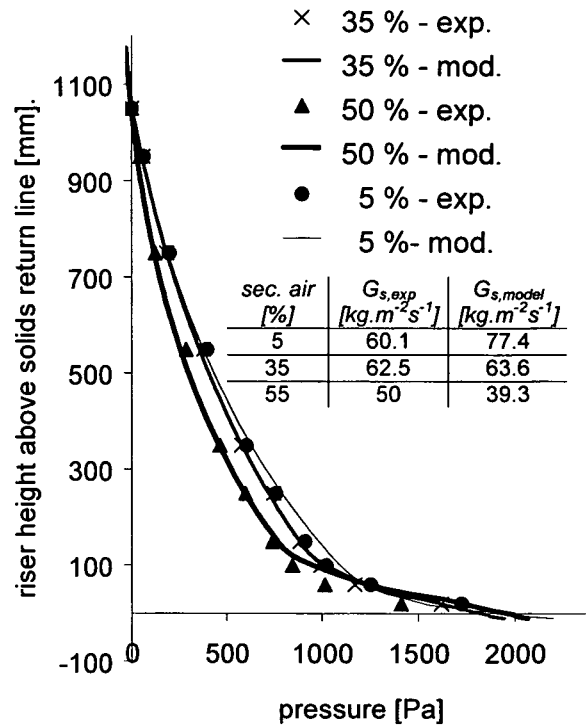


Figure 5-4: Riser pressure profiles for variation of sec. air fraction. (TSI = 18kg, u_{RIS} = 2.74m.s⁻¹)

Riser parameter mapping

The most important output of riser models is the correct prediction of the solids circulation flow rate. This can be seen in Figure 5-5 for the standard case conditions over a wide range of riser pressure drop and riser velocity values. A strong dependency of the solids flux on the riser pressure drop and the riser superficial velocity was found. Although Figure 4-28 shows the same tendency a direct comparison is not possible as for the simulations for the graph below only single parameters (Δp_{RIS} and u_{RIS}) were varied, whereas the experimental results were obtained for the riser when integrated into the overall CFB loop.

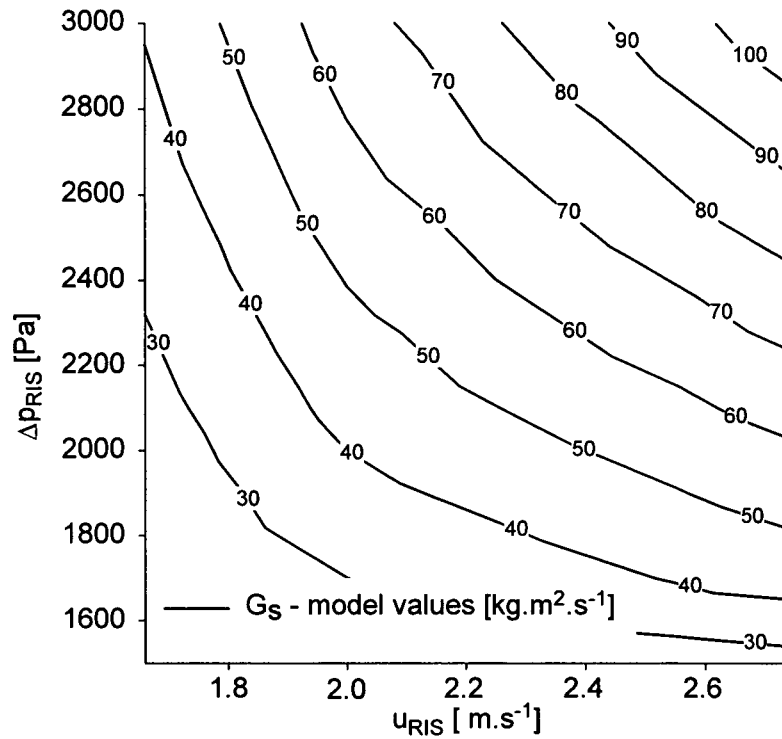


Figure 5-5: Parameter mapping for the riser model. (35% sec. air fraction)

5.2.2 Fuel and air reactor

The fuel reactor and the air reactor in the cold flow model are both designed to have a minimum bed height, which is required for securing the function of the bottom loop seal. The reactors are operating in the bubbling fluidisation regime and the fluid dynamics are described by the modified two-phase theory of Toomey and Johnstone (1952) and the correction factor according to Johnsson et al. (1991).

$$Y = \frac{0.26 + 0.7 \cdot \exp(-3.3 \cdot 10^{-3} \cdot d_p)}{(0.15 + u - u_{mf})^{0.33}} \cdot \left(h + 4 \cdot \sqrt{\frac{A}{n_0}} \right)^{0.4} \quad (5-12)$$

The bubbles are solids free and the mean voidage for the two-phase flow results as

$$\varepsilon_{TP} = \delta_b + (1 - \delta_b) \cdot \varepsilon_{mf} \quad (5-13)$$

with the minimum fluidising velocity following the correlation of Grace (1992) and the voidage at minimum fluidising conditions ε_{mf} the Ergun equation (Ergun, 1952). The bubble volume fraction is determined by using the bubble growth (Darton et al., 1979) and the single bubble rise velocity $u_{b,\infty}$.

$$\delta_b = \frac{1}{1 + \frac{1.3 \cdot (0.15 + u - u_{mf})^{0.33}}{0.26 + 0.7 \cdot e^{-3.3 \cdot d_p}} \cdot (u - u_{mf})^{-0.8}} \quad (5-14)$$

In addition to the bottom fluidisation of the fuel reactor, the fuel gas reaction with the metal oxide causes a change in the volumetric flow within the bed. In the case of methane combustion the molar gas flow increases by a factor of three. In the fuel reactor model this is taken into account and the additional volume flow of gas is distributed evenly along the bed height. The fuel- and air reactor are divided into discrete cells and the pressure drop and mass of each cell is determined based on the hydrostatic solids head of the cell.

5.2.3 Loop seals

Both loop seals were analysed in detail and each loop seal was split into three sections: i) downcomer (A), ii) horizontal flow section (B), iii) standpipe (C) (cf. Figure 5-6).

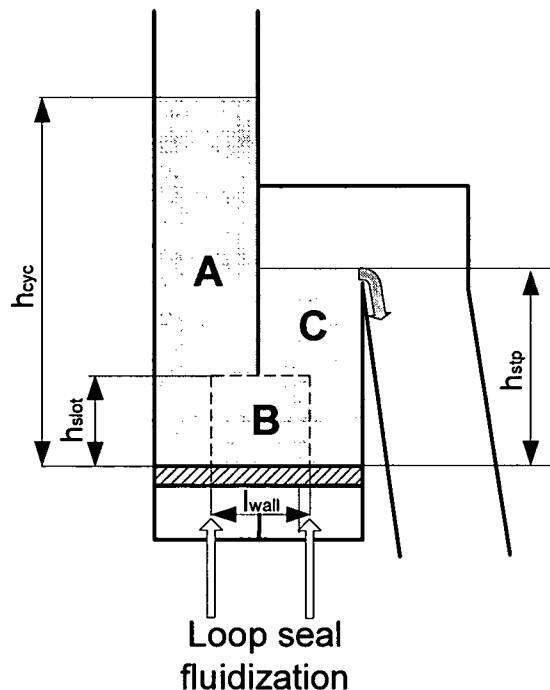


Figure 5-6: Loop seal design (schematic)

The pressure drop and mass content of the fluidised standpipe follows the two-phase flow model approach made for the fuel reactor as demonstrated above, (5-12) - (5-14), wherein h_{stp} is used for the bed height.

The pressure drop of the horizontal section is assumed to be determined by the solids wall friction of the solids particles moving at a velocity u_s and the viscosity of the two-phase flow. Hofbauer (1982) used such an approach and found good agreement to experimental values.

$$\Delta p_{HOR} = \lambda \cdot \frac{u_s^2}{2} \cdot \frac{A_{wall}}{A_{cross}} \cdot \rho_p \cdot (1 - \varepsilon_{LS}) \quad (5-15)$$

where λ is the material-specific friction coefficient. For laminar flow behaviour additionally the correlation in (5-16) is used. The geometric values used are shown in Figure 5-6. A_{cross} is the cross section of the slot and A_{wall} the surface generated by the bottom and the sidewalls of the horizontal section indicated with length l_{wall} .

$$\lambda \propto \frac{1}{Re} \Rightarrow \lambda = k_\lambda \cdot \frac{1}{u_s} \quad (5-16)$$

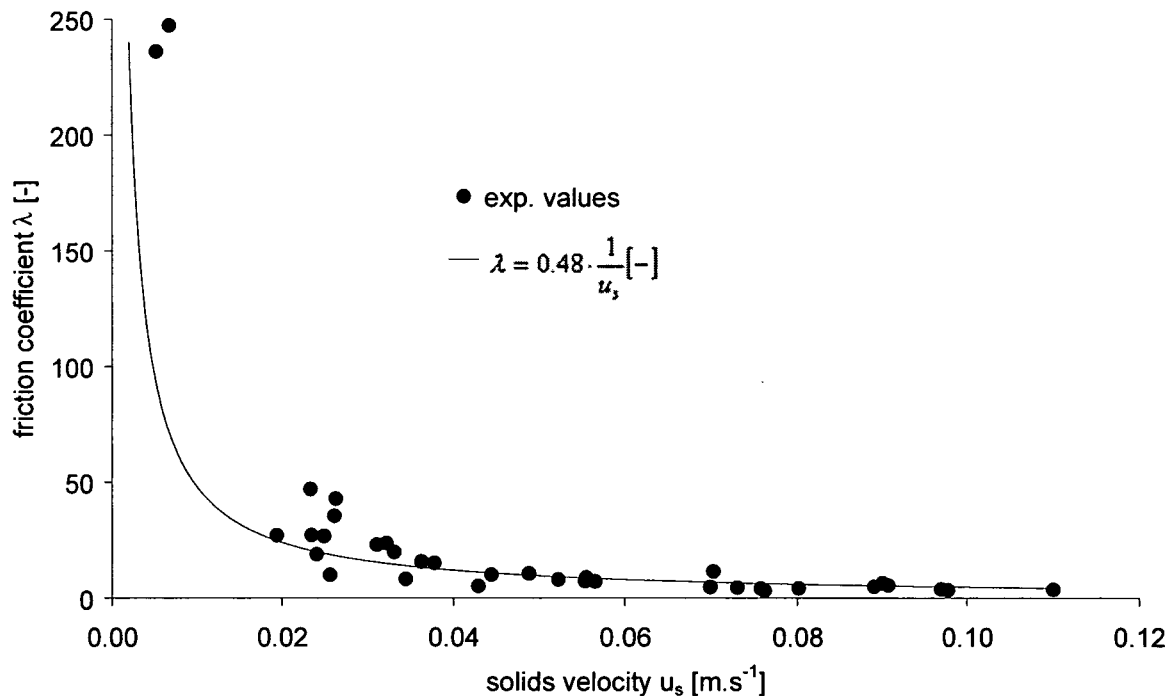


Figure 5-7: Correlation for friction factor λ and solids velocity

Figure 5-7 shows the correlation between the solids velocity and λ which is calculated from pressure drop of both loop seals. The line represents the predicted values for a k_λ of 0.48 s.m^{-1} . It can be seen that the values go along with the correlation and λ is inversely proportional to the solids velocity. Deviations are most likely due to pressure measurement inaccuracies.

According to tracer measurements of the loop seal fluidisation gas flows, the downcomer of the loop seal was not entirely fluidised (cf. 4.5.3). Basu and Cheng (2000) therefore used the Ergun-equation to describe the pressure drop and a fraction of 0.095 of the loop seal fluidisation flow leaving through the downcomer. In this study, analysis of several approaches showed that correlations used in bulk mechanics for fine powder hopper discharge procedures cover better cover the measurements. Equation (5-17) is derived

from the momentum balance in a segment of a hopper. In this correlation only the pressure in the vertical direction is considered. The coefficient μ is used to allow for frictional properties of materials and λ_H is a measure for pressure transmission to the horizontal pressure ($\lambda_H = 0$ for "free-standing" matters, $\lambda_H = 1$ for fluids).

$$\frac{dp_v(h)}{dz} + \frac{P}{A} \cdot \lambda_H \cdot \mu \cdot p_v(h) = \rho_{bulk} \cdot g \quad (5-17)$$

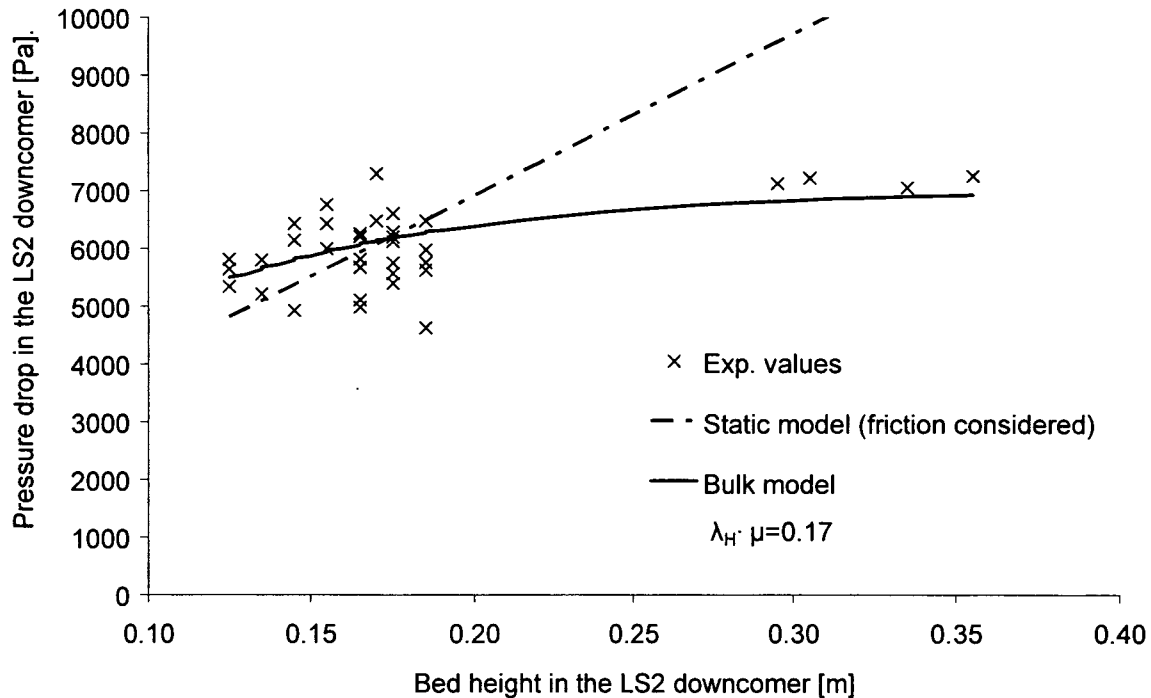


Figure 5-8: Pressure drop in the downcomer of loop seal 2

The graph in Figure 5-8 shows the calculated values of (5-17) approaches compared to measured values. For comparison reasons also the line resulting from the hydrostatic pressure of the fluidised material considering wall-friction is also depicted. Good agreement was found and all experimental. Values were found to be within 20% deviation of the proposed correlation.

The pressure drop situation of the loop seal (LS2) follows from a pressure balance as algebraic sum of the pressure drop of each section of the circulation loop between the cyclone outlet and the fuel reactor outlet (5-18). This includes the loop seal sections and the cyclone vortex tube; the height of the solids column at the side of the cyclone is the unknown variable to be determined.

$$P_{Outlet,cyc} - P_{Outlet,FR} = \Delta p_{CYC,Vortex} + \Delta p_{LS2,Sp} - \Delta p_{LS1,DOW} - \Delta p_{LS2,HOR} \quad (5-18)$$

5.2.4 Cyclone

The pressure drop between the top of the riser and the pressure at the cyclone outlet and the pressure drop of the vortex tube are estimated using a simple empirical correlation in analogy to e.g. Perry et al. (1988), (5-19). Parameters from experimental results are given below. The mass in the cyclone was determined based on the cyclone volume and the solids concentration at the exit of the riser

$$\Delta p_{CYC,i} = k_{CYC,i} \cdot \rho_G \cdot u_{RIS}^2 \quad (5-19)$$

with: $k_{cyc,inlet} = 210$ and $k_{cyc,Vortex} = 350$.

5.3 Simulation results and discussion

5.3.1 Static pressure distribution - pressure loop

The component models were integrated into the global model and a large number of simulation runs were carried out. Input values are the geometries and the parameters as described above as well as the gas pressures at the cyclone and fuel reactor outlet. The pressure drop for the riser is determined from the pressure balance in equation (5-20). This, written for the loop including the riser is:

$$P_{CYC,Outlet} - P_{FR,Outlet} = \Delta p_{CYC,inlet} + \Delta p_{RIS^*} - \Delta p_{LS1,Dow} - \Delta p_{LS1,Hor} + \Delta p_{FR} \quad (5-20)$$

It was already found during experimental work that the pressure situation is stable at all tested operating conditions, which could also be confirmed during simulation work. All component models gave expected results. The relationship between the static pressure (measurement values and model prediction) and the CFB system height is presented for the standard case in Figure 5-5. The total loop is at elevated pressure because of the filter equipment installed for de-dusting of the gas flows of the flow model.

In the diagram the pressure loss of each component is presented and can be identified easily by comparison with the schematic sketch of the unit. It can be seen that the loop seals between oxygen carrier oxidation zone and "combustion" zone are operating at a higher pressure level, which avoids gas mixing between these zones.

The diagram also allows the description of the riser pressure drop Δp_{RIS^*} used in equation (5-20). The situation at the riser solids return line at the height of the air reactor bed surface is such, that the pressure at this location is equal to the pressure of the riser at the same height. The riser pressure drop Δp_{RIS^*} therefore is the pressure drop between the riser exit and the riser height equal to the air reactor bed surface.

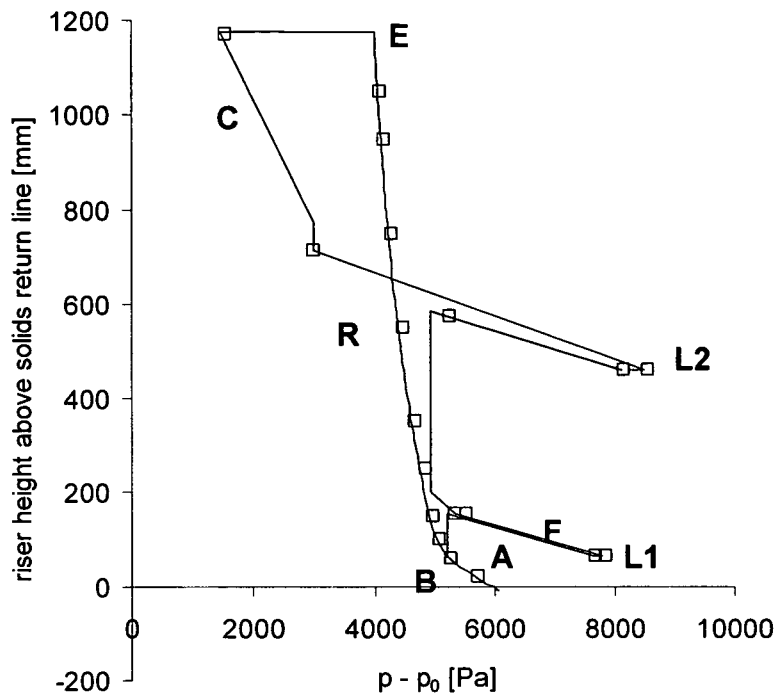


Figure 5-9: Pressure profile of the CFB loop (experimental and modelling data for TSI = 18kg, sec. air fraction = 35%, $u=1.74\text{m}\cdot\text{s}^{-1}$, $G_s=62.5\text{m}^{-1}\cdot\text{s}^{-2}$).

5.3.2 Solids circulation rate

In Figure 5-10 the solids circulation rate is shown for different operating conditions versus the riser pressure drop $\Delta p_{\text{RIS}}^{**}$. The riser pressure drop $\Delta p_{\text{RIS}}^{**}$ is the pressure value taken close above the gas distribution plate because no experimental data exist for the total riser. The air staging in the presented case is 35% secondary air of the total air flow in the riser. The riser fluidisation velocity was altered between 1.66 and $2.74\text{m}\cdot\text{s}^{-1}$ and the total solids inventory for the CFB system was varied between 14 and 20 kg.

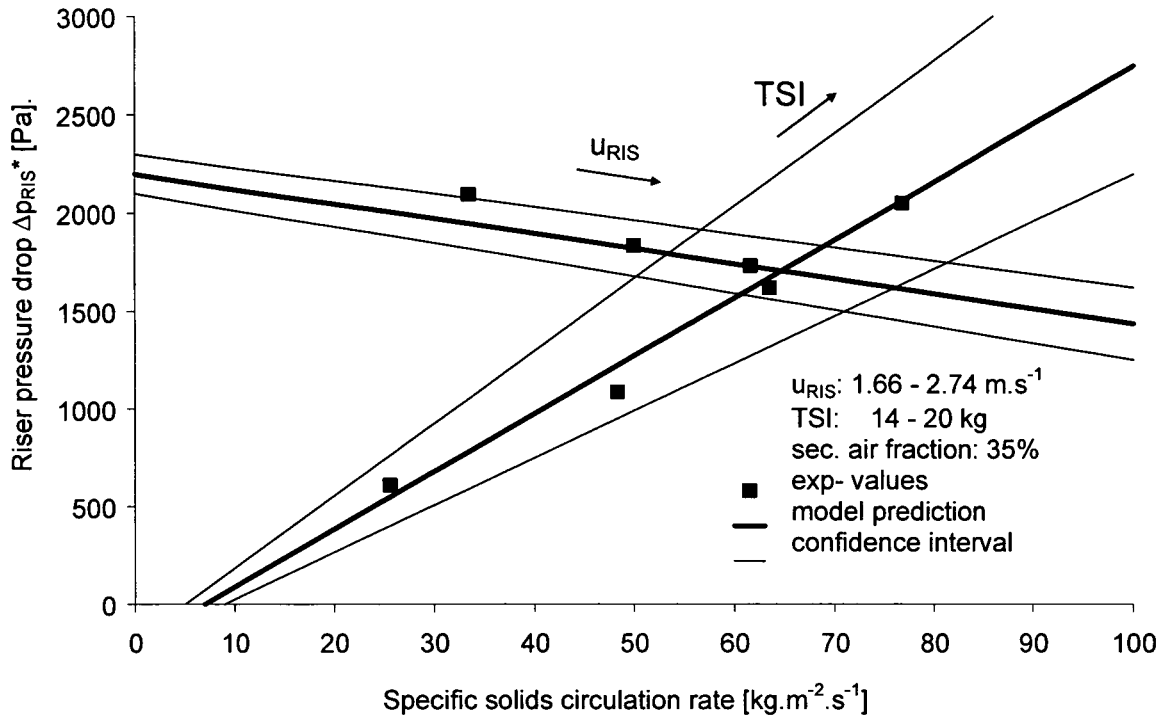


Figure 5-10: CFB loop parameter plot for experimental and modelling results.

Bold lines show results from simulation runs. However, as presented in equation (5-20) the pressure loop includes the modified riser pressure drop Δp_{RIS}^* . As the absolute value is small in comparison to the measurement inaccuracies of the outlet pressures this is a significant source and gives a high sensitivity of the model to the pressure values at the outlets.

The simulation results in Figure 5-10 include deviation indicators. The maximum deviation between the measured and predicted values of Δp_{RIS}^* is determined from comparison of model predictions and experimental results as 6%. As shown in section 5.2 the solids circulation rate is highly dependent on the riser pressure drop and comparison of model predictions and experimental results gives a deviation of maximum 15%. With equal accuracy the model allows determination of mass inventories from the reactor volumes, operating conditions and the solids flux.

5.4 Conclusions

A model for the description of fluid dynamics of a demonstration scale CLC-CFB reactor concept was developed. The present model can reasonably predict the experimentally measured axial solids concentration profile of the riser and the solids circulation rate as well as the pressure drop.

The riser model is characterised by inclusion of a bottom zone, an acceleration zone, transport zone, and effects of the riser exit. Variations of operating parameters could well reproduce the experimental pressure profiles. The implementation of fluidisation staging was successful but further work is required for an exact modelling. Although the acceleration of

solids is integrated it is possibly the disturbance of the annulus flow by the gas injection that causes differences between the model and the measurement data.

The global model for the pressure loop includes numerous details on components existent in many CFB systems and all could be described satisfactorily by empirical equations. Simulation showed that experimental data could be reproduced well for all sections.

It was found that the system is very sensitive to changes of the riser pressure drop by variation of one of the gas exit pressures. The reason for this are the small mass content and the steep pressure profile of the riser. However, if these values can be adjusted correctly the concept is suitable for detailed parameter studies. In addition, the potential of the model can form a basis for fluid dynamic scale-up of the circulating fluidisation bed system.

6 An integrated chemical-looping combustor model

In this section, a modelling and simulation analysis of a CLC-system and the integration into a power plant concept is outlined. A simulation of the power plant concept is set up and the main system parameters are identified. Results of previous sections and experimental data on chemical kinetics, thermodynamics and the CLC - CFB reactor design are used directly in the model. By this, the influence of the metal oxide type and the operating temperatures of the reactors as well as of conditions of the inlet and outlet temperatures are evaluated. Further, design related parameters of a CLC-system based on an interconnected circulating fluidised bed reactor concept are incorporated into the advanced component models of the simulation. Such, the significance of low gas mixing between the reactors and an optimum solid circulation rate are examined.

6.1 Model structure and background

The successful development of the novel power plant concept depends upon the optimisation of single components and component groups such as the power production cycle and the combustor itself. This section focuses on the combustor characteristics and its effects on the process performance. A number of different aspects, analysed by mathematical and physical modelling, form the basis for this simulation model. The following graph gives an overview of the models, combustor parameters and their integration into the simulation model as well as the key target values.

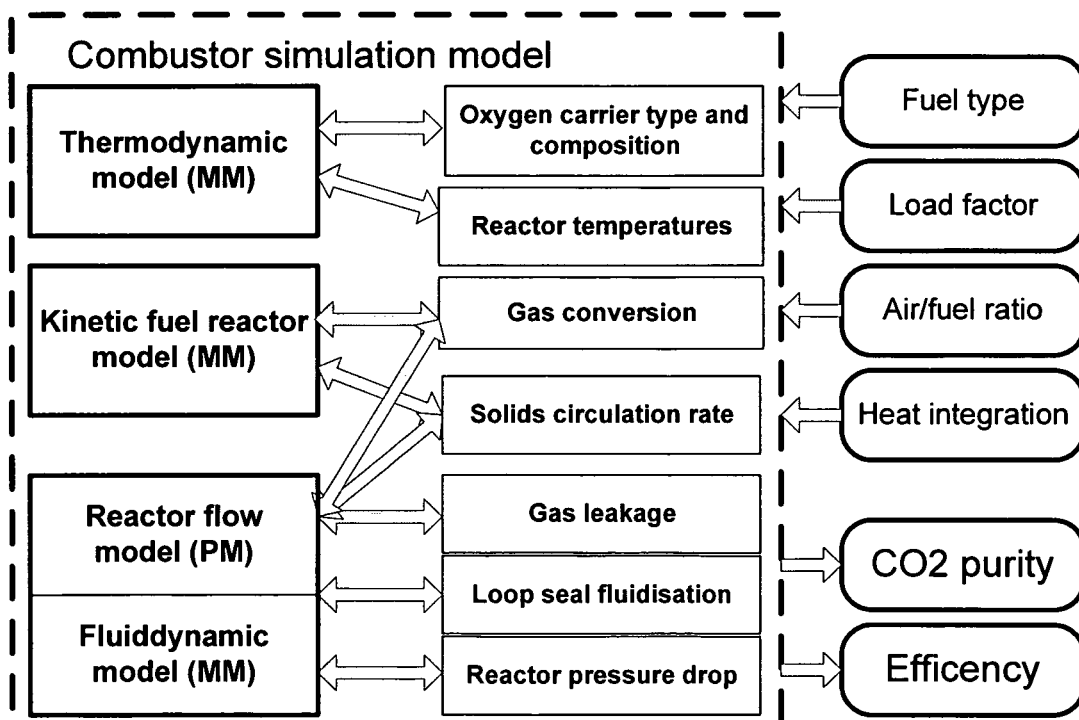


Figure 6-1: Simulation model structure

In Figure 6-1 it can be seen that, in total four detailed models were developed for chemical-looping combustion. These mathematical (MM) and physical models (PM) are for the thermodynamics and fluid dynamics that were introduced in previous chapters. A kinetic model of the fuel reactor reactions was developed by Luisser, 2005 (see also Kronberger et al. 2005a). The model parameters are to a great extent influencing several models, which explains the idea of a single simulation model including all parameters. This so-called combustor simulation model needs in addition the fuel type, the load factor, the air to fuel ratio, and the kind of heat integration, i.e. cooling of the reactors and heat losses as model parameters. As the results of the simulations two key target values, the electrical efficiency and the CO₂ purity (dry CO₂ -concentration) are defined.

6.2 Simulation results and discussion

Although, an analysis of the model is difficult if the system is not integrated into a power cycle arrangement, results are presented for the combustor only. As in this study the focus is given to the combustor, in the following graph the mass and energy balances for a 50MW_{th} combustor are presented (Figure 6-2)

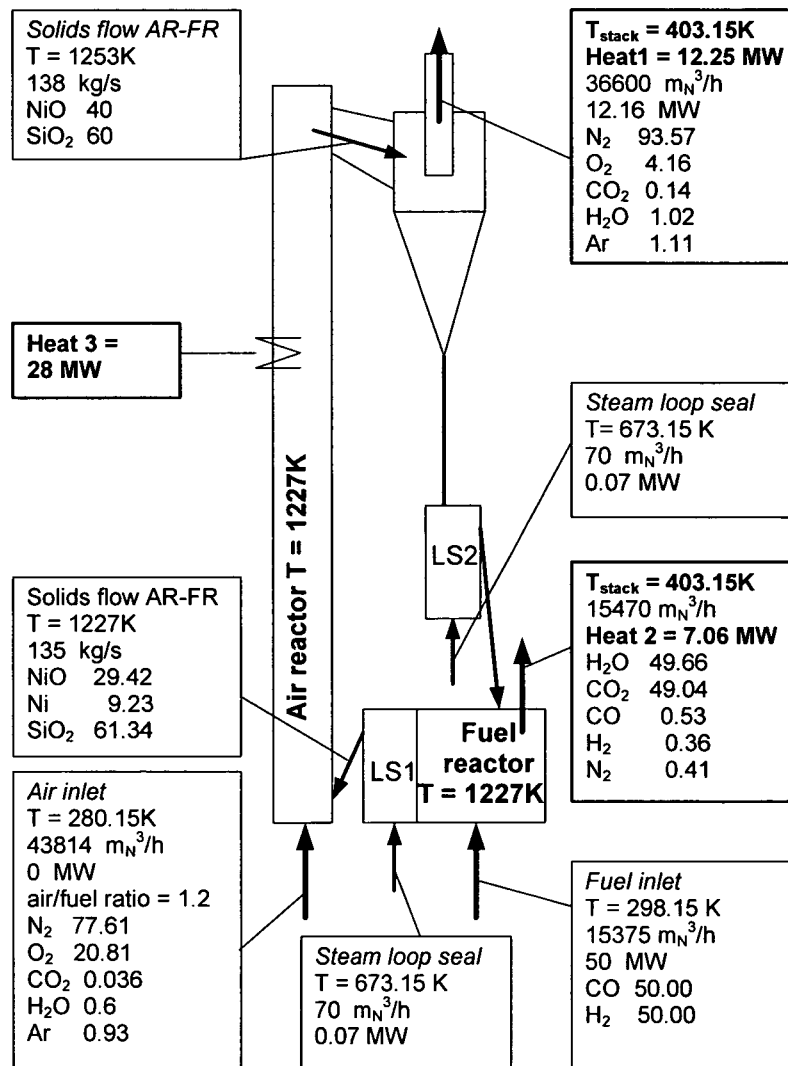


Figure 6-2: Heat and mass balances of chemical-looping combustor (LS = loop seal, gas composition in vol-%)

The boxes show the temperature, the volume flows at standard conditions, the energy and heat flow rates, and the mass concentrations. The heat flow rates at the reactor exit are given on the basis of a stack temperature of 130°C and additional heat duty is performed from tubular walls at the air reactor riser. The bed material assumed is a Nickel based oxygen carrier and the gas conversion for the fuel reactor set to a maximum. Gas leakage was given as 0.5% for both loop seals and reactor pressure drops to zero.

All energy flows are given as heat streams with the exception of the fuel gas, where the calorific energy is used. For the solids flow the sensible heat is super positioned by different chemically bound energy of the two solids flows. In total 41.52 MW of (total) energy are shifted from the fuel reactor to the air reactor against the temperature gradient and reflects the "chemical heat pump" mechanism of chemical-looping as described e.g. by Richter et al., (1983).

An analysis in view of electrical efficiency shows that the incomplete conversion of the fuel due to thermodynamic equilibrium of the NiO – reduction by CO/H₂ causes a reduction of the combustion efficiency by about 1%. Additional combustibles in the fuel reactor flue gas due to incomplete conversion in the fluidised bed reactor further reduce the energetic efficiency of the unit. Another energy penalty is put on the system by the demand of loop seal fluidisation agent. In large-scale boilers steam is used and here the inlet temperature is assumed to be 400°C. Each steam flow requires about 70kW (in total about 0.3% of the thermal power), which in an integrated system would be produced from low temperature heat.

In terms of CO₂ capture and separation the incomplete conversion is the parameter with the largest influence. The CO₂ purity compared to complete conversion decreases at the given conditions by about 2 percentage points. The gas leakage between the reactors further increases the impurity of the CO₂ gas stream because nitrogen from the air reactor is mixed into the CO₂ flow. The requirements on CO₂ purity for transport, storage and the environmental perspective is generally unexplored and the behavior of CO₂ with impurities at high pressures (supercritical) is not well known. Despite this, certainly the energy demand for compression and possible separation of the gases increases significantly. Consequently, the energetic efficiency of the entire CO₂ capture power plant is reduced as well. A second minor effect of the gas leakage is the loss of CO₂ to the air flue gas stream, which for the given conditions equals about 0.7% of the total amount of produced CO₂.

The combustor model forms the basis of a power plant simulation model, which can be used in future to optimise the overall efficiency of a CO₂ capture power plant.

7 A case study of an industrial CLC power plant

Throughout the research work of this thesis a conceptual design of a large-scale CLC demonstration system was developed in cooperation with research partners. The system is based on a refinery scenario (200 MW thermal power, fuel: refinery gas) and an atmospheric circulating fluidised bed (CFB) boiler design. Based on experimental findings and mathematical modelling analysis, scale-up recommendations for CLC were developed. The study confirms that chemical-looping combustion is appropriate for new units and for retrofitting existing atmospheric CFB boilers.

7.1 Development of a conceptual design

A key objective of this research programme was the development of a conceptual design and economic evaluation of a large-scale application of chemical-looping combustion.

The design scenario chosen for this work was prescribed by the research programme management and was taken from one of four real scenarios used to facilitate a comparison of new capture technologies. The selected scenario is based on a refinery and a petrochemical complex, and utilizes CLC to replace existing power boilers. Total thermal boiler power is 200 MW producing 227 tonne/hour of superheated steam for co-generation of power and process steam. The study uses refinery gas as fuel to the boiler, which is in contrast to the laboratory based prototype work, which utilised methane gas as fuel. The main process conditions are given in Table 7-1.

Table 7-1 Industrial plant design criteria:

Process aspect			
Fuel type	Refinery gas	C _x H _y	89 vol-%
		H ₂	8 vol-%
		CO ₂	2 vol-%
		N ₂	1 vol-%
Steam parameter	Temperature	515°C	
	Pressure	126 bar	
	Steam flow	227tonne/h	
Feedwater	Temperature	122°C	
	Pressure	150bar	
Flue gas conditions	Excess air	15%	
	Flue gas temperature at stack	190°C	
Ambient conditions	Ambient temperature	12°C	
	Air humidity	80%	

7.1.1 Boiler layout and process flow diagram

Alstom (Morin and Beal, 2004) has developed a design concept for large-scale chemical-looping combustion boiler, taking advantage of its leading experience in this field (Marchetti et al., 2003). The combustor itself is based on a conventional CFB concept similar to the unit described in chapter 4.5. In this section reference is made to the concept at a 200MW_{th} scale.

The air is fed to the unit as primary air at the bottom of the riser and as secondary air in the lower section of the riser, which also has an increasing cross section. The lower region is refractory lined and the top area is enclosed by water cooled tubes. The possibility of secondary air injection is justified by the improved load control and the possibility for adjustment of the riser pressure profiles. The bed material is entrained through the exit, which is designed as a T-shaped exit allowing adequate particle circulation flow and at the same time and sufficient solids residence time in the oxidizer section. The return leg is formed by: a single cyclone, the loop seal solid splitter, and the downcomers as well as an integrated fluidised bed heat exchanger.

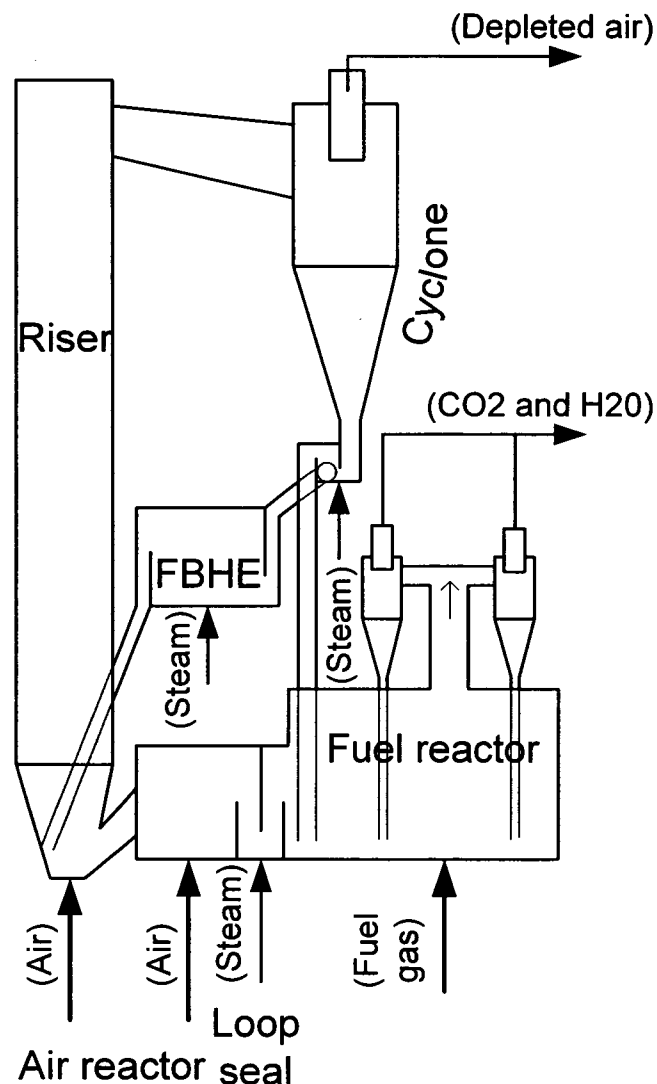


Figure 7-1: Design layout of an industrial CLC boiler.

A major difference from conventional CFB technology is the integration of a novel loop seal design into the solids return system. The gas streams must be prevented from mixing and this requires the development of a loop seal with three solids outlets. Solids can be directed either via a straight return to the riser, extracted to fluidised bed heat exchanger (FBHE) or to the fuel reactor for closing the oxygen carrier flow loop.

Since there is an optimum temperature range for the oxides operation, load follow-up requires close temperature control of the air riser loop. This can be controlled by the directly returning solids after the cyclone separation back into the riser. The second control option is the installation of the fluid bed heat exchanger allowing exact adjustment of the heat withdrawal from the solids loop.

The main downcomer returns the particles into the fuel reactor where the reduction of the oxygen carrier by the gaseous hydrocarbon fuel takes place. The operating conditions in this reactor are determined by a superficial gas velocity of 1.5 times the terminal velocity. The outgoing flow is higher than at the inlet due to the fuel gas volume expansion resulting from the oxidation reaction. The expansion factor of 3 is likely to result in high elutriation rates, and an analysis of the compatibility of the particle characteristics with the required solids loading for the fuel reactor shows that additional cyclones are required. For this a solids separation system as e.g. presented by Goldbach (2001) is considered.

The fuel reactor is directly connected to the air reactor. The chemical-looping boiler concept from Alstom Power Boilers (Morin and Beal, 2005) includes gas barriers between the fuel reactor and the air reactor, which are crucial for the interconnected reactor performance. Because of high velocity in the riser section additional bed material is believed to be necessary for achieving the required mean particle residence time. Also part load operation down to about 40% of the nominal power output is facilitated by this.

The most crucial design parameter for a chemical-looping combustor is the type of oxygen carrier. The encouraging results of the prototype test runs (Lyngfelt et al., 2004b) form the basis for the use of nickel-based oxygen-carrier particles also for the large-scale scenario.

An air-to-fuel ratio of 1.15 was selected, which represents a typical value for industrial applications and the operating temperature is assumed to be 950°C. The resulting heat and mass balances were reviewed and the required solids circulation rates as well as the resulting solids conversion were determined for the CLC boiler arrangement.

The key difference is immediately apparent on inspection of the process block flow diagram, given in Figure 7-2. The chemical-looping combustor requires two separate backpass boiler lines, one for the fuel and one for the air reactor. This split backpass system, however, is similar to existing practice for reheat control.

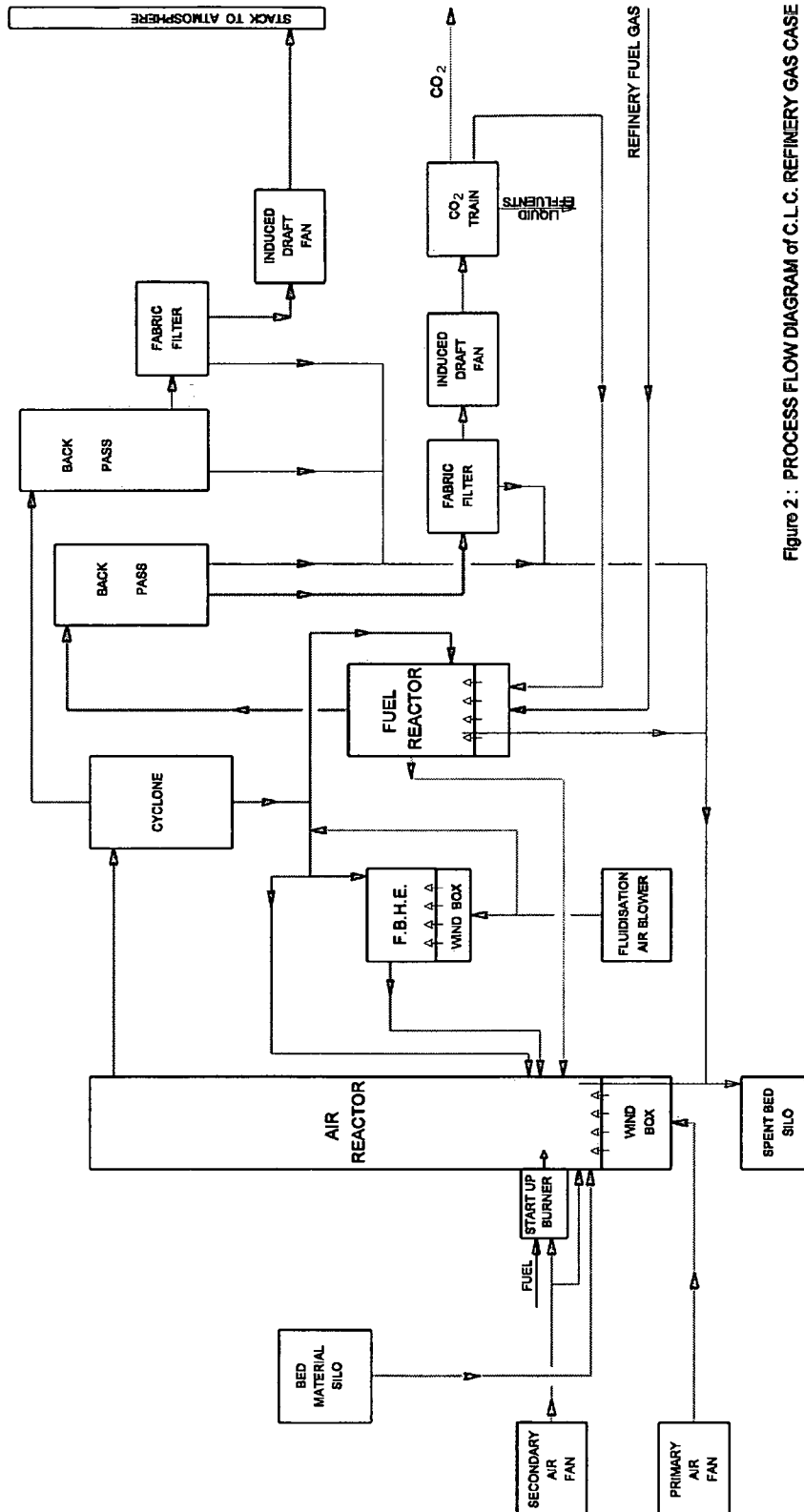


Figure 2: PROCESS FLOW DIAGRAM of C.L.C. REFINERY GAS CASE
ALSTOM Power Boilers

Figure 7-2: Process flow diagram of CLC refinery gas case (Beal and Morin, 2005)

7.1.2 Techno-economic evaluation of the large-scale-concept

From the technical point of view the key issues of a large-scale CLC unit were addressed and satisfactory results were found in the previous section. In the following

section further technical aspects relevant for the set-up of a complete CO₂ capture process are dealt with and results of the economic evaluation are presented.

Development of scale-up guidelines of CLC process

The scale-up (or scale-down) of fluidised bed reactors usually requires the scale-up of three distinguishable sub-processes: fluid dynamic gas to solid contact, heat and mass transfer, and chemical reactions. For successful execution the interaction of these sub-processes has to be considered. From the design point of view the major scale-up technical challenges are with four major components of CFBs: the combustor, the cyclones, the backpass, and the fluid bed heat exchangers. However, the dual-fluidised bed combustor concept coupled by the solids flow gives a rather large degree of freedom for each single reactor.

The fluid dynamic scale-up of the CFB system is primarily determined by the fluidisation regime of the reactors, in particular the CFB riser. The fluid dynamic behaviour of the transport reactor determines the solid circulation rate, which, in turn, is crucial for heat balance of the system and the oxygen transport between the reactors.

With regard to process economics it is desired to minimize the bed material and to optimise the solids circulation rate as this influences the overall energy consumption of the fluidisation. However, with regard to the design of a robust process some margin of safety is advisable as it may give some additional operating flexibility.

The air reactor design can be handled without major difficulties. From determination of reactivity of the various metal oxide types and the fuel gas composition the required particle residence time is determined directly. For scale-up constant mean particle residence time is required.

From the reaction engineering point of view the main focus is to be given to the fuel reactor. Similar fuel gas conversion can only be obtained when the gas-solid contacting is similar at different scales. Reaction rate constants and order of reaction are determined by reactivity tests and, as a consequence of the required gas residence time, the reactor mass is given for a certain thermal power and fuel type. Constant gas residence time has been used as the key scale-up criteria for this issue. For a more general case, however, the mass transfer coefficient X (dimensionless inter-phase mass transfer) and the dimensionless reaction rate k^* as proposed by Grace (1986) are suitable scale-up criteria.

A detailed analysis of the fuel reactor performance was carried out by means of mathematical fuel reactor models by CSIC (Adanez et al., 2003) and TU Vienna (Luisser, 2005). As a result these tools can be used as scale-up instruments for fuel reactor optimisation. A summary of the scale-up criteria is given in Table 7-2.

An additional technical challenge for the process scale-up is given for the cyclone. In scaling-up, a point is reached where the cyclone size gets so large that oxygen carrier particle losses are increasing significantly. Scale-up to larger size cyclones has been gradual

and like the conventional CFB, as the unit size increases, cyclone size is increased or cyclones are added as required to maintain optimum gas velocities, and then optimum cyclone fractional collection efficiency.

Table 7-2: Scaling criteria for chemical-looping combustion

Scaling criteria for CLC reactor systems	
CFB reactor system	$\frac{\text{specific solid flow rate}}{\text{specific fuel mass flow rate}} = \text{const.}$
Air reactor	$\frac{\text{fuel mass flow rate}}{\text{air reactor bed mass}} = \text{const.}$
Fuel reactor	$\frac{\text{fuel mass flow rate}}{\text{fuel reactor bed mass}} = \text{const.}$
	interphase mass transfer coefficient (k^*) = <i>const.</i>
	dimensionless reaction rate constant (X) = <i>const.</i>

Economic evaluation

An economic evaluation of the scenario was conducted during the GRACE project by Alstom Power Boilers. The analysis was based on cost for capital, operation, and energy for the CLC process and calculations are based on similarities with existing large scale CFB power plants.

Two CLC cases, a possible and a conservative one, were analysed based on equal assumptions and terminal conditions for the CO₂ purity but on differences in capital cost requirement for the boiler. The results show that cost and performance of the oxygen carrier are a significant factor for the CLC economics. Based on detailed calculations made by Lyngfelt et al., (2004c) the costs for the oxygen carrier were derived. For the lifetime the number obtained from the prototype operation was used, which suggests a durability of the solids up to 40,000hours. The mass requirement is calculated from reactivity data determined throughout this project. The different assumptions suggest an oxygen carrier cost in the order of 1 €/tonne of CO₂ captured. In Table 7-3 it can be seen that the CO₂ mitigation cost per tonne CO₂ are in the range of €16.7 to €20.8 for the given assumptions.

Table 7-3: Economics of entire CLC system

		CLC boiler conservative case	CLC boiler possible case
CO ₂ mitigation cost (without CO ₂ compression and transport)	€/tonne CO ₂	20.8	16.7

It should be underlined that this analysis is based on estimation at a very early development stage of the technology and thus, two additional factors should be mentioned. Firstly, the reference case does not show the technology to its best advantage as it utilizes a small size boiler, expensive fuel and low pressure steam parameters when compared to

typical utility class boilers. Secondly, the oxygen carrier lifetime is unknown since not tests over more than 300 operating hours were performed.

Despite of these uncertainties a comparison with other CO₂ capture technologies for power plants is given. Within the CCP project an economic evaluation was made for the Grangemouth refinery scenario (Mikus and Melien, 2004). The integration of the capture technologies into scenarios and transfer of data into a comparable and quantified format (equal capacities, calibration of costs and physical conditions) supports a consistent cost evaluation. The technologies included in Figure 7-3 are:

Amine absorption: Amine solvent based absorption process for post combustion for CO₂ capture. This technology is mature for large scale application and forms the baseline technology for the comparison.

Membrane WGS: The pre-combustion decarbonisation concept converts hydrocarbon-based fuels in a reformer or partial combustion unit into synthesis gas (CO and H₂). The CO is further converted into CO₂ via water gas shift reaction to produce additional hydrogen.

Oxyfuel ASU: "Classical" oxyfuel process with flue gas recycling with O₂ separation in a cryogenic air separation unit .

Oxyfuel ITM: Oxyfuel process with inherent O₂ separation by ionic transport membranes (process 2a in Figure 1-3).

Chemical-looping combustion

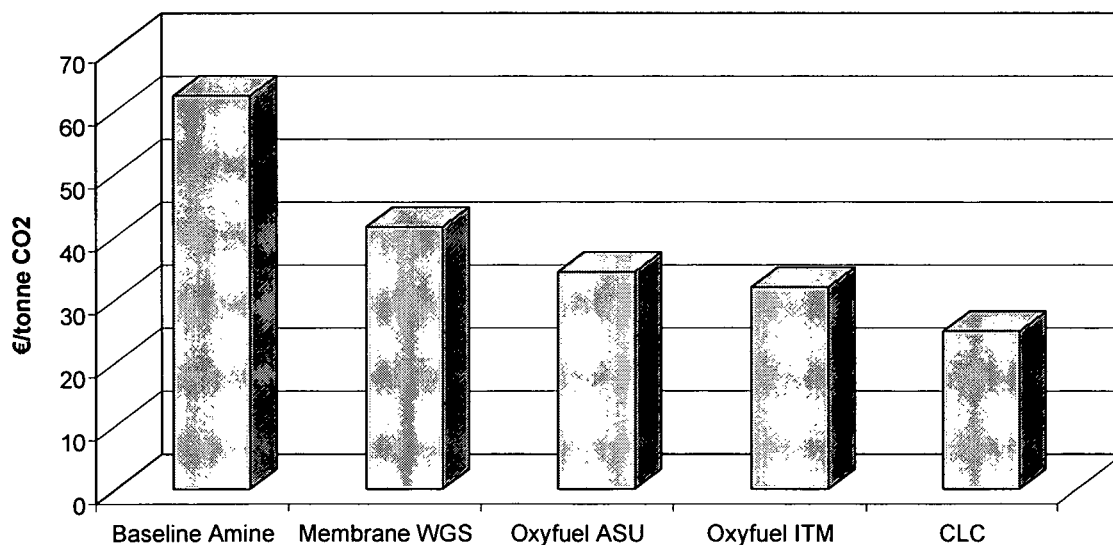


Figure 7-3: CO₂ mitigation cost for the Grangemouth refinery scenario (Mikus and Melien, 2004)

Figure 7-3 shows that a significant reduction for CO₂ mitigation cost can be achieved for all technologies in comparison to the baseline amine absorption technology. Membrane WGS offers, similarly to oxyfuel processes, a reduction of CO₂ avoidance cost of about 30% in comparison to the post-combustion baseline. Oxyfuel-firing can be practiced today using

conventional air separation, along with flue gas recycle, in retrofit or new-built boilers at a cost of about 35€/tonne CO₂ avoided. Further cost reduction in the longer term is possible by using advanced air separation technologies based on high temperature ceramic membranes, to the 20-30 \$/ton range. For chemical-looping combustion a conservative number of 25€/tonne CO₂ was used and it appears in this economic evaluation as the best technology but it must be mentioned that the uncertainties of this evaluation are still significant.

7.1.3 Future development and conclusions for industrial scale CLC boilers

The fluid dynamic testing programme confirms the general suitability of the concept for industrial scale CLC boilers. Scale-up issues have been analysed and it appears that there are no difficult points in terms of technology, in particular as the process uses mostly existing CFB technology. Also cost analysis indicates advantages of the CLC concept in comparison to more conventional CO₂ capture technologies such as amine scrubbing.

In this study safety and environmental aspects of the proposed design have been considered only with respect to the selection of particle materials and the minimisation of emissions. A more detailed analysis is required before a final answer can be given for this point.

The successful results of this study form the basis for future development. A demonstration at pilot scale in long-term prototype operation (10 kW_{th} and 1 MW_{th}) is suggested. The steam cycle parameters in this study are those of the reference industrial boiler and not of the utility type boiler. A CLC process with much higher steam conditions (600/650°C) could offer improved cost benefits and should be considered for future development.

8 Summary and concluding remarks

The research described in this thesis has focused on the further development and especially the gain of fundamental understanding of different aspects for the design of reactor systems for chemical-looping combustion (CLC). This novel method of fuel combustion may be a key process to the energy conversion and the continued use of fossil fuel resources as clean and efficient energy source. This is of particular interest in view of increasing concern about the greenhouse effect, which probably is caused by the increase of anthropogenic CO₂ emissions to the atmosphere.

Chemical-looping combustion is a combustion technology that utilises a novel concept for supplying oxygen to the combustion process. This is, namely, the transfer of oxygen from solid oxide materials in a reducing atmosphere and recycle of those oxide materials to a separate oxidation stage, wherein they are re-oxidised to their original state for re-use in a cyclic fashion. The key feature of this process is its ability to produce an essentially pure CO₂ stream that is ready for sequestration.

For the research work on CLC included in this thesis an integrated approach was chosen. The aspects of particular interest in the development of the process are the oxygen carrier development, the reactor design and the integration of the combustor into a power plant cycle and each of the fields was studied with different intensity. The particle development is covered by a comprehensive literature study. The thermodynamics are studied for two different fuel types and a combustor model, which is also enlarged by integration of "real" power process parameters such as gas leakage. The greatest attention was given to fluidynamics studies by experimental work and mathematical modelling on designs of CLC reactor concepts at different scales. The different aspects for the development of the process are finally considered in a case study of a large-scale power plant.

Particle development for chemical-looping combustion

The development of chemical-looping combustion (CLC) relies on the availability of redox materials able to match the following requirements:

- a. good redox reactivity with high selectivity towards complete oxidation products and air respectively;
- b. high oxygen exchange efficiency, i.e. ratio of the oxygen mass involved in the redox process to the total mass of the solid;
- c. regenerability, i.e. stability during repeated redox cycles at relatively high temperature (above 800°C);

- d. mechanical resistance to the friction stresses associated with recirculation of solid powders;
- e. environmentally sound;
- f. low cost.

Recent research shows that Ni-based carrier particles are preferred because of high reactivity and crushing strength. Issues to be solved are the relatively high production cost and the possibility of causing cancerous dust emissions at industrial scale operation.

The thermodynamics of chemical-looping combustion

In chapter 3 a mathematical model of a CLC system with an integrated solution of the mass and energy balances was set up. The model includes design and operating parameters such as fuel and oxygen carrier type and solids circulation rate.

From the analysis, it follows that for oxides of the metals Fe, Cu, Ni, and Mn and for reasonable small temperature differences between the two reactors an oxygen carrier mass flow of about $0.005\text{kg}\cdot\text{s}^{-1}\cdot\text{kW}^{-1}$ is sufficient for natural gas fuelling. At this value full fuel gas conversion, equivalent to 100% CO_2 purity after H_2O condensation from the fuel reactor exit gas flow, can be expected for all active metal types except Ni, which always produces unconverted CO and H_2 in the range of about 0.5vol-% in the flue gas.

The model allows the identification of possible operating ranges in terms of temperature levels of the reactors in conjunction with purity of the CO_2 . For many parameter variations, limitations in operating conditions for the use of certain types of active metal have been identified, caused either by the attainment of the melting or decomposition point, or by the thermodynamic equilibrium. This information is important for optimisation of CLC systems to secure that additional reactor cooling and oxygen carrier flow are chosen properly to guarantee appropriate temperatures and high efficiency for CO_2 separation. The chemical-looping combustion mass and energy balance model constitutes a suitable tool to support the selection of oxygen carrier types for the process.

Fluid dynamic studies of chemical-looping combustion reactor systems

Fundamental knowledge of fluid dynamic behaviour of the two-phase flow is essential for an optimised design and operation of a chemical-looping combustor. The crucial CLC characteristics can be satisfied for a CLC design based upon circulating fluidised bed (CFB) technology. These are as follows:

- The *solids circulation rate*, which is a very sensitive parameter in operating the system because the solids act as oxygen and heat carrier between the two reactors.

- *Gas leakage* of the two reaction zones has to be prevented as it reduces the CO₂ capture efficiency and/or dilutes the exhaust gas enhancing the CO₂ capture expense.
- *Residence times of gas and solids* need to be sufficient in both reaction zones to ensure high conversions.

In chapters 4 and 5 the development of different reactor system designs focusing on fluid dynamic aspects was presented. The different reactor concepts followed in size, aims, and timescale the research progress of CLC experimentation work: a small unit for oxygen carrier reaction testing, a prototype design for proof of concept, and an industrial design for proof of feasibility at large-scale were analysed.

A laboratory scale two-compartment fluidised bed CLC system was first designed and analysed. The mechanism for the solids circulation is based on the entrainment of particles of high gas velocities in the air reactor. Part of the solids fall down in the downcomer, creating a pressure drop of the column of particles formed. This pressure drop in turn results in a higher pressure in the fuel reactor, pressing particles back into the air reactor via the slot. During experimentation gas velocities and slot designs were varied, and the solids circulation rate and gas leakage between the reactors were measured. The solids flux was found to be sufficient. The gas leakage was somewhat high but could be reduced by altering the slot design. Finally, the design was slightly varied and successfully realised at Chalmers University of Technology, in Gothenborg, Sweden. The two-compartment reactor concept was found to be well suitable for a hot laboratory CLC particle testing system.

A wide range of stable and suitable operating conditions was identified for a prototype bench scale design of a dual fluidised bed combustor for continuous atmospheric chemical-looping combustion. In parallel to parameter studies the design of the fuel reactor and the cyclone could be optimised in respect to solids circulation rate, gas leakage and bed mass in the reactors. The experiments on solids circulation rates showed that high solids flow rates are reached and the circulation rate can be varied in a wide range. This allows adjusting of the oxygen transport capacity in the CLC prototype as well as control of the temperature difference between the air and the fuel reactor. Determination of residence time distribution reveals that a considerable fraction of the bed material may not be included in the mixing process of the bubbling bed. Improvements for the final design are a change of the geometry.

The gas leakage was found to be very low and also the leakage mechanisms were understood. An effective countermeasure is to increase the flow of inert gas for the particle lock fluidisation. Another option is the injection of inert gas, e.g. steam, into the downcomers in order to create a gas barrier for the leakage gases coming from the reactors. Attention must be paid to possible increase of gas leakage in case of extremely porous bed material particles and it is necessary to consider this aspect for the operation of the prototype unit.

The design concept of a large-scale demonstration was explored in order to map suitable conditions for a CLC plant. The concept is featuring industrial CFB system components such as a solids splitter, air staging in the riser, and an external fluidised bed heat exchanger for load control. Intensive experimental analysis and mathematical modelling shows that the concept is very well suited for a large-scale CLC demonstration plant.

The findings of the experimental part of this work package together with mathematical description of chapter 5 provide a reliable foundation for a combustor model described in chapter 6.

An integrated assessment of chemical-looping combustion

By way of a case study the detailed analyses and the developments of other research institutions in this project were reviewed and the potential was assessed. The selected case study was the substitution of a refinery gas boiler at the Grangemouth refinery. A concept for an industrial chemical-looping combustion boiler has been developed and sized. Scale-up issues were analysed and it appeared that there are no difficult points in terms of technology, in particular as the process reuses mostly existing CFB technology. Safety and environmental aspects of the proposed design have been identified.

Costing was conducted showing that CO₂ avoided cost are at the low end of the range given for all CO₂ capture technologies. In terms of cost and durability the oxygen carrier is the main issue. Costing indicates that the CO₂ capture cost could be substantially below that for existing capture technologies if the targeted particle performance is achieved.

Concluding remarks

The results of this thesis as part of two European research programmes help to form a strong basis for future development. The CLC technology is nowadays given a very high potential as being one of the most promising candidates for midterm technologies for fossil fuel combustion with CO₂ capture. Clearly, many issues have to be solved including a pressurisation and/or temperature increase of the concept for high cycle efficiencies, lifetime increase for particles and increasing cost attractiveness by further development of cheap oxygen carriers, and health and safety issues associated with the use of oxygen carriers. However, CLC technology using CFB boilers should appear as a leading technology in terms of competitiveness for CO₂ removal after successful operation of a demonstration unit.

9 List of publications included in this work

Ia Kronberger, B., Löffler, G., Hofbauer, H. (2003). *Simulation of Mass and Energy Balances of a Chemical-Looping combustion System*. In Proceedings of the International Conference in Energy for a Clean Environment. Lisbon, Portugal.

Ib Kronberger, B., Löffler, G., Hofbauer, H. (2005). *Simulation of mass and energy balances of a chemical-looping combustion system*. International Journal on Energy for a Clean Environment, Vol. 6, pp 1-14.

Ila Johansson, E., Kronberger, B., Löffler, G., Mattisson, T., Lyngfelt, A., Hofbauer, H. (2003). *A two-compartment fluidized bed reactor for CO₂ - capture by chemical-looping combustion* In Proceedings of the International Conference in Energy for a Clean Environment. Lisbon, Portugal.

Ilb Kronberger, B., Johansson, E., Löffler, G., Mattisson, T., Lyngfelt, A., Hofbauer, H. (2004). *A Two-Compartment Fluidized Bed Reactor for CO₂ Capture by Chemical-Looping Combustion*, Chemical Engineering Technology, Volume 27, Issue 12, 1318-1326.

III Kronberger, B., Lyngfelt, A., Löffler, G., Hofbauer, H. (2005). *Design and Fluid Dynamic Analysis of a Bench-Scale Combustion System with CO₂ Separation-Chemical-Looping Combustion* Ind. Eng. Chem. Res. 2005; 44, 3, 546-556.

IV Kronberger, B., Löffler, G., Hofbauer, H., (2004). *Residence time distribution of solids in a fluidized bed fuel reactor of a chemical-looping combustion prototype*. In Proceedings of the 16th International Congress of Chemical and Process Engineering, Prague, Czech Republic.

V Kronberger, B., Wopienka, E., Löffler, G., Hofbauer, H. (2005). *Mathematical and experimental modelling of fluid dynamics of a demo-scale dual fluidized bed reactor system for chemical-looping combustion*. submitted to Powder Technology.

VI Kronberger B., Luisser M., Hofbauer H. (2004). *Analysis of a power plant concept with inherent separation of CO₂ - chemical-looping combustion*. In Proceedings of the 16th International Congress of Chemical and Process Engineering, August, Prague, Czech Republic.

VII Kronberger, B., Beal, C., Morin, JX., Hofbauer, H. (2004). *Design, hydrodynamic testing and scale-up recommendations of a conceptual large-scale chemical-looping combustion power plant* In Proceedings of the 3rd Conference on Carbon Sequestration, Alexandria, USA.

VIIIa Kronberger, B. Luisser, M., Löffler, G., Hofbauer, H. (2004). *Chemical-Looping Combustion – Ein neuartiges Kraftwerkskonzept zur CO₂ – Abtrennung* in Proceedings of the XVI. Kraftwerkstechnischen Kolloquium, Dresden, Germany.

VIIIb Kronberger, B. and Hofbauer, H. (2004). *Chemical-Looping Combustion - Ein neuartiges Kraftwerkskonzept zur CO₂ – Abtrennung, (Forschungsstatus und Entwicklungspotential)*. Proceedings (Informationsschriften). of the Expertenforum der VDI-Gesellschaft Energietechnik (GET). on Entwicklungslinien der Energietechnik, Bochum, Germany.

VIIIc Luisser, M., Kronberger, B., Löffler, G. and Hofbauer H. (2005). *Chemical-Looping Combustion eine Methode zur CO₂ freien Stromerzeugung aus fossilen Rohstoffen*. to be presented at the 'Internationale Energiewirtschaftstagung 2005', Vienna, Austria.

IX Kronberger, B., Löffler, G., and Hofbauer, H. (2005). *Chemical-looping combustion – Reactor fluidization studies and scale-up criteria*, Chapter 36 in *The CO₂ Capture and Storage Project (CCP). for Carbon Dioxide Storage in Deep Geologic Formations For Climate Change Mitigation, Volume 1 – Capture and Separation of Carbon Dioxide From Combustion Sources*. Ed.: Thomas, D. Elsevier Science, London. First edition, ISBN: 0-08-044570-5.

X Lyngfelt, A., Kronberger, B., Adanez, J., Morin, J.-X., and Hurst, P. (2004). *The GRACE project. Development of oxygen carrier particles for chemical-looping combustion. Design and operation of a 10 KW chemical-looping combustor*. In *Proceedings of the 7th Conference on Greenhouse Gas Control Technologies (GHGT7)*, Vancouver, Canada.

10 References

Adanez, J., de Diego, L.F., García-Labiano, F., Gayán, P., Abad, A., Palacios, J.M. (2004a). *Selection of oxygen carriers for chemical-looping combustion*. *Energy & Fuels*, 18, 371-377.

Adanez, J., de Diego, L.F., Gayan, P., Armesto, L., Cabanillas, A. (1995a). Modeling of Coal Combustion in Circulating Fluidized Bed Combustors, 13th Int. Conf. On Fluidized Bed Combustion, AMSE, New York, 305-315.

Adanez, J., de Diego, L.F., Gayan, P., Armesto, L., Cabanillas, A. (1995b). *A Model for Prediction of Carbon Combustion in Circulating Fluidized Bed Combustors*, *Fuel*, 74, 7, 1049-1056.

Adanez, J., García-Labiano, F., de Diego, L., Gayán, P., Abad, A., and Celaya, J. (2004b). *Development of Oxygen Carriers for Chemical-Looping Combustion*, Chapter 34 in *Carbon Dioxide Capture for Storage in Deep Geologic Formations –Results from the CO₂ Capture Project, Volume 1 - Capture and Separation of Carbon Dioxide From Combustion Sources*. Ed.: Thomas, D. Elsevier Science, London. First edition, ISBN: 0-08-044570-5.

Adanez, J., García-Labiano, F., de Diego, L. F., Plata, A., Celaya, J., Gayán, P., Abad, A. (2003). *Optimizing the fuel reactor for chemical looping combustion*. In *Proceedings of the 17th International Conference on Fluidised Bed Combustion*. Paper 63, Jacksonville, Florida.

Adanez, J., Gayan, P., Garcia-Labiano, F., de Diego, L.F. (1994). *Axial Voidage Profiles in Fast Fluidized Beds*, *Powder Technol.* 81, 259-268.

Alstom (2003), *Greenhouse gas emissions control by oxygen firing in circulating fluidized beds boilers Phase 1 – A preliminary system evaluation (Vol. I and II) Final Report by Alstom Power Inc.*. PPL Report NO. PPL-03-CT-09.

Anheden, M. (2000). *Analysis of Gas Turbine Systems for Energy Conversion*. PhD Thesis KTH Royal Institute of technology, Dept. of Chem. Eng. & Tech., Energy Processes Stockholm. ISSN 1104-3466, ISRN KTH/KET/R—112—SE.

Anheden, M. and Svedberg, G. (1996). *Chemical-Looping Combustion in Combination with Integrate Coal Gasification*. *Proceedings of 31st Intersociety Energy Conversion Conference IECEC'96 Washington, USA*. Vol. 3, 2045-2050.

Anheden, M. and Svedberg, G. (1998). *Exergy analysis of chemical-looping combustion systems*. *Energy Conversion Management*, 1998, 39, 16-18, 1967-1980.

Bader, R., Findlay, J., Knowlton, T.M. (1988). *Gas/Solid Flow Patterns in a 30.5 cm Diameter Circulating Fluidized Bed*, P. Basu and J.F. Large (Eds.), in *Circulating Fluidized Bed Technology II*, Pergamon Press, Oxford, England, 123-128.

Barin I. (1995). *Thermochemical Data of Pure Substances*, Vol. I and II, 3rd Edition VCH Publishers.

Basu, B. and Cheng, L. (2000) *An analysis of loop seal operations in a circulating fluidized bed*, *Trans IChemE*, Vol. 78, Part A, p991-998.

Bi, H.T. and Grace, J.R. (1995). *Flow Regime Diagrams for gas-Solid Fluidization and Upward Transport*, *Int. J. Multiphase Flow* 21 (6), 1229-1236.

- Blom, R. Bolland, O., Brandvoll, Ø., Olafsen, A., Larring, Y., Bredesen, R. (2004) *New materials for chemical looping combustion of natural gas*, The Second Trondheim Conference on CO₂ Capture, Transport and Storage, Trondheim, Norway. <http://www.energy.sintef.no/arr/co2%5F2004/> (last visited on Feb., 1st, 2005).
- Bolland O., Ertesvaag I.S., and Speich D., (2001) Exergy analysis of gas-turbine Combined Cycle with CO₂ capture using auto-thermal reforming of natural gas, in Proceedings of the International Conference Power Generation and Sustainable Development, Liège, Belgium.
- Brandvoll, Ø. and Bolland, O. (2002a). *Inherent CO₂ capture using chemical-looping combustion in a natural gas fired cycle*. In Proceedings of the ASME TURBO EXPO 2002, Amsterdam, Netherlands.
- Brandvoll Ø., Kolbeinsen L., Olsen N., Bolland O., (2002b) *Chemical Looping Combustion - Reduction of NiO:NiAl₂O₄ with hydrogen*, Chem. Eng Trans., vol. 3, p. 105-110.
- Burcat A. (2001). *Third Millennium Ideal Gas and Condensed Phase Thermochemical Database for Combustion*, Technion Aerospace Engineering (TAE). Report # 867.
- Capes, C.E. and Nakamura, K. (1973). Vertical Pneumatic Conveying: an Experimental Study with Particles in the Intermediate and Turbulent Flow Regimes, Can. J. Chem. Eng. 52, 31.
- Chan, H. and Louge, M. (1992). *Fluid dynamics similarity of circulating fluidized beds*. Powder Tech., 70, 259-270.
- Cho, P., Mattisson, T., Lyngfelt, A. (2002). *Reactivity of iron oxide with methane in a laboratory fluidized bed - application of chemical-looping combustion*. In Proceedings of the 7th International Conference on Circulating Fluidized Beds, Niagara Falls, Ontario, 599-606.
- Cho, P., Mattisson, T., Lyngfelt, A. (2004). *Comparison of iron-, nickel- copper- and manganese-based oxygen carriers for chemical-looping combustion*. Fuel, 83, 9, 1215-1225.
- Chong, Y. O., Nicklin, D. J., and Tait, P. J. (1986). *Solids exchange between adjacent fluid beds without gas mixing*, Powder Techn., 47, 151.
- Clift, R., Grace, J.R., and Weber, M.E.,(1978). *Bubbles, Drops, and Particles* Academic Press, New York.
- Consonni, S., Lozza, G., Pelliccia, G., Rossini, S., Saviano, F. (2004). *Chemical-looping combustion for combined cycles with CO₂ capture*. In Proceedings of the ASME Turbo Conference GT2004-53503, Vienna, Austria.
- Copeland, R.J., Alptekin, G., Cessario, M., Gerhanovich, Y. (2000). *A Novel CO₂ Separation System*. The 8th International Symposium on Transport Phenomena and Dynamics of Rotating Machinery, Honolulu, Hawaii, USA.
- Copeland, R.J., Alptekin, G., Cessario, M., Gerhanovich, Y. (2001). *A Novel CO₂ Separation System*. First National Conference on Carbon Sequestration, National Energy Technology Laboratory (NETL), Washington., USA.
- Copeland, R. J., G. Alptekin, M. Cesario and Y. Gershanovich, (2002). *Sorbent Energy Transfer System (SETS) for CO₂ Separation with High Efficiency* In Proceedings of the 27th International Conference on Coal Utilization and Fuel Systems, Clearwater, Florida, 719-729.
- Darton, R.C. (1979). *A Bubble Growth Theory of Fluidized Bed Reactors*, Trans. Instn. Chem. Engrs. 57, 134.

- Eklund, H., Sundkvist, S.G., Wilhelmsen, K., Åsen, K.I., Griffin, T. (2003). *Development of a membrane based CO₂ emission free gas turbine system* In Proceedings of the Clean Air 2003, Seventh International Conference on Energy for a Clean Environment, Lisbon, Portugal.
- Ergun, S. (1952). *Fluid Flow through Packed Columns*, Chem. Eng. Prog. 48, 89-94.
- Fang, M.; Yu, C.; Shi, Z.; Wang, Q.; Luo, Z.; Cen, K. (2003) *Experimental research on solid circulation in a twin fluidized bed system*, Chemical Engineering Journal, 94 ,3, 171-178.
- Fournal, A.B., Bergougnou, M.A., and Baker, C.G.J. (1973). *Solids Entrainment in a Large Gas Fluidised Bed*, Can. J. Chem. Eng., 51, 401-404.
- Franke, H.J., Shimizu, T., Hori, S., Takano, Y., Tonsho, M., Inagaki, M., Tanaka, M. (2001). *Simultaneous reduction of NO_x emissions and unburned hydrocarbon emission during plastic incineration in fluidized bed*, In Proceedings of the 16th International Conference on Fluidized Bed Combustion, Reno, Nevada, 1056-1064.
- Foscolo, P.U., Di Felice, R., Gibilaro, L.G., Pistone, L. and Piccolo, V. (1990). *Scaling relationships for fluidisation, The generalised particle bed model*, Chem. Eng Sci., 45 (6). 1647-1651.
- Geldart, D. (1985). *Elutriation, in Fluidization*, Second Edition, J.F. Davidson, R. Clift, and D. Harrison (Eds.), Academic Press, London, UK, 383-412.
- Geldart, D. (1986). *Gas Fluidization Technology*, Geldart, D. (Ed.), John Wiley & Sons, Chichester, New York, Brisbane, Toronto, Singapore, 1986.
- Geldart, D., Cullinan, J., Georghiades, S., Gilvray, D., Pope, D.J. (1979). *The Effect of Fines on Entrainment from Gas Fluidised Beds*, Trans. Instn. Chem. Eng. 57, 269-275.
- George, S.E. and Grace, J.R. (1978). *Entrainment of Particles from Aggregative Fluidized Beds*, AIChE Symp. Ser. 74, 67-74.
- Glicksman, L.R. (2004). *Scaling relationships for fluidized beds, recent progress*, Fluidization XI Present and Future for Fluidization Engineering, Naples, Italy.
- Glicksman, L.R. (1984). *Scaling Relationships for Fluidized Beds*, Chem. Eng. Sci. 39 (9), 1373-1379.
- Glicksman, L.R., Hyre, M. and Woloshun, K. (1993). *Simplified Scaling Relationships for Fluidized Beds*, Powder Technology. 77, pp. 177 - 199.
- Goldbach, G. and Tanca, M. (2001). *Firing Coal Washing Wastes in a FI-CIRCTM Steam Generator - Redbank Project* in Proceedings of the 6th International Conference on Fluidized Bed Combustion, Reno.
- Göttlicher, G. (2004) *The energetics of carbon dioxide capture in power plants*. US Department of Energy. Office of Fossil Energy, National Energy Technology Laboratory
- Grace, J.R. (1986a). *Fluidized Bed Hydrodynamics*, in Handbook of Multiphase Systems, G. Hetsroni (Ed.), Washington Hemisphere Publishing, Washington
- Grace, J.R., (1986b). *Fluidized Beds as Chemical Reactors*, in *Gas Fluidization Technology*, Geldart, D. (Ed.), John Wiley & Sons, Chichester, New York, Brisbane, Toronto, Singapore.
- Grace, J.R., Avidan, A.A. and Knowlton, T.M. (1997). *Circulating Fluidized Beds*, Blackie Academic & Professional, New York, USA.

- Gupta, S.K. and Berruti, F. (2000). *Evaluation of the Gas-solid Suspension Density in CFB Risers with Exit Effects*, Powder Technol. 108, 21-31.
- Habermann, A., Winter, F., Hofbauer, H., Gogolek, P. (1998). *Residence time distribution of particles in fluidized bed reactors for metallurgical processes*. In Proceedings of the Engineering Foundation Conference on Fluidization, 9th, Durango, CO, United States.
- Harvey, P.S. (1994) *Reversibility of Combustion Processes* PhD Thesis at the Thayer School of Engineering, Dartmouth College.
- Harris, A. T., Davidson J. F., and Thorpe R. B. (2002). *A novel method for measuring the residence time distribution in short time scale particulate systems*, Chemical Engineering Journal, 89, 1-3, 28, 127-142.
- Harris, B.J. and Davidson, J.F. (1994). *Modeling Options for Circulating Fluidized Beds: A Core/Annulus Deposition Model*, in A.A. Avidan (Ed.), *Circulating Fluidized Bed Technology IV*, AIChE, New York, 32-39.
- Haslinger, W., Hofbauer, H., Gavriil, L., Boukis, I. (1999). *Scale-up guidelines for a circulating fluidized bed biomass pyrolyser*. In *Circulating Fluidized Bed Technology VI* (ed. Werther, J.), DEHEMA, Frankfurt; Germany, 899-905.
- Hatanaka, T., Matsuda, S., and Hatano, H. (1997). *A new-concept gas-solid combustion system "MERIT" for high combustion efficiency and low emissions*, Proceedings of the 32nd Intersociety Energy Conversion Engineering Conference, Honolulu, Hawaii, 944-947.
- He, Y., Rudolph, V., Nicklin, D.J. and Chong, Y-O. (1993) *Circulating fluidized oil shale retort*, Fuel, 72, 6, 879-883
- Hofbauer, H. (1982). *Experimentelle Untersuchung an einer zirkulierenden Wirbelschicht mit Zentralrohr*, PhD. Thesis, Vienna University of Technology.
- Hofbauer, H. (1995). *Internally Circulating Fluidized Beds, Fundamental and Applications*, Proceedings of the 1st SCEJ Symposium on Fluidization, Tokyo, 275.
- Horio, M., Nonaka, A., Sawa, Y. and Muchi, L. (1986). *A new similarity rule for fluidized bed scale-up*. AIChE Journal, 32, (9). 1466-1482.
- Hugi, E. (1997). *Auslegung hochbeladener Zyklonabscheider für zirkulierende Gas/Feststoff-Wirbelschicht-Reaktorsysteme*. PhD Thesis, ETH Nr. 12171.
- IEA, (2002). *World Energy Outlook 2002*, ISBN 92-64-19835-0.
- IPCC, (2001). *Climate Change - The Scientific Basis*, Cambridge University Press.
- Ishida M. and Jin H. (1994a). *A novel combustor based on chemical-looping reactions and its reaction kinetics*, Journal of Chemical Engineering of Japan, 27 296-301.
- Ishida M. and Jin H. (1994b). *A new advanced power generation system using chemical-looping combustion*, Energy, 19, 4, 415.
- Ishida, M. and Jin, H. (1996). *A novel chemical-looping combustor without NO_x formation*. Ind. Eng. Chem. Res. 35, 2469-2472.
- Ishida, M. and Jin, H., Okamoto, T. (1997). *Hydrogen fuelled gas turbine cycle with chemical-looping combustion*, Proceedings of the 3rd International Conference on New Energy Systems and Conversions, Russia, 69-73.

- Ishida, M. and Jin, H., Okamoto, T. (1998). *Kinetic behaviour of solids particles in chemical-looping combustion: Suppressing Carbon Deposition in Reduction*, Energy & Fuels, 12, 223.
- Ishida, M., Yamamoto, M. and Ohba, T. (2002). *Experimental results of chemical-looping combustion with NiO/NiAl₂O₄ particle circulation at 1200°C*. Energy Conversion and Management, 43, 1469-1478.
- Jin, H. and Ishida, M. (1997) *A new advanced IGCC power plant with chemical-looping combustion*. In Proceedings of Thermodynamic Analysis and Improvement of Energy Systems (TAIES'97) Beijing, China 548-553.
- Jin, H. T. Okamoto and M. Ishida (1998). *Development of a Novel Chemical-Looping Combustion: Synthesis of a Looping Material with a Double Metal Oxide of CoO-NiO*. Energy & Fuels;12, 1272-1277.
- Jin, H. T. Okamoto and M. Ishida (1999). *Development of a Novel Chemical-Looping Combustion: Synthesis of a Solid Looping Material of NiO/NiAl₂O₄*. Industrial and Engineering Chemistry Research;38, 126-132.
- Jin H. and M. Ishida (2001) *Reactivity study on novel hydrogen fueled chemical-looping combustion*. International Journal of Hydrogen Energy;26, 889-894.
- Jin H. and M. Ishida (2002) *Reactivity Study on Natural-Gas-Fueled Chemical Looping Combustion by a Fixed-Bed Reactor*. Industrial and Engineering Chemistry Research; 41, 4004-4007.
- Johansson, E. (2005). PhD thesis at the Chalmers University of Technology, Gothenborg, Sweden (in progress).
- Johansson, E., Kronberger, B., Löffler, G., Mattisson, T., Lyngfelt, A., Hofbauer, H. (2003) *A two-compartment fluidized bed for chemical-looping combustion - Design and Experiments*. In Proceedings of the Clean Air 2003, Seventh International Conference on Energy for a Clean Environment, Lisbon, Portugal.
- Johansson, E., Lyngfelt, A., Mattisson T., Johnsson F. (2002) *A Circulating Fluidized Bed System with Inherent CO₂ Separation - Application of chemical-looping combustion*, In Proceedings of the 7th International Conference of Circulating Fluidized Beds (J. R. Grace, J. Zhu and H. d. Lasa eds.), 2002, Canada, 717-724,
- Johnsson, F., Andersson, S., Leckner, B. (1991). *Expansion of a Freely Bubbling Fluidized Bed*, Powder Technol. 68, 117-123.
- Johnsson, F., Vrager, A., Leckner, B. (1999). *Solids flow pattern in the exit region of CFB furnace-influence if exit geometry*, In Proceedings of the 15th Conference on Fluidized Bed Combustion, Savannah.
- Kaiser, S., Löffler, G., Bosch, K., Hofbauer, H. (2003). *Hydrodynamics of a dual fluidized bed gasifier. Part II: simulation of solid circulation rate, pressure loop and stability*, Chem. Eng. Sci. , 58, 18, 4215-4223.
- Knoche K. F. and Richter, H. (1968). *Verbesserung der Reversibilität von Verbrennungs-prozessen*. Brennstoff-Wärme-Kraft, 20, 205-211.
- Krishnaiah, K. Y., Pydi Setty, Varma, Y.B.G. (1982). *Residence Time Distribution of Solids in Multistage Fluidization*, Chem. Eng. Sci. 37, 1371-1377.
- Kronberger, B., Löffler, G. Hofbauer, H. (2004). *Residence time distribution of solids in a chemical-looping fluidized bed fuel reactor*. Proceedings of the 16th International Congress of Chemical and Process Engineering, Prague, Czech Republic.
- Kronberger, B., Löffler, G., and Hofbauer, H. (2005a). *Chemical-looping combustion – Reactor fluidization studies and scale-up criteria*, Chapter 35 in Carbon Dioxide Capture for Storage in Deep Geologic Formations –

Results from the CO₂ Capture Project, *Volume 1 – Capture and Separation of Carbon Dioxide From Combustion Sources*. Ed.: Thomas, D. Elsevier Science, London. First edition, ISBN: 0-08-044570-5

Kronberger, B., Lyngfelt, A., Löffler, G., Hofbauer, H. (2005b). *Design and Fluid Dynamic Analysis of a Bench-Scale Combustion System with CO₂ Separation-Chemical-Looping Combustion* Ind. Eng. Chem. Res. 2005; 44, 3, 546-556.

Kunii, D. and Levenspiel, O. (1991). *Fluidization Engineering*, Second Edition, Butterworth-Heinemann, Boston.

Lackermeier, U. and Werther, J. (2002) Flow phenomena in the exit zone of a circulating fluidized bed *Chemical Engineering and Processing* 41, 771- 783.

Lackner, K.S. and Ziock, H.-J. (2001) The US Zero Emission Coal Alliance Technology, VGB Power Tech 12.

Leithner, R. (2004). *Energy Conversion Processes with Intrinsic CO₂ Separation*. SME (Society for Mining, Metallurgy and Exploration) Annual Meeting, Denver, Colorado

Leretaille, P.-Y., Werther, J., Briand, P., Montat, D. (1999) Modeling of hydrodynamics of large-scale atmospheric circulating fluidized bed coal combustors, in: R.B. Reuther (Ed.), *Proceedings of the 15th International Conference on Fluidized Bed Combustion (FBC99-0024)*, ASME, New York.

Löffler, G., Kaiser, S., Bosch, K. and Hofbauer, H. (2003a) *Hydrodynamics of a dual fluidized-bed gasifier—Part I: simulation of a riser with gas injection and diffuser*, Chem. Eng. Sci. 58, 18, 4197-4213

Löffler G., T. Pröll, (2003b) Effekte der Gipszugabe in den Vergasungsteil des Biomassevergasers Güssing, Internal report TU Wien.

Luisser, C. (2005a). PhD thesis in progress, TU Vienna.

Luisser, M., Kronberger, B., Löffler, G. and Hofbauer H. (2005b). *Chemical-Looping Combustion eine Methode zur CO₂ freien Stromerzeugung aus fossilen Rohstoffen*. to be presented at the 4rd Internationale Energiewirtschaftstagung, Vienna, Austria.

Lyngfelt A. (2004a), Chalmers University of Technology, Gothenborg, Sweden.

Lyngfelt, A., Kronberger, B., Adanez, J., Morin, J.-X., and Hurst, P. (2004b). *The GRACE project. Development of oxygen carrier particles for chemical-looping combustion. Design and operation of a 10 KW chemical-looping combustor*. In *Proceedings of the 7th Conference on Greenhouse Gas Control Technologies (GHGT7)*., Vancouver, Canada.

Lyngfelt A, and Thunman, H. (2004c). *Chemical-looping combustion: Design, construction and 100 h of operational experience of a 10 kW prototype*. *Carbon Dioxide Capture for Storage in Deep Geologic Formations – Results from the CO₂ Capture Project, Volume 1 - Capture and Separation of Carbon Dioxide From Combustion Sources*. Chapter 36, Ed.: Thomas, D. Elsevier Science, London. First edition, ISBN: 0-08-044570-5

Lyngfelt, A., Leckner, B. and Mattisson, T. (2001b). *A Fluidized-Bed Combustion Process with Inherent CO₂ Separation, Application of Chemical-Looping Combustion*, *Chemical Engineering Science*, 56, 3101-3113.

Marchetti, M.M., Czarnecki, T.S. Semedard, S.C., Devroe, S. and Lemasle, J-M. (2003). *Alstom's Large CFBs and Results*, *Proceedings of FBC 2003, 17th International Fluidized Bed Combustion Conference*, Jacksonville, Florida USA.

- Marion, J., Mohn, N., Liljedahl, G.N., Nsakala, N., Morin, J.-X. Henriksen, P.P. (2004). *Technology options for controlling CO₂ emissions from fossil-fuelled power plants*, Proceedings of the Third Annual Conference on Carbon Capture and Sequestration, Alexandria, USA.
- Mattisson, T., Johansson, M., Lyngfelt, A. (2004a) *Multi-cycle reduction and oxidation of different types of iron oxide particles - application to chemical-looping combustion*. Energy & Fuel, 18(3), 628-637.
- Mattisson T., Lyngfelt, A. (2001a). *Applications of chemical-looping combustion with capture of CO₂*, Second Nordic Minisymposium on Carbon Dioxide Capture and Storage, Göteborg, Sweden. available at <http://www.entek.chalmers.se/anly/symp/symp2001.html#46>,
- Mattisson, T., Lyngfelt, A., (2001b). *Capture of CO₂ using chemical-looping combustion*. First Biennial Meeting of Scandinavian-Nordic Section of the Combustion Institute, Göteborg, Sweden, 163-168.
- Mattisson, T., Lyngfelt, A., Cho, P. (2001c). *The use of iron oxide as an oxygen carrier in chemical-looping combustion of methane with inherent separation of CO₂*. Fuel, 80, 1953. First Biennial Meeting of Scandinavian-Nordic Section of the Combustion Institute, Göteborg, Sweden, 163-168.
- Mattisson, T., Lyngfelt, A., Cho, P., (2000). *Possibility of Using Iron Oxide As an Oxygen Carrier for Combustion of Methane with Removal of CO₂ - Application of chemical-looping combustion*. In Proceedings of the 5th International Conference on Greenhouse Gas Control Technologies, Cairns, Australia, 205-210.
- Mattisson, T., Zafar, Q., Lyngfelt, A. and Gevert, B., (2004b), *Integrated hydrogen and power production from natural gas with CO₂ capture*, 15th World Hydrogen Energy Conference, Yokohama.
- Mikus, T. Melien, T. (2004) *CCP Economics overview* In Proceedings of the 3rd Conference on Carbon Sequestration, Alexandria, USA.
- Miwa, K., S. Mori, T. Kato, and I. Muchi, (1972). *Behavior of Bubbles in a gaseous Fluidized Bed* Int. Chem. Eng., 12, 1.
- Mori, S., and C.Y. Wen, (1975). *Estimation of Bubble Diameter in Gaseous Fluidized Beds* AIChE J., 21, 1.
- Morin, J.-X., and Béal, C. (2005) *Chemical Looping Combustion of Refinery Fuel Gas with CO₂ Capture*, chapter 37 in Carbon Dioxide Capture for Storage in Deep Geologic Formations –Results from the CO₂ Capture Project, Volume 1 - Capture and Separation of Carbon Dioxide From Combustion Sources, , Ed.: Thomas, D. Elsevier Science, London. First edition, ISBN: 0-08-044570-5.
- Nakano Y, Iwamoto S, Maeda T, Ishida M, Akehata T. (1986) *Characteristics of Reduction and Oxidation Cycle Process by Use of aFe₂O₃ Medium*. Iron & Steel Journal of Japan, 72, 1521-1528.
- Naqvi, R., Bolland, O., Brandvoll, Ø., Helle, K. (2004a) *Chemical Looping combustion: Analysis of Natural Gas Fired Power Cycles with Inherent CO₂ capture.*, The Second Trondheim Conference on CO₂ Capture, Transport and Storage, Trondheim, Norway. <http://www.energy.sintef.no/arr/co2%5F2004/> (last visit 1.2.2005).
- Naqvi, R. R., Bolland, O., Helle, K., Brandvoll, Ø. (2004b). *Chemical Looping Combustion-Analysis of Natural Gas Fired Power Cycles With Inherent CO₂ Capture* In Proceedings of the ASME Turbo Conference (GT2004-53359), Vienna, Austria.
- Olazar, M., San Jose, M. J., Penas, F. J., Aguayo, A. T., Arandes, J. M., Bilbao, J. *A simplified model for gas flow in conical spouted beds*. Chemical Engineering Journal, 1995
- Perry, R. H. (1988). *Perry's Chemical Engineers Handbook*, 6th Ed., McGraw Hill International Ed.

- Prasad Babu, M. and Pydi Setty Y. (2003). *Residence Time Distribution of Solids in a Fluidized Bed*, The Canadian Journal of Chemical Engineering, 81.
- Pugsley, T.S. and Berruti, F. (1995). *A Core-Annulus Solids Interchange Model for Circulating Fluidized Bed and FCC Risers*, in Fluidization VIII, 379-388.
- Pugsley, T.S. and Berruti, F. (1996). *A Predictive Hydrodynamic Model for Circulating Fluidized Bed Risers*, Powder Technol. 89, 57-69.
- Pugsley, T.S., Berruti, F., Godfroy, L., Chaouki, J., Patience, G.S. (1994). *A Predictive Model for the Gas-Solid Flow Structure in Circulating Fluidized Bed Risers*, in Circulating Fluidized Bed Technology IV, A.A. Avidan (Ed.), AIChE, New York, USA, 41-48.
- Rhodes, M., Zhou, S., Hirama, T., Cheng, H. (1991). *Effects of Operating Conditions on Longitudinal Solids Mixing in a Circulating Fluidized Bed Riser*, AIChE J., 37, 10, 1450-1458.
- Richter H. and K. Knoche (1983). *Reversibility of combustion processes. Efficiency and Costing* ACS Symposium Series, 235: 71-86.
- Rivière la, R., Hartholt, G.P., Hoffmann, A.C., Janssen, L.P.B.M. (1996). *Methods for the determination of particle residence time distribution in continuous gas fluidized beds*, IChemE Symp. Ser. 140, 283-294.
- Rizeq, G., West, J., Frydman, A., Subia, R., Zamansky, V. (2003). *Advanced Gasification-Combustion Technology for Production of Hydrogen, Power and Sequestration-Ready* In Proceedings of Gasification Technologies, San Francisco, USA.
- Rudolph, V. and Judd, M.P. (1985) *Circulation and slugging in a fluid bed gasifier*, in: P. Basi (Ed.), Circulating Fluidized Bed Technology, pp. 437-441.
- Ryu, H.J., Bae, D.H., Han, K.H., Lee, S.-Y. Jin, G.-T. and Choi, J.-H. (2001) *Oxidation and Reduction Characteristics of Oxygen Carrier Particles and Reaction Kinetics by Unreacted Core Model* Korean Journal of Chemical Engineering, 18, 6, 831-83.
- Ryu, H.J., Bae, D.H., Jin, G.T. (2002a). *Carbon deposition characteristics of NiO based oxygen carrier particles for Chemical-Looping Combustion*. In Proceedings of the Sixth International Conference on Greenhouse Gas Control Technologies - GHGT-6, Kyoto, Japan.
- Ryu, H.J., Bae, D.H., Jin, G.T. (2003a) *Effect of Temperature on Reduction Reactivity of Oxygen Carrier Particles in a Fixed Bed Chemical-Looping Combustor* Korean Journal of Chemical Engineering, 20, 5, 960-966
- Ryu, H.-J., Bae, D.-H., Lee, S.-Y., Jin, G.-T. (2002b). *Conceptual Design of 50kWth Chemical-Looping Combustor* Theories and Applications of Chem. Eng., 8, 2, 3798-3792, (in Korean)..
- Ryu, H.J., Jin, G.T (2004a) *Development of CO₂/NO_x free Chemical-Looping Combustor: Fluidized Bed Experiment*, Korean Chem. Eng. (in print).
- Ryu, H.J., Jin, (2004b) *Criteria for Selection of Metal Component in Oxygen Carrier Particles for Chemical-Looping Combustor*, Korean Chem. Eng. Res., 42, 5, 588-597 (in Korean).
- Ryu, H.J., Jin, G.T., Yi, C.K. (2004c) *Demonstration of inherent CO₂ separation and no NO_x emission in a 50kW Chemical Looping Combustor: Continuous Reduction and oxidation experiments*, In Poster and Paper at the 7th Conference on Greenhouse Gas Control Technologies (GHGT7), Vancouver, Canada.

- Ryu, H.J., Lim, N.Y., Bae, D.H., Jin, G.T. (2003b) *Carbon Deposition Characteristics and Regenerative Ability of Oxygen Carrier Particles for Chemical-Looping Combustion* Korean Journal of Chemical Engineering, 20, 1, 157-162.
- Salvador, C., Lu, D., Anthony, E.J., Abanades, J. C. (2003). *Novel CO₂ control method by means of CO₂ chemical looping* In Proceedings of the Clean Air 2003, Seventh International Conference on Energy for a Clean Environment, Lisbon, Portugal.
- Schlichthaerle, P. and Werther, J. (1999). *Axial Pressure Profiles and Solids Concentration Distributions in the CFB Bottom Zone*, Chem. Eng. Sci. 54, 5485-5493.
- Schut, S.B., van der Meer, E.H., Davidson, J.F., Thorpe, R.B. (2000). *Gas-solid Flow in the Diffuser of a Circulating Fluidized Bed Riser*, Powder Technol., 111, 94-103.
- Simbeck D., (2004). *Overview and Insights on the Three Basic CO₂ Capture Options* Proceedings at the Third Annual Conference on Carbon Capture and Sequestration, Alexandria, USA.
- Stiess, M. (1992). *Mechanische Verfahrenstechnik 1&2* Springer Verlag, Berlin-Heidelberg ISBN 3-540-55778-4.
- Stobbe, E.R. (1999) *Catalytic routes for the conversion of methane to synthesis gas*. PhD Thesis, Utrecht University.
- Stokes, R.L. and Naumann, E.B. (1970). *Residence Time Distribution Functions for Stirred Tanks in Series*, Can. J. Chem. Eng. 48, 723-725.
- Song, K., Seo, Y., Yoon, H., and Cho, S., 2003. Characteristics of the NiO/Hexaaluminate for Chemical Looping Combustion, *Korean Journal of Chemical Engineering* Vol. 20, No. 3: 471-475.
- Tagwerker, C. (2003) *Aufbau und Betrieb eines Labormodells zur Untersuchung der Fluidodynamik eines Chemical Looping Combustion Wirbelschichtsystems* Diploma thesis, Vienna University of Technology.
- Toomey, R.D. and Johnstone, H.F. (1952). *Gaseous Fluidization of Solid Particles*, Chem. Eng. Prog. 48, 220.
- Valenciano, R., (2001). *Effect of Solids Residence Time Distribution on Fuel Reactor Performance of Chemical Looping Combustor*, Master thesis, Vienna University of Technology.
- Villa, R., Cristiani, C., Groppi, G., Lietti, L., Forzatti, Pio., Cornaro, U., Rossini, S. (2003). *Ni based mixed oxide materials for CH₄ oxidation under redox cycle conditions*. Journal of Molecular Catalysis A: Chemical 202-204, 637-646.
- Wein, J.W. (1992). *Das Expansionsverhalten von Gas/Feststoff Wirbelschichten bei höheren Geschwindigkeiten*, PhD. thesis, TU Hamburg-Harburg, Germany.
- Werther, J. (1993). *Fluid Mechanics of Large-Scale CFB Units*, in Circulating Fluidized Bed Technology IV, A.A. Avidan (Ed.), AIChE, New York, USA, 1-4.
- Wolf, J. (2005). *CO₂ Mitigation on Advanced Power Cycles*, PhD. Thesis, at KTH Stockholm.
- Wolf, J., Anheden, M., Yan, J. (2001). *Performance Analysis of Combined Cycles with chemical Looping Combustion for CO₂ Capture Requirements for the Oxidation and Reduction Reactors*, International Pittsburgh Coal Conference, Newcastle, New South Wales, Australia.

Wolf, J. and Yan, J. (2004) *Cogeneration of hydrogen and electrical power in an extended chemical-looping combustion* 17th International Conference on Efficiency, Costs, Optimization, Simulation and Environmental Impact of Energy and Process Systems, Guanajuato, México.

Wu, S.Y. and J. Baeyens, (1991). *Effect of Operating Temperature on Minimum Fluidization Velocity* J. Powder Technol., 67, 217.

Zenz, F.A. and Weil, N.A. (1958). *A Theoretical-Empirical Approach to the Mechanism of Particle Entrainment from Fluidized Beds*, AIChE J. 4, 472-479.

Zhang M.C, and Yang, R.Y.K. (1987). *On the scaling laws for bubbling gas-fluidized bed dynamics*, Powder Tech., 51, 159-165.

Zheng, Q.-Y. Zhang, H. (1995) *Effect of geometry of bed exit (end effect) on hydrodynamic behaviour of gas-solid flow in CFB combustor*, in: J.-F. Large, C. Laguerie (Eds.), Fluidization VIII, Engineering Foundation, New York, p. 453.

11 Nomenclature

a	decay constant of the riser	$[m^{-1}]$
A	cross section area of reactor/bed	$[m^2]$
A_{cross}	area of cross section of loop seal opening	$[m^2]$
A_{wall}	area of defined wall surface	$[m^2]$
A_0	cross section of return slot	$[m^2]$
Ar	Archimedes number	[-]
c	concentration	$[kg.kg^{-1}]$
c_0	start concentration	$[kg.kg^{-1}]$
C_D	drag coefficient	[-]
d_p	particle diameter	[m]
d_p^*	dimensionless particle diameter $\propto Ar^{1/3}$	[-]
dz	vertical length increment	[m]
D	diameter	[m]
D_e	exit diameter	[m]
D_h	hydraulic diameter	[m]
E_0	ejection flux of solids	$[kg.m^2.s^{-1}]$
$E(\theta)$	age distribution function	[-]
f_s	friction factor	[-]
Fr	Froude number	[-]
$F(\theta)$	cumulative RTD function	[-]
g	gravity	$[m.s^{-2}]$
G_s	specific solids circulation rate	$[kg.m^{-2}.s^{-1}]$
$G_{s,min}$	minimum required specific solids circulation rate	$[kg.m^{-2}.s^{-1}]$
ΔG_f	Gibbs free energy in a chemical reaction	$[J.mol^{-1}]$
h	height	[m]
$h_{AR,RS}$	AR bed height at return slot level (from distributor)	[m]
$h_{FR,RS}$	FR bed height at return slot level (from distributor)	[m]
h_{slot}	height of loop seal slot	[m]
h_{stp}	height of loop seal standpipe	[m]
H	height	[m]
H_e	riser exit height	[m]
H_j	enthalpy of stream j	$[J.mol^{-1}]$
ΔH_{red}	heat of reduction	$[J.mol^{-1}]$
ΔH_{ox}	heat of oxidation	$[J.mol^{-1}]$
ΔH_c	heat of combustion	$[J.mol^{-1}]$
k	decay constant	$[m^{-1}]$
k^*	dimensionless reaction rate	[-]
$k_{CVC,inlet}$	parameter for cyclone	[-]
$k_{CVC,Vortex}$	parameter for cyclone	[-]
k_λ	friction constant	$[s.m^{-1}]$
K	constant in equation (5-2)	[-]
$K_{i,\infty}$	elutriation rate constant	$[kg.m^{-2}.s^{-1}]$
K_x	equilibrium constant in molar fraction	[-]
K_D	discharge coefficient	[-]
l_{wall}	wall length for loop seal wall area	[m]
L	length	[m]
m	mass	[kg]
m_{AR}	bed mass in the air reactor	[kg]

m_{circ}	circulating mass flow	$[\text{kg}\cdot\text{s}^{-1}]$
m_{FR}	bed mass in the fuel reactor	$[\text{kg}]$
m_{ox}	mass of oxygen carrier when fully oxidised	$[\text{kg}]$
m_{O_2}	mass flow of oxygen	$[\text{kg}\cdot\text{s}^{-1}]$
$m_{\text{s,down}}$	downward solids mass flow	$[\text{kg}\cdot\text{s}^{-1}]$
$m_{\text{s,up}}$	upward solids mass flow	$[\text{kg}\cdot\text{s}^{-1}]$
M_{actual}	actual molar mass of oxygen carrier	$[\text{kg}\cdot\text{mol}^{-1}]$
$M_{\text{f,ox}}$	molar mass of oxygen carrier in fully oxidised state	$[\text{kg}\cdot\text{mol}^{-1}]$
$M_{\text{f,red}}$	molar mass of oxygen carrier in fully reduced state	$[\text{kg}\cdot\text{mol}^{-1}]$
n	Richardson Zaki coefficient	$[-]$
n_0	number number of orifices in the distributor	$[-]$
N_{De}	dimensionless form of exit diameter	$[-]$
N_{Gs}	mass number	$[-]$
N_{Gst}	terminal mass number	$[-]$
N_{He}	dimensionless form of projected height	$[-]$
N_{α}	dimensionless exit angle	$[-]$
p_v	pressure in vertical direction in bulk material	$[\text{Pa}]$
p_{fric}	frictional pressure drop	$[\text{Pa}]$
Δp_{FR}	pressure drop of the fuel reactor	$[\text{Pa}]$
Δp_{HOR}	pressure drop in horizontal section of loop seal	$[\text{Pa}]$
Δp_{L}	pressure difference between fuel reactor and downcomer	$[\text{Pa}]$
Δp_{RS}	pressure drop across return slot	$[\text{Pa}]$
Δp_{RIS}	riser pressure drop	$[\text{Pa}]$
Δp_{RIS}^*	modified riser pressure drop (solids return line to top)	$[\text{Pa}]$
$\Delta p_{\text{RIS}}^{**}$	riser pressure drop(20mm above gas distributor to top)	$[\text{Pa}]$
$\Delta p_{\text{AR,RS}}$	bed pressure drop of AR at $h_{\text{AR,RS}}$	$[\text{Pa}]$
$\Delta p_{\text{FR,RS}}$	bed pressure drop of FR at $h_{\text{FR,RS}}$	$[\text{Pa}]$
p_0	atmospheric pressure	$[\text{Pa}]$
P	perimeter	$[\text{m}]$
PSD	particle size distribution	$[-]$
R_0	oxygen ratio	$[-]$
R	universal gas constant	$[\text{J}\cdot\text{mol}^{-1}\cdot\text{K}^{-1}]$
Re_p	particle Reynolds number	$[-]$
SF	gas split factor	$[-]$
t	time	$[\text{s}]$
T	temperature	$[\text{K}]$
TSI	total solids inventory	$[\text{kg}]$
u	superficial velocity	$[\text{m}\cdot\text{s}^{-1}]$
$u_{\text{a,s}}$	solids velocity in the annulus	$[\text{m}\cdot\text{s}^{-1}]$
$u_{\text{c,s}}$	solids velocity in the core	$[\text{m}\cdot\text{s}^{-1}]$
u_{AR}	AR fluidisation velocity	$[\text{m}\cdot\text{s}^{-1}]$
u_{FR}	FR fluidisation velocity	$[\text{m}\cdot\text{s}^{-1}]$
u_g	gas velocity	$[\text{m}\cdot\text{s}^{-1}]$
u_s	solid velocity	$[\text{m}\cdot\text{s}^{-1}]$
u_t	terminal particle settling velocity	$[\text{m}\cdot\text{s}^{-1}]$
u_{mf}	minimum fluidisation velocity	$[\text{m}\cdot\text{s}^{-1}]$
u_c	superficial velocity at maximum pressure fluctuation amplitude	$[\text{m}\cdot\text{s}^{-1}]$
u_{se}	onset velocity of significant solids entrainment	$[\text{m}\cdot\text{s}^{-1}]$
u_{RIS}	superficial gas velocity in the riser	$[\text{m}\cdot\text{s}^{-1}]$

U^*	dimensionless velocity	$[\text{m}\cdot\text{s}^{-1}]$
V	volume flow	$[\text{m}^3\cdot\text{s}^{-1}]$
V_{LS}	loop seal fluidisation volume flow	$[\text{m}^3\cdot\text{s}^{-1}]$
$V_{LS,FR}$	loop seal fluidisation volume flow leaving through the fuel reactor	$[\text{m}^3\cdot\text{s}^{-1}]$
W	width	$[\text{m}]$
w_{MeO}	mass content of active phase in oxygen carrier in fully oxidised state	$[-]$
x_i	molar fraction of the species i	$[-]$
$x_{\text{CO}_2,FR,\text{exit,dry}}$	molar fraction CO_2 in the FR exit gas flow (dry basis)	$[-]$
X	dimensionless interphase mass transfer	$[-]$
X_{OC}	oxygen carrier conversion	$[-]$
ΔX_{OC}	oxygen carrier conversion difference	$[-]$
Y	correction factor for the two-phase theory	$[-]$

11.1 Greek letters

α	exit angle equ. (5-12)	$[\text{°}]$
δ_b	bubble fraction	$[-]$
ε	voidage	$[-]$
η	dynamic viscosity	$[\text{Pa}\cdot\text{s}]$
η_B	reflection coefficient	$[\text{kg}\cdot\text{m}^{-1}\cdot\text{s}^{-1}]$
η_{CO_2}	purity of CO_2	$[-]$
$\eta_{\text{CO}_2,FR,\text{exit,dry}}$	purity of CO_2 at FR exit, dry basis	$[-]$
γ	half angle of the diffuser	$[-]$
λ	friction coefficient	$[-]$
λ_H	measure for pressure transmission of bulk material	$[-]$
μ	coefficient	$[\text{°}]$
ϕ	particle sphericity	$[-]$
ρ	density	$[\text{kg}\cdot\text{m}^{-3}]$
ψ	slip factor	$[-]$
σ	RMS (root mean square) deviation	$[-]$
τ	space time	$[-]$
ξ	ratio of volume of ejected particle to the bubble volume	$[-]$
Θ	dimensionless time	$[-]$

11.2 Acronyms

AR	air reactor
BZ	bottom zone
CCCC	CO_2 capture in coal combustion
CCS	CO_2 capture and storage
CCP	CO_2 capture project
CFB	circulating fluidised bed
CLC	chemical-looping combustion
CON	connection
CSTR	continuous stirred tank reactor
CYC	cyclone
DOW	downcomer
FBHE	fluidised bed heat exchanger
FM	flow model
FCC	fluid catalytic cracking
FR	fuel reactor

GB	glass beads
GRACE	Grangemouth Advanced CO ₂ Capture Project
LHV	lower heating values
LS1	loop seal 1
LS2	loop seal 2
Me	metal
MeO	metal oxide
PSD	particle size distribution
RTD	residence time distribution
TDH	transport disengagement height
TGA	thermo gravimetric analyser
TIT	turbine inlet temperature
TSI	total solids inventory
ZECA	zero emission coal alliance

11.3 Indices

a	annulus
AR	air reactor
b	bubble phase
bed	bed
bulk	bulk solids material
BZ	bottom zone
c	core
corr	corrected
cross	cross sectional area
CON	connection
CYC	cyclone
dyn	dynamic
DOW	downcomer
f	fluid
fric	friction
FR	fuel reactor
g	gas
hor	horizontal
inlet	at the inlet
i	counter
k	reaction number
LS1	loop seal 1
LS2	loop seal 2
mf	minimum fluidisation
OUT	at the outlet
p	particle
RIS	riser
RS	return slot
s	solid
stp	standpipe
t	terminal
Top	at top of
Tol	tolerance

TP	two phase
tracer	tracer
Vortex	vortex tube of cyclone
wall	wall
∞	above transport disengaging height
0	at bottom of transport zone

12 CURRICULUM VITAE

Bernhard Kronberger

In der Straß 4
4816 Gschwandt

geb. am 24.09.1973 in Gmunden

Familienstand: ledig



Ausbildung

1980 – 1984	Volksschule Gschwandt
1984 – 1988	Hauptschule Vorchdorf
1988 – 1993	HTBLA Vöcklabruck Abteilung Maschinenbau, Gebäudetechnik und Energieplanung Matura im Juni 1993 mit Auszeichnung
1994 - 2000	Studium der Verfahrenstechnik and der TU Wien, Studienzweig Apparate-, Anlagenbau und Prozesstechnik Diplomarbeitstitel: "Defluidization of Fine Powder Fluidized Beds Caused by Changing the Fluidizing Gas" Diplomprüfung im Oktober 2000
Jän.1999 – Jun.1999	Studienaufenthalt am UMIST - Manchester, UK. Department of Civil and Structural Engineering.

Berufslaufbahn

Jän. 2001 - Jän. 2002	Wissenschaftlicher Mitarbeiter am Institute for Systems, Informatics and Safety an der Gemeinsamen Forschungsstelle der Europäischen Kommission (JRC) in Ispra, Italien.
seit Feb. 2001	Vortragender an der Fachhochschule für Verfahrens- und Umwelttechnik Innsbruck
seit Jän. 2002	Dissertation und Forschungsassistent am Institut für Verfahrenstechnik, Umwelttechnik und Technische Biowissenschaften der TU-Wien. Thema: "Modelling Analysis of Fluidised Bed Reactor Systems for Chemical-Looping Combustion"